Marine and Petroleum Geology 173 (2025) 107288

Contents lists available at ScienceDirect

Marine and Petroleum Geology

journal homepage: www.elsevier.com/locate/marpetgeo

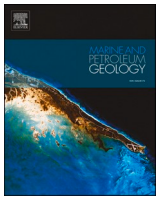

Research Paper

Hydrological isolation of the Paratethys in the late Middle-Late Miocene: Integrated stratigraphy, palaeoenvironments and biotic record of the Caspian Basin, Karagiye, Kazakhstan

Sergei Lazarev [a,b,*], Oleg Mandic [c], Marius Stoica [d], Pavel Gol'din [e], Stjepan Ćorić [f], Mathias Harzhauser [c], Wout Krijgsman [g], Dias Kadirbek [h], Davit Vasilyan [a,b]

[a] Department of Geosciences, University of Fribourg, Fribourg, Switzerland
[b] JURASSICA Museum, Porrentruy, Switzerland
[c] Geological-Paleontological Department, Natural History Museum Vienna, Vienna, Austria
[d] Faculty of Geology and Geophysics, University of Bucharest, Bucharest, Romania
[e] Schmalhausen Institute of Zoology, National Academy of Sciences of Ukraine, Kyiv, Ukraine
[f] GeoSphere Austria, Vienna, Austria
[g] Department of Earth Sciences, Utrecht University, Utrecht, the Netherlands
[h] School of Mining and Geosciences, Nazarbayev University, Astana, Kazakhstan

ARTICLE INFO

Keywords:
Caspian basin
Eastern Paratethys
Serravallian-Tortonian
Magnetostratigraphy
Biostratigraphy
Vertebrate fauna

ABSTRACT

The hydrological connectivity of semi-isolated basins with the global ocean drives remarkable ecosystem turnover and regional climate shifts, making palaeoenvironmental and palaeohydrological studies of the epicontinental basins of high relevance. During the late Middle–Late Miocene, the Paratethys Sea, which occupied vast areas of the West Eurasian Interior, underwent a notable hydrological isolation from the global ocean. Between 12.65 and 7.65 Ma, the Paratethys experienced significant water level fluctuations and eventually near-total ecosystem collapse. The causes and timing of these hydrological and biotic changes remain unclear, especially in the understudied Caspian Sea region. Our study presents an integrated stratigraphic framework of the 136-m-thick Karagiye section on the east coast of the Caspian Sea (Mangystau region, Kazakhstan). The fauna-rich deposits document the pre- (Konkian), syn- (Volhynian, Bessarabian and Khersonian) and post-isolation (Maeotian) phases of Paratethys evolution at its eastern margin. We reconstruct the palaeoenvironmental history of the Caspian Basin by combining palaeomagnetic dating with biostratigraphic analyses of microfauna, molluscs, marine vertebrates and calcareous nannoplankton. Our key findings in the studied section include: 1. Konkian (incomplete): Open lagoonal environments with restricted connectivity to the global ocean in the early Konkian followed by a middle Konkian faunal influx and establishment of normal marine environments; 2. Volhynian (incomplete, 12.3–12.05 Ma): Onset of Paratethys hydrological isolation with marginal lagoonal environments, new endemic species, plus rare surviving Konkian taxa; 3. Bessarabian (12.05–9.9 Ma): Transgression and offshore setting at ~12.05 Ma with maximum flooding at 11.6 Ma and Intra-Bessarabian Carbonate Surge at ~10.7 Ma, followed by upper Bessarabian (10.7–9.9 Ma) carbonate platform interior settings; 4. Khersonian (9.9–7.65 Ma): Khersonian Ecological Crisis, carbonate platform to backshore environments with hiatus between 9.5 and ~8.0 Ma representing an extreme lowstand. 5. Maeotian (incomplete 7.65–7.0 Ma): Transgression at 7.65 Ma, followed by a delayed invasion of Maeotian faunas at 7.5 Ma, linked to the reconnection of the Caspian Basin with the rest of the Eastern Paratethys. The well-dated biotic record of Karagiye enhances understanding of Paratethyan hydrological and ecological events in the Caspian Basin and provides a foundation for further palaeoclimatic and palaeobiogeographic studies across Eurasia.

1. Introduction

The hydrological evolution of enclosed basins (i.e. surrounded by land), with irregular connectivity history to the global ocean (Healy and Kenichi, 1991), is a complex and fascinating process. In these systems, the interplay of tectonics and climate controls the water budget

* Corresponding author. Department of Geosciences, University of Fribourg, Fribourg, Switzerland.sergei.lazarev@unifr.ch

https://doi.org/10.1016/j.marpetgeo.2025.107288
Received 18 September 2024; Received in revised form 3 January 2025; Accepted 4 January 2025
Available online 11 January 2025

(evaporation vs precipitation) and defines the basin connectivity mode with the global ocean (Meijer, 2012; Simon et al., 2019). Any change in the gateway configuration may significantly impact the basinal water level and, with this, change regional palaeoclimate (precipitation and temperature) (Zhao et al., 2022; Voigt et al., 2017; Frisch et al., 2019; Hoyle et al., 2020). Further, water level fluctuations (Paramonova, 1994; Popov et al., 2010), erosional processes on land (Schobben et al., 2016) and connectivity changes with the global ocean (or other basins) (Flecker et al., 2015; Andreetto et al., 2021) strongly control basinal water chemistry and aquatic ecosystems. Detailed palaeoenvironmental and palaeohydrological reconstructions of epicontinental basins are vital for understanding palaeoprecipitation dynamics and faunal dispersal pathways.

An outstanding example of an epicontinental basin with a dynamic connectivity history is the Paratethys – a former Cenozoic Sea in the West Eurasian interior that, at its maximum extension, spread from modern Kazakhstan to France (Laskarev, 1924). Since its birth in the early Oligocene from the Tethys Sea/Ocean, the Paratethys, consisted of numerous basins that were periodically connected with the global ocean via tectonically-controlled gateways (Rögl, 1999; Schulz et al., 2005).

During the late Middle – early Late Miocene (Serravallian-Tortonian), the Paratethys underwent a major phase of hydrological isolation (Fig. 1). At 12.65 Ma, the restriction and closure of the Slovenian Strait disconnected Paratethys from the global ocean. Between 12.65 and 7.65 Ma, during the Volhynian, Bessarabian and Khersonian (sub)stages, the restricted marine basin transformed into a large anomalohaline lake (Rögl, 1999; Popov et al., 2022). Later, at 11.7 Ma, the uplift of the Carpathian mountains separated the Eastern Paratethys from the Central Paratethys, with the latter transforming into the Lake Pannon (ter Borgh et al., 2014). The marine cut-off made the Eastern Paratethys water budget (evaporation vs precipitation) highly sensitive to climatic changes, resulting in extreme water level fluctuations (Popov et al., 2010). During the Bessarabian, the Eastern Paratethys underwent a gigantic water surface expansion, flooding the vast territories of Central Asia and the northern Black Sea margin (Iljina et al., 1976). During the Khersonian, the Eastern Paratethys experienced water level drops of ~300 m amplitude that repetitively disconnected the Caspian, Euxinian and Dacian subbasins, exposing large areas of the former shelf (Popov et al., 2010).

The aquatic Paratethyan ecosystems faced remarkable diversification and expansion to near-total extinction. Right after the isolation, during the Volhynian, the aquatic faunal communities gradually radiated and thrived in the Bessarabian. However, at the transition to the Khersonian lowstand, the ecosystem collapsed: the biodiversity of molluscs shrunk by about 90%, the entire foraminifera fauna vanished and the marine vertebrate fauna such as fishes, dolphins, whales and seals went nearly entirely extinct (Paramonova, 1994; Maissuradze and Koiava, 2011; Popov et al., 2022; Gol'din and Startsev, 2017).

The diversity dynamics of Eastern Paratethys biota are well understood, but the drivers behind the extreme water level fluctuations and biodiversity rise and demise remain elusive. This is mainly related to the lack of continuous geological outcrops with reliable age constraints. In

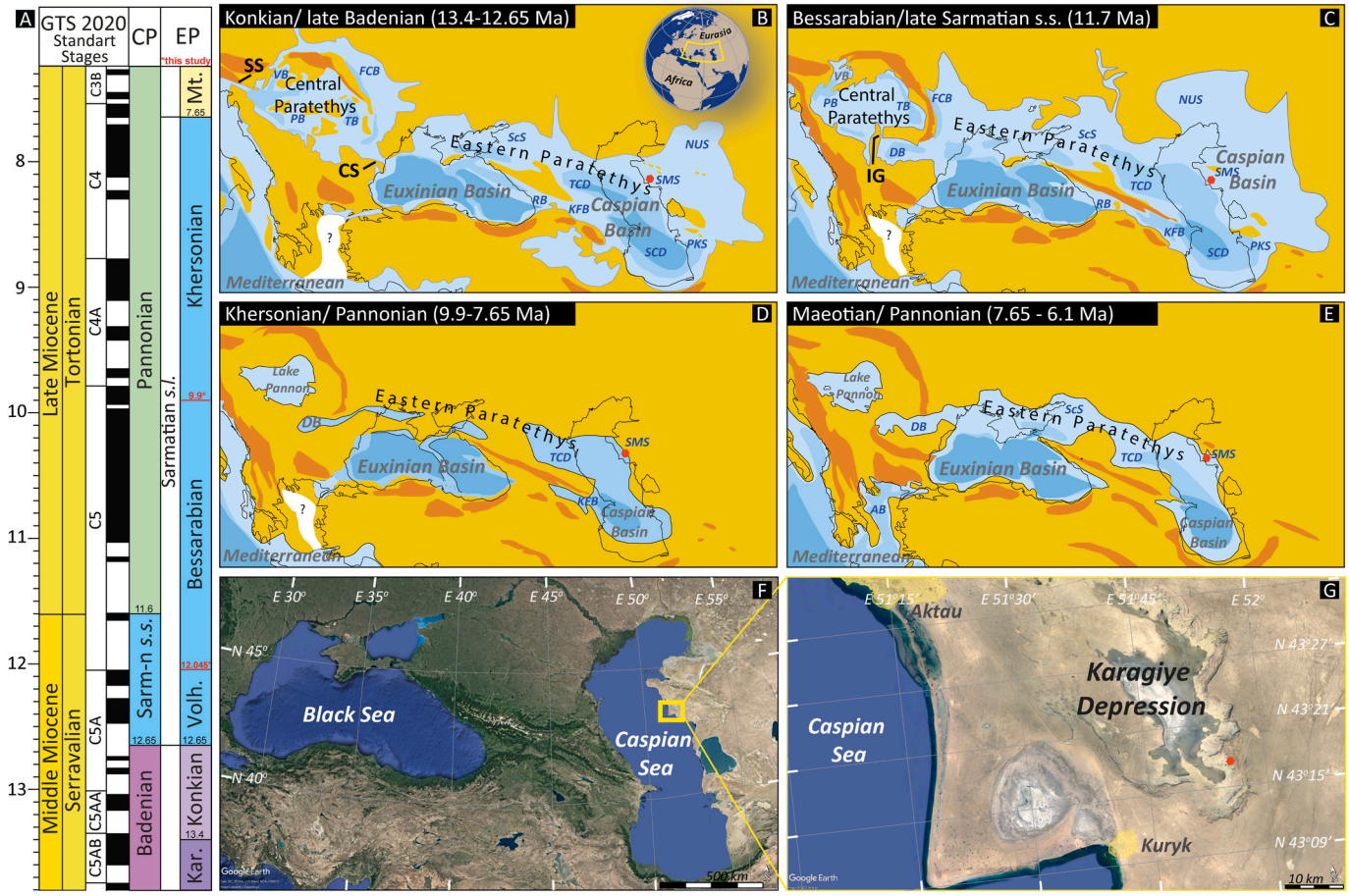

Fig. 1. Serravallian-Tortonian regional stages of the Central (CP) and Eastern Paratethys (EP) (A), palaeogeographic evolution of the region (B–E) (redrawn from (Paramonova, 1994; Popov et al., 2010), (F–G) geographic location (red dot) of the studied outcrop Karagiye (maps are taken from Google Earth©). Abbreviations (in column) Kar. – Karaganian, Mt. – Maeotian; (on the maps): SS – Slovenian Strait, CS – Carasu Strait, IG – Iron Gate Strait, NUS – North-Ustyurt Shelf, SMS – South Mangyshlak Shelf, PKS – Pre-Kopet Dag Shelf, SCd – South Caspian Depression, KFB – Kura Foreland Basin, TCD – Terek-Caspian Depression, RB – Rioni Basin, ScS – Scythian Shelf, DB – Dacian Basin, TB – Transylvanian Basin, PB – Pannonian Basin, VB – Vienna Basin, FCB – Fore-Carpathian Basin.

line with the Oligocene-Early Miocene Maikopian Series, the Volhynian-Bessarabian-Khersonian Stages remain one of two poorly dated intervals in the Paratethys history. Moreover, most of the palaeoenvironmental recontructions are based on biotic records from the Dacian (Carpathian Foreland) and the Euxinian (Black Sea) basins (Popov et al., 2016). Its large easternmost segment – the Caspian Sea misses robust constraints.

In this paper, we present an integrated stratigraphy of the 136-m-thick Karagiye section in Kazakhstan (Fig. 1), which comprises one of the most complete Middle–Late Miocene sedimentary successions of the Caspian Basin. A combination of high-resolution magnetostratigraphy, sedimentary facies observations, molluscs, microfauna (foraminifera and ostracods) and calcareous nannoplankton reveals the palaeoenvironmental evolution of the Eastern Paratethys before, during and after the Serravalian–Tortonian hydrological isolation. Moreover, we provide a continuous and well-dated record of marine vertebrate fauna (whales, dolphins, seals, fishes) for the first time, allowing us to better understand their responses to palaeoenvironmental perturbations. The paper aims to create a well-dated biotic and palaeoenvironmental record for the Volhynian – Khersonian of the Caspian Basin, further contributing to a broad range of interregional palaeoenvironmental studies concerning the hydrological evolution of the Paratethys, palaeobiogeography of aquatic groups and palaeoclimatic reconstructions of Eurasian Interior.

2. Geological setting and stratigraphy

2.1. Serravallian-Tortonian stratigraphy of the Eastern Paratethys

The Paratethys's semi-isolated nature throughout its history made it an important hotspot of diverse endemic faunas, whose correlation to the Geological Time Scale has been problematic (Harzhauser et al., 2024b; Popov et al., 2022). Because of that, the Paratethys has its own regional stratigraphic subdivision, which is mainly based on the endemic mollusc fauna (Nevesskaya et al., 2003).

The Serravallian-Tortonian stratigraphy of the Eastern Paratethys comprises the following regional stages: Karaganian, Konkian, Sarmatian s.l. and Maeotian (Popov et al., 2022; Raffi et al., 2020), with the first one being not present in our study and thus not discussed below (but see Harzhauser et al., 2024a). The term "Sarmatian" was introduced in 1866 for the Central Paratethys (CP) (Suess, 1866) and was later adopted for the Eastern Paratethys (EP). However, later it was shown that the Sarmatian in the CP comprises a much shorter stratigraphic interval (e.g. 12.65–11.6 Ma) than in the EP (e.g. 12.65–7.6 Ma). In order to resolve the conflict on the term use, the stratigraphic committee adopted a temporal solution by calling the Sarmatian in the CP as Sarmatian *sensu stricto* and in the EP – Sarmatian *sensu lato* (Papp et al., 1974a). Nowadays, some of the authors use the Sarmatian s.l. substages – the Volhynian (lower), Bessarabian (middle) and Khersonian (upper), as independent stages (Palcu et al., 2019; Lazarev et al., 2020). In our work, we follow this nomenclature and show that these substages have distinct biostratigraphic signatures that allow us to show and recognise these units as independent regional stages.

The Konkian Stage dated between 13.4 and 12.65 Ma (Palcu et al., 2017) is subdivided into three substages: the lower (Kartvelian) marked by the dominance of the molluscs *Barnea* and *Ervillia*; the middle (Sartaganian) characterised by a massive influx of euhaline faunas dominated by *Limacina*, *Aequipecten* and *Loripes* molluscs and upper (Veselyankian) with *Timoclea konkensis* and *Ervilia podolica* (Popov et al., 2022).

The Volhynian Stage characterises the onset of the hydrological isolation of the Eastern Paratethys. The base of Volhynian is marked by the Badenian-Sarmatian Extinction Event (BSEE) (Harzhauser and Piller, 2007; Palcu et al., 2015) and by the first occurrence of the molluscs *Polititapes vitalianus* and *Sarmatimactra eichwaldi* (Muratov and Nevesskaya, 1986; Paramonova, 1994). The base of the Volhynian (known as the base of the Sarmatian s.l.) is concurrent with the base of the Sarmatian s.s. in the Central Paratethys and has an age of 12.65 Ma (Palcu et al., 2017).

The Bessarabian Stage begins as a large-scale transgression followed by the occurrence of new mollusc fauna with *Sarmatimactra vitaliana*, *Plicatiformes plicatofittoni* and *Obsoletiformes* spp. (Paramonova, 1994; Popov et al., 2022; Muratov and Nevesskaya, 1986). The base of the Bessarabian lacks any conclusive age constraints and was previously estimated between 12.2 Ma (Chumakov et al., 1992) and 11.9 Ma (Harzhauser and Piller, 2004). The lower part of the Bessarabian correlates with the upper Sarmatian s.s. in the Central Paratethys, while the upper part (e.g., from 11.6 Ma) corresponds there to the Pannonian Stage.

The **Khersonian Stage** signifies a massive decline of biodiversity and the occurrence of new endemic mollusc genera *Chersonimactra* with only a few species such as *Ch. caspia*, *Ch. balcica* and *Ch. bulgarica* (Kojumdgieva et al., 1989; Paramonova, 1994). They become extinct prior to the Khersonian–Maeotian boundary and the uppermost part of the Khersonian is therefore referred to as the "Barren biozone" (Kojumdgieva et al., 1989; Paramonova, 1994). The Bessarabian – Khersonian boundary is placed between 8.9 and 8.6 Ma in GPTS 2020; Raffi et al., (2020) but has recently been dated in the Panagea outcrop of the Euxinian Basin at 9.6 Ma with a potential window between 9.8 and 9.6 Ma (Palcu et al., 2021).

The Maeotian Stage begins with a transgression event that terminated the Khersonian lowstand and probably reconnected the Eastern Paratethys with the global ocean (Vasiliev et al., 2021; Popov et al., 2022). The faunal record is usually characterised by the occurrence of fresh-to brackish water mollusc taxa such as *Andrusoviconcha panticapea*, *Sinzowinaia subhoernesi* and *Viviparus moldavicus* followed by marine taxa with *Dosinia maeotica*, *Polititapes abichi* and *Mactra superstes* (Lazarev et al., 2020; Popov et al., 2016). The Khersonian – Maeotian boundary has been dated with magnetostratigraphy in the Dacian and Euxinian Basins at 7.65 Ma (Lazarev et al., 2020; Palcu et al. 2019, 2021).

2.2. On the way to isolation: Paratethys and Caspian Basin during the Serravallian-Tortonian

During most of the Serravallian, the Paratethys Sea combined two large realms: the Central Paratethys, consisting of the Pannonian, Vienna, Transylvanian, Dacian and Forcarpathian basins (up to Volhynian), and the bigger Eastern Paratethys, with the Caspian, Euxinian (Black Sea) and Dacian and Forcarpathian basins (both, starting from Volhynian) (Fig. 1). During that time, the westernmost Central Paratethys was directly connected with the global ocean via the Slovenian Strait. The Eastern Paratethys did not have a direct connection to the global ocean and only connected with the Central Paratethys by a Carasu/Barlad Strait (until 12.65 Ma) and by an Iron Gate Strait (until 11.7 Ma) (Fig. 1) (Palcu et al., 2017; Popov, 2004). The Caspian Basin, as the easternmost part of the Eastern Paratethys, consisted of several subbasins with three major depocentres –the South Caspian Depression in the south, the Kura Foreland Basin in the southwest and the Terek-Caspian Depression in the north-west. The northern and eastern parts were shallow water shelves – The North Pre-Caspian, Ustyurt and Mangyshlak and Pre-Kopetdag (Fig. 1). The Caspian Basin was connected with the Euxinian Basin in the north-west via the Scythian Shelf – Terek-Caspian Depression and in the south-west via the Transcaucasian Strait (Kura Foreland Basin – Rioni Basin) (Fig. 1) (Popov, 2004).

Before the main endorheic phase, the Paratethys had already experienced repetitive episodes of restriction and widening of hydrological connectivity with the global ocean (Rögl, 1999; Popov et al., 2022; Vernyhorova et al., 2023). The early Serravallian was marked by Slovenian Strait restriction (Simon et al., 2019; Palcu et al., 2017). Accompanied by a negative water budget, restricted marine inflow caused thick evaporite formation in the Fore-, Transcarpathian and Transylvanian basins – a period known as the Badenian Salinity Crisis

(13.8–13.4 Ma) (De Leeuw et al., 2010; Simon et al., 2019; Peryt, 2006). At the same time, the restriction of the Carasu Strait resulted in the Eastern Paratethys freshening and endemic fauna radiation (e.g. Karaganian Stage, 13.8–13.4 Ma) (Palcu et al., 2017). At 13.4 Ma, restored connectivity through the Slovenian and Barlad Straits re-established near-marine environments in the entire Paratethys – an interval known as upper Badenian in the CP and Konkian in the EP (13.4–12.65 Ma) (Palcu et al., 2017; Popov et al., 2022).

During the Konkian, the Eastern-Central Paratethys connectivity was unstable. After a short reconnection event at the base of the early Konkian (Kartvelian), an isolation phase occurred marked by *Barnea*-dominated mollusc fauna (Popov et al., 2022). The sudden influx of middle Konkian (Sartaganian) euhaline fauna indicates the restoration of connectivity with marine Central Paratethys (Vernyhorova, 2015). However, during the upper Konkian (Veselyankian), the new rise of endemics along with the euhaline taxa potentially points to a gradual decline of connectivity with the global ocean (Popov et al., 2022).

The eventual termination of the Slovenian Strait at 12.65 Ma (Palcu et al., 2015) completely isolated the unified Paratethys from the global ocean, marking the onset of a main endorheic phase. The basin's salinity decreased, which provoked the massive extinction of stenohaline faunas at 12.65 Ma, known as the Badenian-Sarmatian Extinction Event (Harzhauser and Piller, 2007; Harzhauser et al., 2024b).

The hydrological isolation made the Paratethyan water budget (evaporation vs. precipitation) highly sensitive to climatic oscillations (Palcu et al., 2021). During the Volhynian/early Sarmatian s.s., the Paratethyan water level was generally at a similar level as during the pre-isolation Konkian/late Badenian (Popov et al., 2010). In contrast, at the onset of Bessarabian/late Sarmatian s.s., a large-scale transgression extended far landwards into the northern Black Sea region and Central Asia (Iljina et al., 1976) (Fig. 1).

In the beginning of Tortonian, the uplit of the Carpathians isolated the CP from the rest of the Paratethys and transformed it into the Lake Pannon (ter Borgh et al., 2014). In the terminal Bessarabian, uplift of the Caucasus and the closure of the Transcaucasian Strait took place (Cavazza et al., 2024; Mosar et al., 2010; Nemčok et al., 2013; Sokhadze et al., 2018). During the Khersonian, a series of sudden high-amplitude water level drops in the Eastern Paratethys not only disconnected its subbasins (including the Caspian Basin) but also provoked a near-total extinction of all faunal groups (Paramonova, 1994; Popov et al., 2010; Gol'din and Startsev, 2017; Maissuradze and Koiava, 2011). The Eastern Paratethys endorheic phase was terminated by the Maeotian transgression that shortly reconnected the basin with the global ocean, presumably via the Aegean Basin (Lazarev et al., 2020; Palcu et al., 2019; Vasiliev et al., 2021).

3. Methodology

3.1. Logging

The 136-m-thick Karagiye section, located in the south-eastern part of the Karagiye Depression, comprises three transects (A, B and C), whose correlation in between was checked by laterally tracing marker beds (Fig. 2N and O). A series of trenches were dug along each transect, enabling sampling for palaeomagnetic and biostratigraphic analysis and lithofacies observations.

The Karagiye section was measured with a Jacob's staff and a geological compass. Bedding orientation is mostly horizontal, locally deepening $<5°$. Logging was performed with a resolution of 10–20 cm, focusing on sediment colour, granulometry, sedimentary structures and type of bed contact. The outcrop was photographed with a Mavic Air 2 drone, and a 3D model was constructed using Agisoft© software (Fig. 2N and O).

3.2. Biostratigraphy

3.2.1. Molluscs

For the analysis of mollusc fauna and for the biostratigraphic subdivision of the outcrop, 132 hand samples were taken. Silicone casts were made in some beds, where the mollusc fauna was fragile or present as imprints. The samples were usually 0.5–1 kg in weight and were either washed and picked over 1 mm sieve or, in case of high fragility, were gently cleaned, surfaced-glued and studied under the microscope. Mollusc fauna was identified at the Vienna Natural History Museum, Austria using Kojumdgieva (1969); Iljina et al., (1976); Nevesskaja et al., (1993); Paramonova (1994); Iljina (1993); Harzhauser (2021); Harzhauser et al., (2023); Sladkovskaya (2017).

3.2.2. Microfauna

In total, 126 micropalaeontological samples, weight of 300–1000 taken with an average resolution of 1 m, were analysed for ostracods and foraminifera. Sample processing was performed at the Faculty of Geology and Geophysics, University of Bucharest, Romania. The samples were first completely dried for the elimination of interstitial water. Next, samples were boiled for 30–60 min in a sodium carbonate solution for better disintegration, washed through a battery of sieves (63–500 μm) and dried. Samples were picked under a ZEISS–GSZ microscope. A ZEISS – Stemi SV11 microscope with a NIKON digital camera was used to illustrate the key foraminifera and ostracod species.

For identification and palaeoecological evaluations of ostracod, we used Méhes (1908) and Zalányi (1913) for the Central Paratethys species and Schneider (1953; Schneider, 1939, 1949), Suzin (1956), Pobedina et al. (1956) for the northern Black Sea, Caucasus and Caspian areas. Then, the works of Cernajsek (1974); Jiřiček (Jiřiček, 1974, 1983); Stancheva (Stancheva, 1963, 1972, 1990); Olteanu (Olteanu, 1989, 1998, 1999, 2006); Zelenka (1990); and the newer contributions of Fordinál et al. (2006); Gross (2006); Tóth (2008); Tóth et al. (2010); Gebhardt et al. (2009); Stoica in ter Borgh et al., 2013 and ter Borgh et al., 2014 were used; We also referred to studies of Filipescu et al., (2014); Dumitriu et al., (2017); Harzhauser et al., (2018); Szuromi-Korecz et al., (2021).

Foraminifera identification and biostratigraphic significance from the Central Paratethys was based on the historical monograph of d'Orbigny (1846), revised by Papp and Schmid (1985), as well as the works of Korecz-Laky (1968), Brestenská (1974), Papp et al. (1974b), Papp et al. (1978), Görög (1992) and ter Borgh et al. (2013).

From the Transylvanian and Dacian basins (including the Moldavian platform) we used the contributions of Filipescu (1996), (2005), (2014), Silye (2015), Popescu (1995), Popescu and Grihan (Popescu and Grihan, 2002, 2004, 2005, 2008), Brânzilă (1999), Ionesi (2006), ter Borgh et al. (2014) and Dimitriu (2017).

From the Transcarpathian and modern Ukraine areas of the Eastern Paratethys, we used the studies of Bogdanovich (1952), Venglinsky (1953, 1958, 1962, 1975), Serova (1955), Subbotina et al. (1960), Didkowski (1961), Didkowski and Satanovskaja (1970) and Pishanova (1969). For other areas of Eastern Paratethys related to the Caucasus, Black and Caspian seas Voloshinova (1952), 1958; Krasheninnikov (1959); Zhizhtschenko (1959); Maisuradze (1971), 1980; Maissuradze and Koiava (2011); Vernyhorova et al., (2023) were used. For the Polish part of the Paratethys, we used the papes of Łuczkowska (1974) and Szczechura (1982). For the interpretation of the foraminifera palaeoecology, we mainly used Murray (2009).

3.2.3. Calcareous nannofossils

For the investigation of calcareous nannofossils, 103 samples were prepared using the standard protocol of Perch-Nielsen (1985). Nannofossil assemblages were studied quantitatively and qualitatively (presence/absence). For biostratigraphic interpretation, standard nannoplankton zonation defined by Martini (1970) was used. From all samples containing calcareous nannofossils, at least 300 specimens were

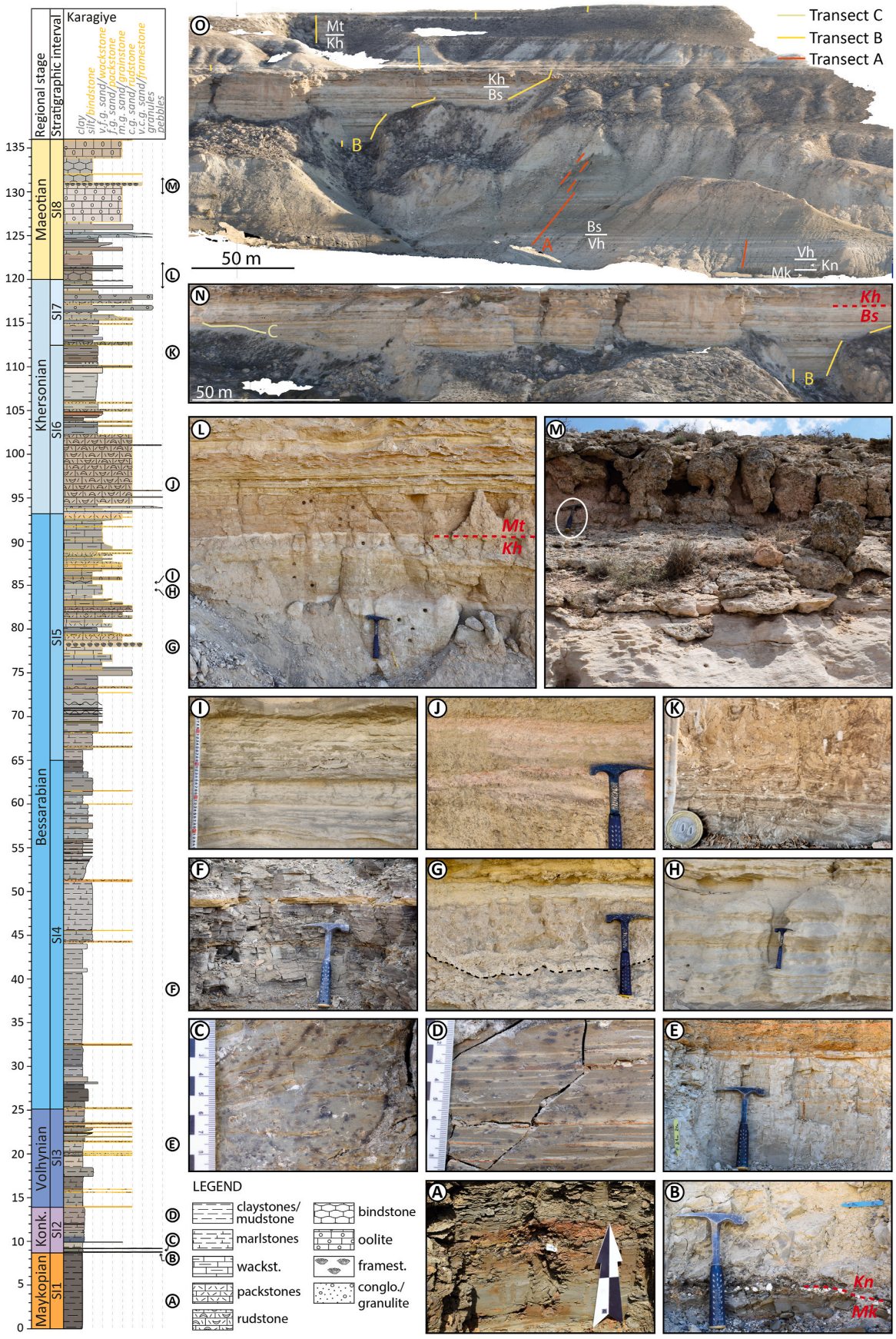

Fig. 2. Lithological log, stratigraphic units and representative photographs of some lithologies along the section. Explanations for photos from A to M can be found in Chapter 4.1, subchapters on lithology. N, O: 3D models of the studied outcrop with indicated stratigraphic units and logging paths, N. for transects A and B, O. for transects B and C. Abbreviations: Mk – Maikopian, Vh – Volhynian, Bs – Bessarabian, Kh – Khersonian, Mt – Maeotian.

counted to reconstruct palaeoecologic environments. For samples containing poor nannoplankton assemblages, i.e. less than 1 specimen in 10 fields of view under the microscope, only presence/absence analyses were applied.

3.3. Marine vertebrate fauna

Marine vertebrate fauna remains were collected both *in situ* and *ex situ* (surface findings/debris), registering their exact stratigraphic levels or, in the case of an *ex situ* find, the relative stratigraphic position. The fragile fragments were glued in place and, together with other remnants, packed for further preparation and taxonomic interpretation. Partial skeletons and isolated bones were identified using Brandt (1873) Mchelidze (1964, 1984) and Kazár (2006) and compared with type specimens when available in museum collections.

3.4. Magnetostratigraphy

To determine magnetic polarity patterns, 344 standard cylindrical doublet samples were taken throughout the section with a resolution of 0.1–0.5 m. Samples were extracted using a portable battery-powered drill machine with a 25-mm diamond crone and a pressurised water tank. Samples were then oriented using a measuring table and a compass, and two parameters (sample tilt and sample azimuth) were documented.

Palaeomagnetic measurements were done at the Palaeomagnetic laboratory "Fort Hoofddijk", Utrecht, the Netherlands. Thermal demagnetisation (th) was performed on a horizontal 2G Enterprises DC SQUID magnetometer (noise level 3×10^{-12}Am^2) in a shielded room with an effective internal field of 0–0.1 mT. Each sample was measured in multiple positions with temperature increments of 20–40 °C either up to a maximum of 690 °C or to the remanent magnetisation dropping below 10% from the initial natural remanent magnetisation (NRM). For the determination of magnetic carriers, 10 samples were measured for thermomagnetic properties in air on a horizontal type Curie balance (noise level 5×10^{-9} Am^2) (Mullender et al., 1993). In addition, for 30 samples, different coercivity fractions of IRM were thermally demagnetised along three orthogonal axes following the method of Lowrie (1990). For that, samples were first magnetised in a horizontal 2G Enterprises DC SQUID magnetometer along axes x, z and y in 700, 150 and 50 mT fields, respectively and then step-wise thermally demagnetised up to 700 °C in a shielded room with zero field.

Palaeomagnetic data associated with this manuscript, such as the interpretation of magnetic components (Supplementary 1) and statistical tests (Mean directions, 95%-cutoff, reversal test, E/I shallowing test, Supplementary 2) were done using an online platform Paleomagnetism.org (Koymans et al., 2016). In our manuscript, we refer to the Geomagnetic Polarity Time Scale (GPTS) 2020 (Raffi et al., 2020).

4. Results

4.1. Stratigraphic intervals and associated fauna

4.1.1. Stratigraphic interval 1 (Pre-Konkian, 0–8.7 m)

4.1.1.1. Lithology. Description: The studied outcrop begins with Stratigraphic interval (SI) 1, represented by grey to dark greenish grey thinly (2–4 mm) parallel-laminated claystones (Fig. 2A). On the surface, the claystones have a paper shale appearance with brownish-red secondary oxidation, secondary gypsum or yellowish powder of jarosite. In the studied section, the claystones have a thickness <9 m but become thicker and better exposed westwards towards the Karagiye Depression centre. No fossil fauna has been detected in SI1.

Interpretation: The thinly parallel-laminated claystones were accumulated from hemipelagic suspension fall-out in a low-energy depositional setting (van der Merwe et al., 2010; Jorissen et al., 2018). The paper shale appearance and abundant jarosite powder on the surface point to the oxidation of iron sulfide minerals and may suggest accumulation in anoxic settings (van et al., 2016a). We interpret the depositional settings of SI1 as offshore. Similar, clay-dominated low--energy offshore depositional environments are common around the globe and are usually described as shelf or offshore facies associations (Yoshida, 2000; Lazarev et al., 2020).

4.1.2. Stratigraphic interval 2 (Konkian, 8.7–13.9 m)

4.1.2.1. Lithology. Description: SI2 begins with a sharp erosional contact bounded by secondary gypsum crystals and rare intraformational pebbles followed by a set of one to two 10-cm-thick beds of matrix-supported conglomerates (Fig. 2B). These conglomerates are usually separated by siltstones and laterally, they either disappear or transform into thicker, up to 1-m-thick beds with highly irregular bases (Fig. 2B). Above the conglomerates, the package is represented by greenish grey to pale yellowish brown (almost white) marlstones with interchangeable sedimentary structures: 1. speckled, with tiny abundant rusty brown to black spots (Fig. 2C); 2. thinly (3–4 mm) parallel-laminated, lenticularly bedded with thin sandy lenses and troughs (Fig. 2D). Except for the conglomerates, the marlstone beds have gradual basal surfaces.

Interpretation: The matrix-supported sharp-based intraformational breccia at the base of the Konkian represents transgressive lag deposits. The laterally extensive incisive conglomerate beds may represent periods of rapid shoreface progradation related to water level oscillation within shallow water marginal environments (Nichols, 2009). The following marsltones with alternating speckled, thinly-laminated and lenticular structures were formed in shallow water lagoonal environments. Here, the alternation of speckled and laminated structures may suggest different levels of the bottom oxygenation and thus facilitate more and less bioturbation, respectively (Damholt and Surlyk, 2004). The lenticular bedding with thin sandy stripes and ripple marks was formed by wave winnowing or tidal processes with bidirectional or oscillatory currents sorting the sediments at the lagoon bottom (Reineck and Wunderlich, 1968). Similar lagoonal depositional environments were previously described in the Upper Cretaceous marginal marine strata of the Straight Cliffs Formation, USA (Allen and Johnson, 2011).

4.1.2.2. Mollusc fauna. SI2 consists of two mollusc units – 2a and 2b. Unit 2a is represented by several monospecific shell-concentrations of disarticulated pholadid bivalve *Barnea pseudoustjurtensis* (Samples KDM 8.8—KDM 12.0 m, Figs. 3 and 4). They mostly form pavements of horizontally oriented, up to 17-mm-long valves, counting occasionally the juveniles. The uppermost pholadid pavement is recorded at 12.0 m. Unit 2b (KDM 13—KDM 13.6 m, Fig. 3) begins in yellowish-grey bioturbated marlstones containing *Limacina konkensis*, *Varicorbula gibba and Apporhais alata*. *Varicorbula gibba* is common and dominantly present by articulated shells. Shiny, translucent microscopic shells of the pteropod gastropod *L. konkensis* are, in general, badly preserved due to compaction and leaching and occur as single individuals or accumulated thin lenses.

4.1.2.3. Foraminifera. Rich Konkian benthic foraminifera assemblages were recorded at levels 12.6 and 13.7 m (Figs. 5 and 6A). No planktonic foraminifera have been detected. Agglutinated foraminifera are represented by the species *Pseudogaudryna karreriana*. Miliolids are richer and represented by several species, e.g. *Pseudotriloculina* ex. gr. *consobrina*, *Quinqueloculina haueriana*, *Qu. gracilis*, *Qu. pseudoangustissima, Qu. collaris*, *Qu. tortonica*, *Adelosina longirostra*, *Pyrgoella controversa* and *Sigmoilina mediterranensis*. Strongly and heavily ornamented tests of *Cycloforina serovae*, *Adelosinia poligonia* and *Adelosina schreibersi* are common.

Lagenids are moderately recorded, being observed by a few

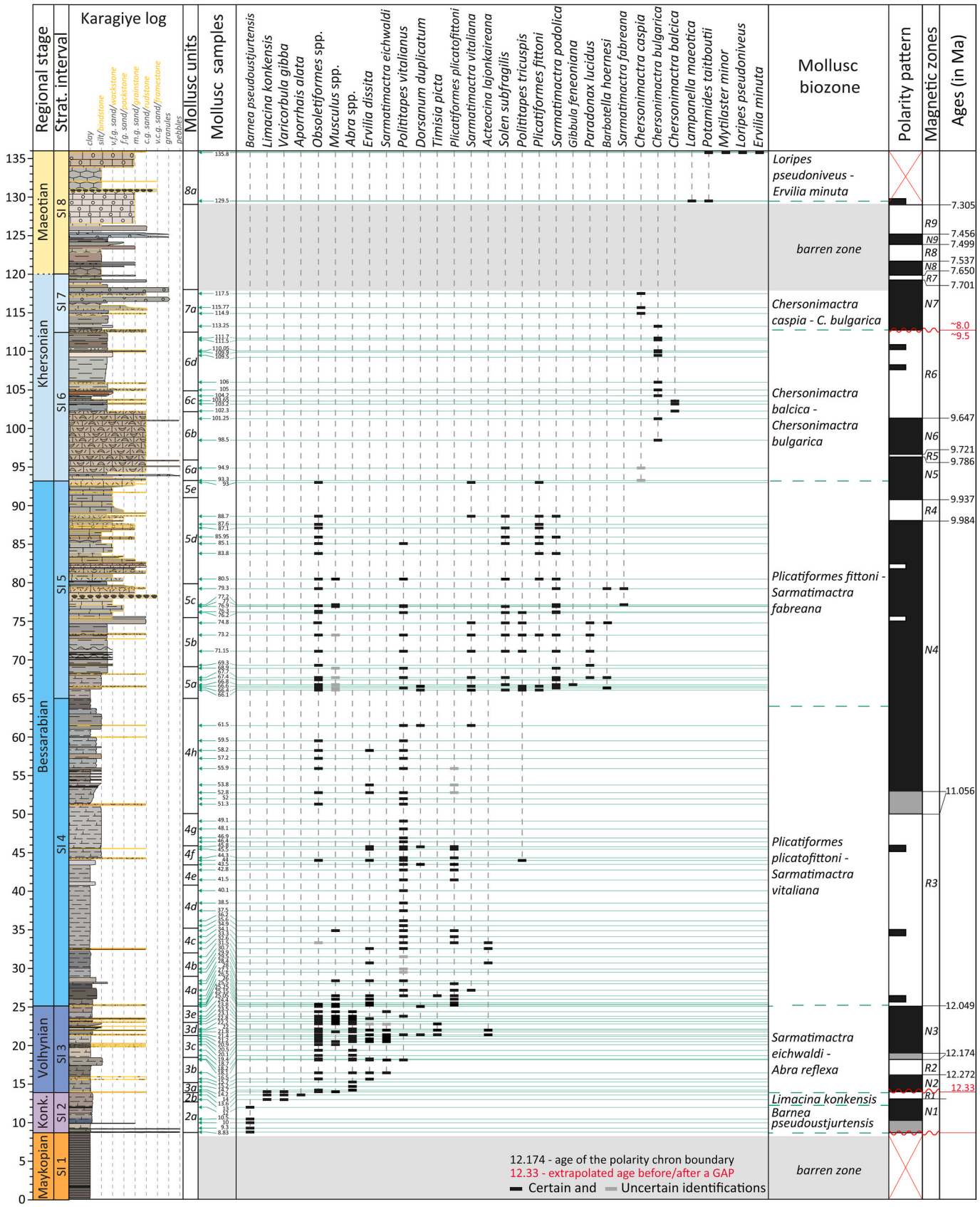

Fig. 3. Stratigraphic distribution of fossil mollusc fauna in the Karagiye Section and defined biozones plotted against the polarity patterns. The age of magnetic zones is discussed in Chapter 5.

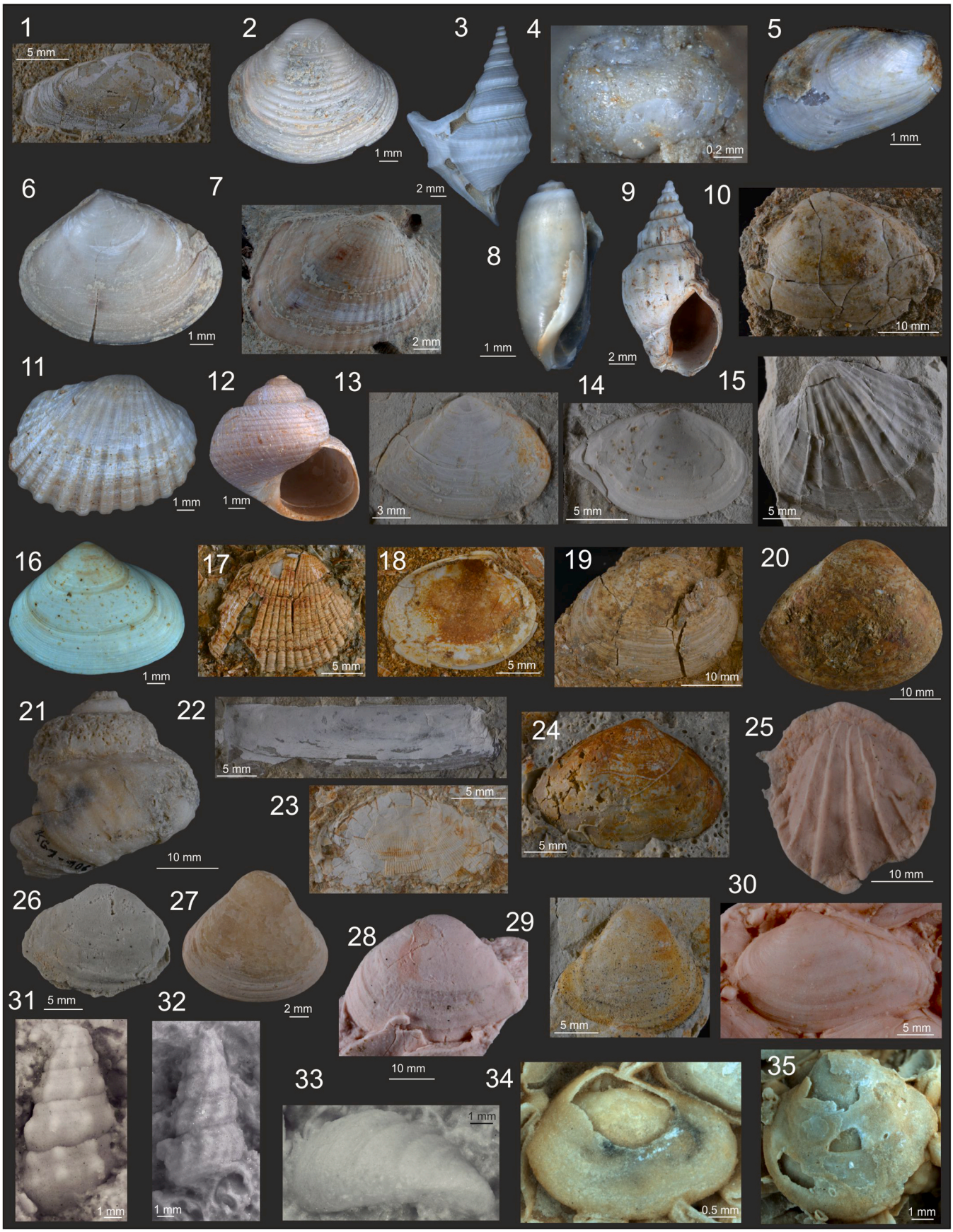

(caption on next page)

Fig. 4. Molluscs from Karagiye with indication of the stratigraphic positions (in meters) in the section. Konkian forms: 1. *Barnea pseudoustjurtensis*, 9.3 m; 2. *Varicorbula gibba*, 13.0 m; 3. *Apporhais alata*, 13.0 m; 4. *Limacina konkensis*, 14.0 m. Volhynian forms: 5. *Musculus naviculoides*, 14.0 m; 6. *Abra alba*, 14.2 m; 7. *Obsoletiformes lithopodolicus*, 18.7 m; 8. *Acteocina lajonkaireana*, 21.4 m; 9. *Dorsanum duplicata*, 21.4 m; 10. *Sarmatimactra crassa*, 21.4 m; 11. *Plicatiformes praeplicata*, 21.4 m; 12. *Timisia plicata*, 21.4 m, 13. *Abra scythica*, 22.0 m; 14. *Abra reflexa*, 23.8 m. Lower Bessarabian forms: 15. *Plicatiformes plicatofittoni*, 26.0 m; 16. *Ervilia dissita*, 43.5 m; 17. *Obsoletiformes obsoletus*, 44.0 m; 18. *Polititapes tricuspis*, 44.0 m; 19. *Polititapes vitalianus*, 44.0 m; 20. *Sarmatimactra vitaliana*, 61.5 m. Upper Bessarabian forms: 21. *Barbotella hoernesi*, 66.4–79.3 m; 22. *Solen submarginatus*, 71.15 m; 23. *Paradonax lucidus*, 74.8 m; 24. *Sarmatimactra podolica*, 76.3 m; 25. *Plicatiformes fittoni*, 85.95 m. Lower Khersonian forms: 26. *Chersonimactra* cf. *caspia*, 94.9 m; 27. *Chersonimactra bulgarica*, 101.25 m; 28. *Chersonimactra balcica*, 103.2 m; 29. *Chersonimactra bulgarica*, 105 m. Upper Khersonian forms: 30. *Chersonimactra caspia*, 114.9 m. Lower Maeotian forms: 31. *Lampanella maeotica*, 129.5 m; 32. *Potamides taitboutii*, 129.5 m; 33. *Mytilaster minor*, 129.5 m; 34. *Ervilia minuta*, 135.8 m; 35. *Loripes pseudoniveus*, 135.8 m.

specimens of *Grigelis pyrula, Dentalina antenula* and *Laevidentalina communis*. Buliminids are represented by frequent specimens of *Bulimina elongata*, *B. subulata*, *Globobulimina pyrula*, and *Fursenkoina acuta* together with the frequent bolivinid *Bolivina* aff. *dilatata*. The small-sized uvigerinids *Angulogerina esuriens* and *Angulogerina angulosa* are frequently observed in our samples. Rotaliid foraminifera are moderately present in the Konkian of Karagiye. We identified specimens of the species *Cibicides konkensis*, *Melonis soldanii*, *Porosononion martkobi*, *Anomalinoides transcarpathicus* and *Elphidium aculeatum*.

4.1.2.4. Ostracods. In contrast with foraminifera, the Konkian (Unit 2, 8.7–13.9 m) contains a less diverse ostracod association (Figs. 5 and 6B). We identified four forms, the most frequent being small-sized *Cytherois gracilis*. At 10 m, *Cythereis caucasica* appears in very large numbers. *Olimfalunia plicatula* and *Sclerochilus* sp. are very rare.

4.1.2.5. Nannofossils. Ten samples from SI2 were investigated for calcareous nannofossils (Fig. 7). Five samples from the lower part (9.8–11.1 m) contain rare, poorly to moderately preserved nannofossils with *Coccolithus pelagicus*, *C. miopelagicus, Cyclicargolithus floridanus, Reticulofenestra pseudoumbilicus* and *Sphenolithus moriformis* (Figs. 7 and 8). The upper part (five samples from 12.8 to 13.8 m) is rich in well-preserved nannofossils with regular occurrences of *Braarudosphaera bigelowii, Coccolithus pelagicus, Holodiscolithus macroporus, Rhabdosphaera sicca, Reticulofenestra pseudoumbilicus* and *Syracosphaera mediterranea*. In addition, there are also *Acanthoica cohenii*, *Calciosolenia fossilis, Cyclicargolithus floridanus, helicoliths (Helicosphaera carteri, H. wallichi)*, *Nivisolithus kovacici*, *N. vrabacii, Pontosphaera multipora, Umbilicosphaera rotula etc.* The upper interval (12.8–13.8 m) of SI2 is also characterised by a stepwise increase of *Coccolithus pelagicus* from the bottom (min. value 0.7% in sample 12.8 m) to the top (max. value 96.8% in sample 13.8 m). The percentages of *R. pseudoumbilicus* in this interval follow an opposite trend, with a maximum presence at the bottom (30.5% in sample 12.8 m) and absence in the uppermost sample (13.8 m). Similar to *R. pseudoumbilicus*, the percentages of holococcolith *H. macroporus* decrease from sample 12.8 m (13.2%) to the top of SI2 (0.6% in sample 13.8 m). Moreover, very rare reworked specimens from the Cretaceous and Paleogene were observed.

4.1.3. Stratigraphic interval 3 (Volhynian, 13.9–25.1 m)

4.1.3.1. Lithology. Description: Generally, SI3 has a remarkably white appearance in the outcrop (Fig. 2O). SI3 starts at 13.9 m with an irregularly-based 10-cm-thick orange-brown horizon mainly built of reworked bivalve shells and rare intraclasts. In the interval 14–18 m (Fig. 2E), SI2 is represented by an alternation of light brown, light yellowish brown (in dry condition, almost white) marlstones with thin (2–4 mm) parallel-lamination, speckled structure with mm-scale horizontally elongated black and brown spots, and lenticular bedding with occasional sandy troughs and wave ripple marks. Among the marlstones, there are also single 5-cm-thick sharp-based orange-brown coquina beds. Between 18 and 25.1 m, the coquina beds become more frequent and up to 30 cm thick (Fig. 2, log). Between 18.4 and 19.6 m, there are three 10–20 cm thick levels with remarkable perforated structures with abundant 1–2 mm holes. At 21.3 m is a remarkable sharp-based coquina bed with highly reworked shells, intraclasts, and abundant cm-scale rootlets. The marlstone beds in SI3 usually have gradual bases, while the coquina beds have sharp, slightly irregular basal surfaces.

Interpretation: The depositional environments of SI3 are similar to those of SI2. Here, the marlstones were accumulated in the low-energy lagoonal settings. The speckled marlstones and horizons with tiny unfilled burrows represent serpulid bioturbation (BI = 3–4). The lenticular bedding may either represent a wave winnowing process or stand for the microtidal activity (Reineck and Wunderlich, 1968). At the same time, the abundance of shell debris and the presence of rootlet horizons point to much shallower, lagoonal margin environments that periodically experienced episodes of subaerial exposure.

4.1.3.2. Mollusc fauna. SI3 (Volhynian) is divided into two parts delimited by an erosive boundary at 21.3 m, followed by the introduction of three new gastropod species (Fig. 3). According to the faunal changes, five units (3a—3e) are distinguished.

Unit 3a (KDM 14–KDM 15.2 m, Fig. 3). At 13.9 m, the reworked bed comprises shell fragments and articulated bivalve shells of small-sized *Obsoletiformes ruthenicus* and *Musculus naviculoides* as well as largely disarticulated shells of *Varicorbula gibba* (sample KDM 14.0 m, Fig. 3). Microscopic planktonic gastropod *Limacina konkensis* and minute hydrobiid steinkerns are likely present. Above, at 14.1 m, a light yellowish grey marlstone exhibits a pavement on its top surface with densely packed, size-sorted and horizontally oriented articulated bivalve shells of *Abra alba* and random small-sized cardiid shells (sample KDM 14.2 m, Sup.1). The lying above light yellowish-brown marlstone contains scattered shells of *A. alba* and of some minute cardiids (samples KDM 14.7—KDM 15.2 m, Fig. 3).

Unit 3b (Samples KDM 15.7—KDM 18.2 m, Fig. 3**).** At 15.7 m, orange-brown coarse shell-debris concentration contains small disarticulated whole shells, mainly of *Ervilia dissita*, accompanied by *O. ruthenicus* and *Mohrensternia* sp. (KDM 15.7 m, Fig. 3). Above, the greenish-brown mudstone includes scattered disarticulated shells of *Sarmatimactra eichwaldi*, *A. alba*, *E. dissita* and *Obsoletiformes* sp. (KDM 15.7 m, Fig. 3), grading into a mollusc-barren interval (16.5—18.1 m). The latter is intercalated at its very top by several thickening upwards, mm-to few-cm-thick shell concentrations of horizontally oriented disarticulated *Obsoletiformes obsoletus*, *A. alba*, *E. dissita*, *S. eichwaldi* and *Polititapes vitalianus* (KDM 18.1—KDM 18.2 m, Fig. 3).

Unit 3c (KDM 18.7–KDM 21.2 m, Fig. 3**).** The following beige-coloured interval begins with a 20-cm thick limestone bed with frequent up to 4-cm-long and 1-mm-broad tubes of bristle worms (polychaetes) adjoined by a few single and articulated shells of *A. alba* and *Obsoletiformes* sp. and minute hydrobiid gastropods (KDM 18.7 m). Above, the pale yellowish-grey marlstone comprises in its lower part common, predominantly horizontally oriented and disarticulated shells of latter species (KDM 19.4 m); its middle part is barren of molluscs, whereas in its top part, several thin, densely packed concentrations of horizontally oriented shells of *Obsoletiformes* sp. and *Musculus naviculoides* appear (KDM 20.1 m). The three following samples (KDM 19.4—KDM 21.2 m) represent occasional thin horizontal shell concentrations of disarticulated *Obsoletiformes* sp., *M. naviculoides*, *A. alba*, *E. dissita* and *S. eichwaldi*.

Unit 3d (KDM 21.4–KDM 22.8 m). The erosional contact at 21.3 m is overlain by an orange-brown rudstone with shell debris bearing

Fig. 5. Stratigraphic distribution of foraminifera and ostracod faunas and other micropalaeontological groups of the Karagiye section plotted against the age model.

Fig. 6a. Konkian foraminifera from the Karagiye section. 1-4. *Pseudogaudryna karreriana*; 5, 6. *Quinqueloculina haueriana*; 7, 8. *Quinqueloculina gracilis*; 9,10. *Cycloforina serovae*; 11, 12. *Adelosinia poligonia*; 13, 14. *Adelosina schreibersi*; 15, 16. *Quinqueloculina tortonica*; 17, 18. *Pyrgoella controversa*; 19, 20. *Pseudotriloculina* ex. gr. *consobrina*; 21, 22. *Quinqueloculina pseudoangustissima*; 23–26. *Adelosina longirostra*; 27, 28. *Sigmoilina mediterranensis*; 29, 30. *Grigelis pyrula*; 31, 32. *Dentalina antenula*; 33, 34. *Laevidentalina communis*; 35, 36. *Fursenkoina acuta*; 37, 38. *Bulimina elongata*; 39, 40. *Bulimina subulata*; 41,42. *Angulogerina esuriens*; 43, 44. *Angulogerina angulosa*; 45, 46. *Bolivina* aff. *dilatata*; 47–49. *Cibicides konkensis*; 50–52. *Melonis soldanii*; 53,54. *Porosononion martkobi*; 55–57. *Anomalinoides transcarpaticus*; 58.59. *Elphidium aculeatum.*

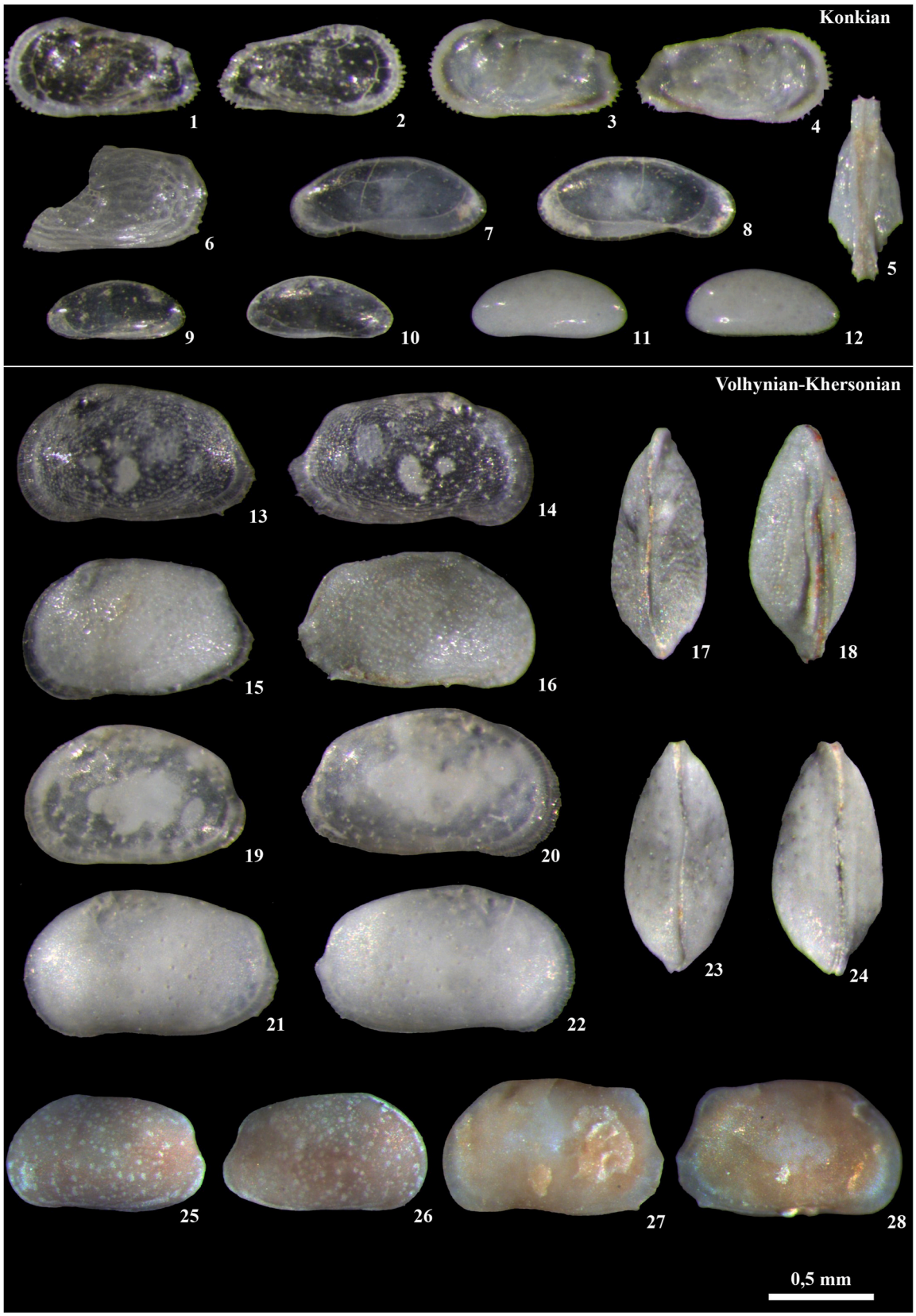

Fig. 6b. Konkian (1–12) and Volhynian–Khersonian (13–28) ostracods from the Karagiye section. 1-5. *Cythereis caucasica*; 1,3. Left valve (LV), external view; 2, 4. Right valve (RV), external view; 5. C, ventral view; 6. *Olimfalunia plicatula*. LV, fragmented valve; 7,8. *Sclerochilus* sp.; 7. LV, external view; 8. RV, external view; 9–12. *Cythereis gracilis*; 9, 11. LV, external view; 10, 12. RV, external view. 13–18. *Aurila merita*; 13, 15. LV, external view; 14, 16. RV, external view; 17. C, dorsal view; 18. C, ventral view; 19–24. *Aurila mehesi*; 19, 21. RV, external view; 20, 22. RV, external view; 23. C, dorsal view; 24. C, ventral view; 25, 26. *Aurila* sp; 25. LV, external view; 26. RV, external view; 27, 28. *Aurila angularis*; 27. LV, external view; 28. RV, external view.

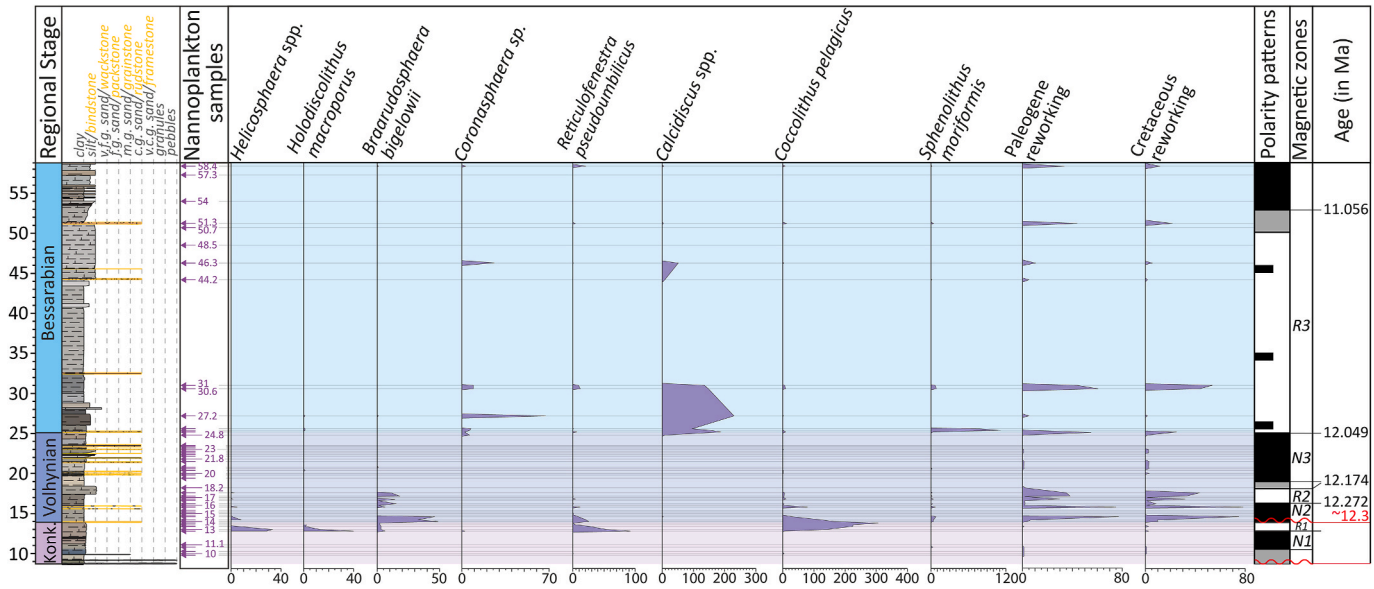

Fig. 7. Distribution of the age-indicative/stratigraphically important calcareous nannoplankton taxa from the Karagiye section.

common *Dorsanum duplicatum*, *Timisia picta*, *Plicatiformes praeplicatus* and *S. eichwaldi*, adjoined by rare *E. dissita*, *Polititapes vitalianus*, as well as a few fretted shells of *Varicorbula gibba* (KDM 21.4 m). A yellowish-grey marlstone follows above, showing thin shell concentrations of horizontally oriented *A. alba*, *M. naviculoides* and *Obsoletiformes* sp. (KDM 21.8 m), overlain by a 15-cm-thick densely packed shell-bed similar in composition to penultimate one with the exception of present *A. alba* and absent *D. duplicatum*, *P. praeplicatum*, *P. vitalianus* and *V. gibba* (KDM 22.0 m). The overlaying two samples represent occasional shell debris lenses (KDM 22.2 m) and thin shell-bed intercalations (KDM 22.8 m) in marlstones with horizontally oriented shells dominated by *A. alba*.

Unit 3e (KDM 23.1–KDM 25.05 m). At 23 m, the orange-brown shell-debris with clay intercalations bear whole large-sized shells of *O. obsoletus* and *O. lithopodolicus* (KDM 23.1 m), grading upwards into marlstone with lenses of shell-debris additionally comprising *E. dissita* (KDM 23.5 m). The pale yellowish-grey marlstone above includes sporadic horizontally-oriented shells of *A. abra*, *A. reflexa*, *M. naviculoides*, *O. lithopodolicus*, *S. eichwaldi* and *P. vitalianus* (KDM 23.8—KDM 24.4 m). In its upper part, the marsltone bears a densely packed concentration of bristle worm tubes. The marlstone interval is finally overlain by a greenish claystone (KDM 25.05 m) bearing small-sized bivalve shells of *O. obsoletus*, *P. vitalianus*, *M. naviculoides* horizontally oriented and commonly taking articulated butterfly position. The gastropod shells of *D. duplicatum* are additionally present.

4.1.3.3. Foraminifera. The part between 13.9 and 19 m is dominated by *Pseudotriloculina* ex. gr. *consobrina, Porosononion martkobi, Bulimina elongata, Quinqueloculina pseudoangustissima, Quinqueloculina gracilis, Quinqueloculina collaris*, which survived from the Konkian (Figs. 5 and 9A-B). They are associated with newly occurring species *Sinuloculina angustioris*, *Varidentella latelacunata*, *Nonion bogdanowiczi*, *Elphidium crispum*, *Elphidium hauerinum*, *Elphidium antoninum* and *Elphidium fichtellianum*. The sample from 18.2 m shows abundant presence of the euryhaline species *Ammonia* ex. gr. *beccarii*.

A diversification of foraminifera starts at 19 m, with the presence of rotaliid species such as *Porosononion* ex. gr. *granosum*, *P.* ex. gr. *subgranosum* as well as diverse species of *Fissurina* genus, like *F. cubanica*, *F. bicaudata*, *F. bessarabica*, *F. carpathica*, *F. elongata*, *F. daraensis* and the polymorphinid *Guttulina austriaca* (Fig. 5). The Volhynian index species *Varidentella reussi* appears in small numbers at 19 m and between 19 and 21 m becomes abundant marking the *Varidentella reussi* Zone (Popescu, 1995).

Samples from 21 to 25.1 m mark the presence of *Elphidium* species that show different degrees of development of the marginal spines, starting with relatively small ones in *Elphidium aculeatum,* going to forms with more developed, long spines, as *Elphidium josephinum* up to *Elphidium reginum* var. *caucasica* (Fig. 9B). Many transitional forms are observed, making taxonomic classification difficult. In the same interval, the *Articulina* genus appears with the species *Articulina problema*. The large number of *Elphidium* species with marginally developed spines and associated with miliolid foraminifera of the genus *Articulina*, defines the so-called *Elphidum reginum* Zone (Popescu, 1995).

4.1.3.4. Ostracods. The Volhynian stage marks a progressive diversification of the ostracod assemblage, especially towards the top of this interval (Figs. 5, 6B and 9C-D). Only the small-sized *Cytherois gracilis* passed the boundary to Volhynian.

The basal part of SI3 (13.9–19 m) is characterised by the dominance of leptocytherids, among them the most abundant being *Amnicythere tenuis*, associated with *Euxinocythere* aff. *marginata*. The *Loxoconcha* genus is represented by *Loxoconcha subcrassula*.

Like the foraminifera, starting from 19 m, a greater diversification of the ostracod fauna is observed. New are the index species *Aurila merita* and *Aurila mehesi*. The loxoconchids are well represented by *L. subcrassula, L.* aff. *subcrassula, Loxocorniculum schmidi* and the rare thin-shelled *Phlyctocythere fragilis*. Besides *A. tenuis* and *E. marginata,* the leptocyderids are also represented by *Euxinocythere* ex. gr. *praebosqueti*, *Callistocythere naca* and two more species – *Euxinocythere* sp. 1 and *Euxinocythere* sp. 2. Three xestolebrids species are identified at this stratigraphic interval – *Xestoleberis* aff. *dispar*, *Xestoleberis fuscata* and *Xestoleberis glabrescens*. The top part of SI3 displays the maximum diversification and abundance of the Volhynian ostracods.

4.1.3.5. Nannofossils. In total, 35 samples from SI3 were investigated on calcareous nannofossils. The lowermost part (samples at 14 m, 14.2 m and 14.6 m) is rich in lower salinity indicator species *Braarudosphaera bigelowii*. Nannoplankton assemblages from 14.1 to 18.2 m are generally scarce, moderately preserved and are mostly dominated by species reworked from the Upper Cretaceous (*Arkhangelskiella cymbiformis*, *Micula staurophora*, *Prediscosphaera cretacea*, *Watznaueria barnesiae* etc.) and Paleogene (*Coccolithus formosus*, *Reticulofenestra bisecta*, *Reticulofenestra dictyoda*, *Isthmolithus recurvus*, *Zygrhablithus bijugatus* etc.). Autochthonous assemblages are comparable with those from SI2

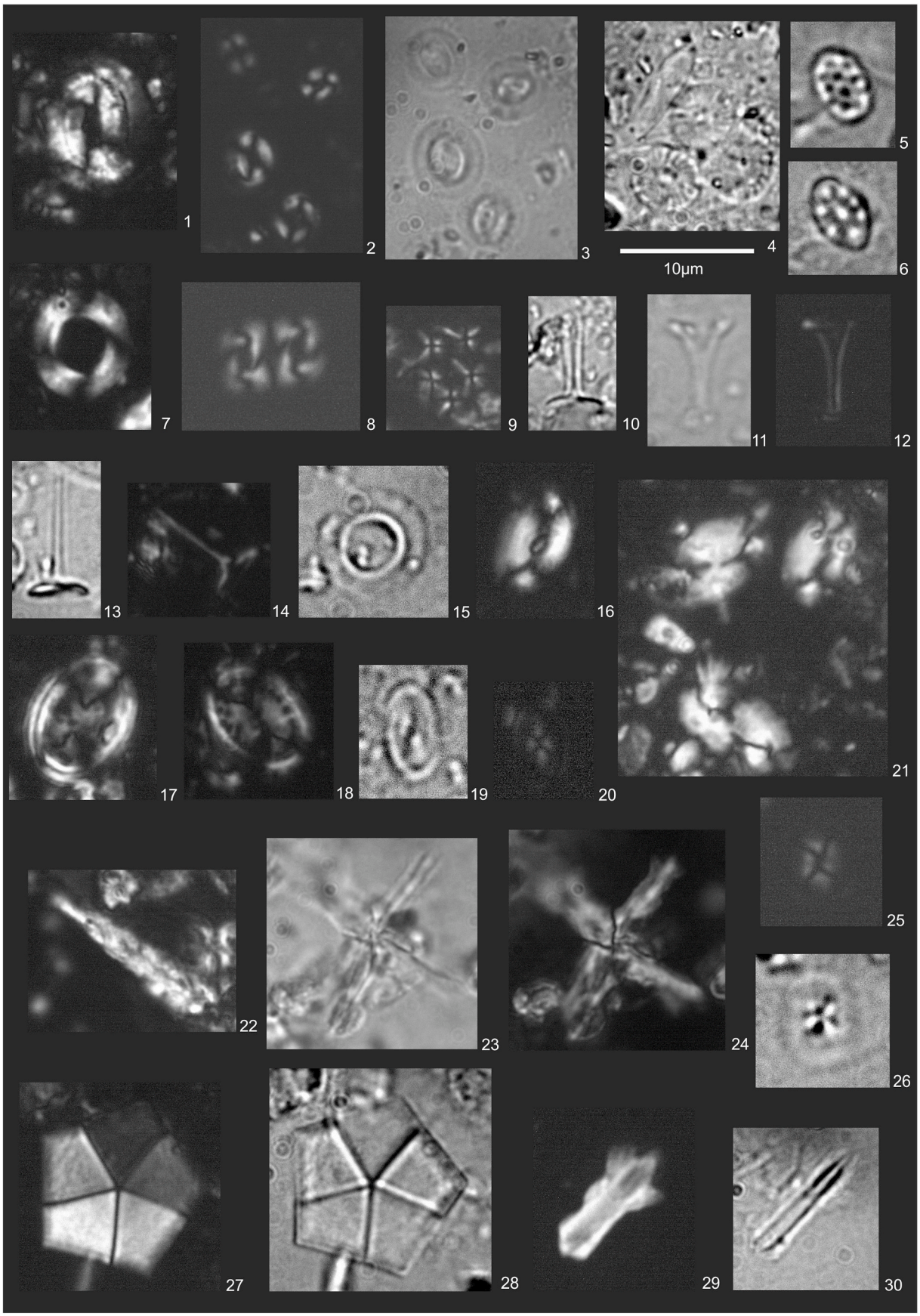

(caption on next page)

Fig. 8. Calcareous nannofossils from the Karagiye outcrop. 1. *Coccolithus miopelagicus*, sample KD22-88, 17.5; 2, 3. *Coccolithus pelagicus*, sample KD22-27, 11.4 m; 4. *Calcidiscus leptoporus*, sample KD22-88, 17.5 m; 5, 6. *Holodiscolithus macroporus,* sample KD22-23, 11 m; 7. *Reticulofenestra pseudoumbilicus*, morphotype >7 μm, sample KD22-88; 8. *Reticulofenestra pseudoumbilicus*, morphotype 5–7 μm, sample KD22-23, 11 m; 9. *Sphenolithus moriformis*, sample KD22-88, 17.5 m; 10. *Rhabdosphaera clavigera*, sample KD22-23, 11 m; 11, 12. *Discosphaera tubifera*, sample KD22-23, 11 m; 13, 14. *Rhabdolithus siccus*, sample KD22-23, 11 m; 15. *Umbilicosphaera rotula*, sample KD22-23, 11 m; 16. *Helicosphaera euphratis*, sample KD22-23, 11 m; 17. *Pontosphaera discopora*, sample KD22-23, 11 m; 18. *Pontosphaera desuetoidea*, sample KD22-23, 11 m; 19, 20. *Syracosphaera* sp., sample KD22-23, 11 m; 21. *Helicosphaera wallichii*, sample KD22-23, 11 m; 22. *Nivisolithu vrabacii*, sample KD22-23, 11 m; 23, 24, 29, 30. *Nivisolithus kovacicii*, sample KD22-23, 11 m; 25, 26. *Syracosphaera fragilis*, sample KD22-23, 11 m; 27, 28. *Braarudosphaera bigelowii*, sample KD22-23, 11 m. The scale bar applies to all figured fossils.

(Konkian) containing: *Acanthoica cohenii*, *Coccolithus pelagicus*, *Reticulofenestra pseudoumbilicus, Nivisolithus kovacici*, *N. vrabacii, Syracosphaera mediterranea etc.* Samples from 19.4 m to 21.45 m are rich in well-preserved diatoms accompanied by very rare nannofossils. Samples above the diatoms layer (21.8–24.8 m) are generally barren in nannofossils, containing just a few specimens reworked from the Cretaceous and Paleogene.

4.1.4. Stratigraphic interval 4 (lower Bessarabian, 25.2–65 m)

4.1.4.1. Lithology. Description: SI4 begins with a remarkable orange-brown double shell bed separated by a thin claystone intercalation. Further up, it continues with an alternation of speckled yellowish-grey claystones and dark greenish grey thinly (1–2 mm) parallel-laminated 0.4–0.6 m thick claystone beds. Starting from 30 m, the claystones have thin, silty, to very fine-grained sandy laminae (Fig. 2F). From 34 m, among claystones appear occasional beds of pale yellowish-grey massive marlstones, locally with speckled structure and concave-down oriented bivalve shells. From 44 m until the top of SI4, the marlstones prevail and occasional 20-30 cm-thick orange-brown coquina beds appear with sharp undulating bases and locally, with swaley cross-stratification. All the beds except for sharp-based coquinas have gradual basal surfaces. *Interpretation*: The basal coquina bed containing both, reworked Volhynian and new Bessarabian taxa was formed as a transgressive lag. The thin parallel lamination in the claystone suggests accumulation from suspension fallout in low-energy offshore settings (Jorissen et al., 2018; van der Merwe et al., 2010). The laterally-delimited sharp-based shell debris are tempestites deposited within the storm-wave base or offshore transition zone (Raaf et al., 1977; Dott and Bourgeois, 1982; Nichols, 2009). Later appearance and thickening of marlstones intervals point to progradation of a carbonate platform (Tucker, 1985; Reading, 1996). Similar examples of low-energy offshore settings and storm-dominated offshore transition zones were previously described in Cretaceous deposits of the Wasatch Plateau (USA) (Gani, M. R. et al., 2015) and as offshore-lower shoreface deposits in Cretaceous Upper Almond Formation (USA) (Kieft et al., 2011).

4.1.4.2. Mollusc fauna. Based on changes in mollusc distribution, we divided SI4 into 7 units (4a—4f, Fig. 3).

Unit 4a (KDM 25.2–KDM 28.4 m) begins with a 20-cm-thick orange-coloured, densely packed mollusc-debris concentration delineated by thin clay intercalation. Samples taken below and above the claystone (KDM 25.15—24.25 m) include a small number of detectable shells, including only *E. dissita* in the lower, accompanied in the upper sample by *Obsoletiformes* sp., *Musculus naviculoides* and *Plicatiformes plicatofittoni*. The claystones include articulated shells of *P. plicatofittoni*, (KDM 25.5—28.4 m). *E. dissita* and *M. naviculoides* are present throughout the entire interval, with the first being especially common in KDM 26.5 m, where *Polititapes vitalianus* starts regularly occurring and *Sarmatiamactra vitaliana* is detected. Except for a few thin *Ervilia* layers, shell concentrations are absent in this unit.

Unit 4b (KDM 29.5–KDM 31.5 m), located in dark greenish-grey claystones, exhibits badly preserved shells of *P. vitalianus*. In its upper part, monospecific pavements of E. *dissita* with concave up-oriented single valves are present.

In Unit 4c (KDM 32.6–KDM 34.9 m), the greenish grey claystones passing upwards into yellowish grey marlstones are marked by concomitant occurrence of *P. plicatofittoni* and *P. vitalianus* (KDM 32.6—KDM 34.9 m). The former, represented by single and articulated valves in butterfly position and floating in sediments or concentrated in lenses, is very common in the upper part of the interval. Between KDM 30.7 m and KDM 33.3 m, lenses with numerous *Acteocina lajonkaireana* specimens occur, comprising additionally *E. dissita*. *Musculus naviculoides* occurs in the topmost sample.

Unit 4d (KDM 35.6–KDM 40.1 m, Fig. 3) continues with similar lithology, but the mollusc content is reduced solely to *P. vitalianus* (KDM 35.6—40.1 m). In the lowermost part of the interval, its shells are concentrated in lenses; above, they are present randomly floating in the muddy sediment.

Unit 4e (KDM 40.6–KDM 43.5 m, Fig. 3), represented by similar claystones as in the previous unit**,** bears thin shell concentrations with partly articulated *P. plicatofittoni* and *P. vitalianus* (KDM 41.5—KDM 43.5 m). The topmost sample comprises a 10-cm-thick beige limestone intercalation with steinkerns of the latter two taxa adjoined by a few *D. duplicatum* shells.

Unit 4f (KDM 44–KDM 45.8 m, Fig. 3). At 44.5 m, a composite, clay-intercalated, orange-coloured 20-cm-thick shell-debris bed bears nicely preserved shells of *Obsoletiformes obsoletus*, *E. dissita* and *P. vitalianus* (KDM 44m, Fig. 3). Lower and thicker bed shows large-sized concave-down bivalve shells at the base (Sample KDM 44.0 m). The reworked bed is overlain by greyish brown mudstone that starts with a thin concentration of single valves of *P. vitalianus* followed by a horizon with cluster-accumulated *P. plicatofittoni* shells (KDM 44.3 m). The greenish-grey claystone (45.3–45.95 m) begins with rare *P. vitalianus* followed upwards by several up to 10-cm-thick coquinas with small-sized *P. plicatofittoni*. In the coquinas *E. dissita* is common, followed by *P. vitalianus*, *P. plicatofittoni*, *M. naviculoides* and *D. duplicatum* (KDM 45.5—45.8 m).

Unit 4g (KDM 46.4–KDM 49.1 m, Fig. 3) within the pale yellowish-grey marlstones contains monotypic shell pavements and lenses of *P. vitaliana*.

Unit 4h (KDM 51.3–KDM 61.5 m, Fig. 3). The topmost mollusc bearing interval starts with a 30-cm-thick orange-coloured shell-debris concentration bearing horizontally oriented shells of *O. obsoletus* and *P. vitalianus*, intercalated by mollusc bearing marl. The shell-debris bed is overlain by about 10-m-thick alternation of dark and light grayish to brownish coloured mudrocks with occasional up to 10 cm thick coquinas. In its upper sandier part, three up to 4-cm-thick shell-debris layers occur. Below, several pavements with disarticulated *P. vitalianus* shells are present, marked by a regular occurrence of *P. vitalianus* usually accompanied by *Obsoletiformes* sp. *E. dissita*. The interval ends with a 15-cm-thick orange shell-debris layer bearing whole single valves of *P. vitalianus* and *S. vitaliana* along with *D. dorsanum* shells.

4.1.4.3. Foraminifera. The lower Bessarabian foraminifera assemblage is less diverse than in Volhynian, but in general, the abundance of individuals is higher. The most common taxa in SI4 (Figs. 5 and 9A-B) are *Porosononion* ex. gr. *granosum* and *P.* ex. gr. *subgranosum*. The difference between these two species is often very difficult to observe. In addition, *N. bogdanowiczi* appears frequently. *Elphidium* is not as common as in the previous stratigraphic interval, being identified by rare specimens of *E. crispum* and *E. hauerinum* species. Miliolids are represented mainly by *Pseudotriloculina* ex. gr. *consobrina* and *Varidentella sarmatica*.

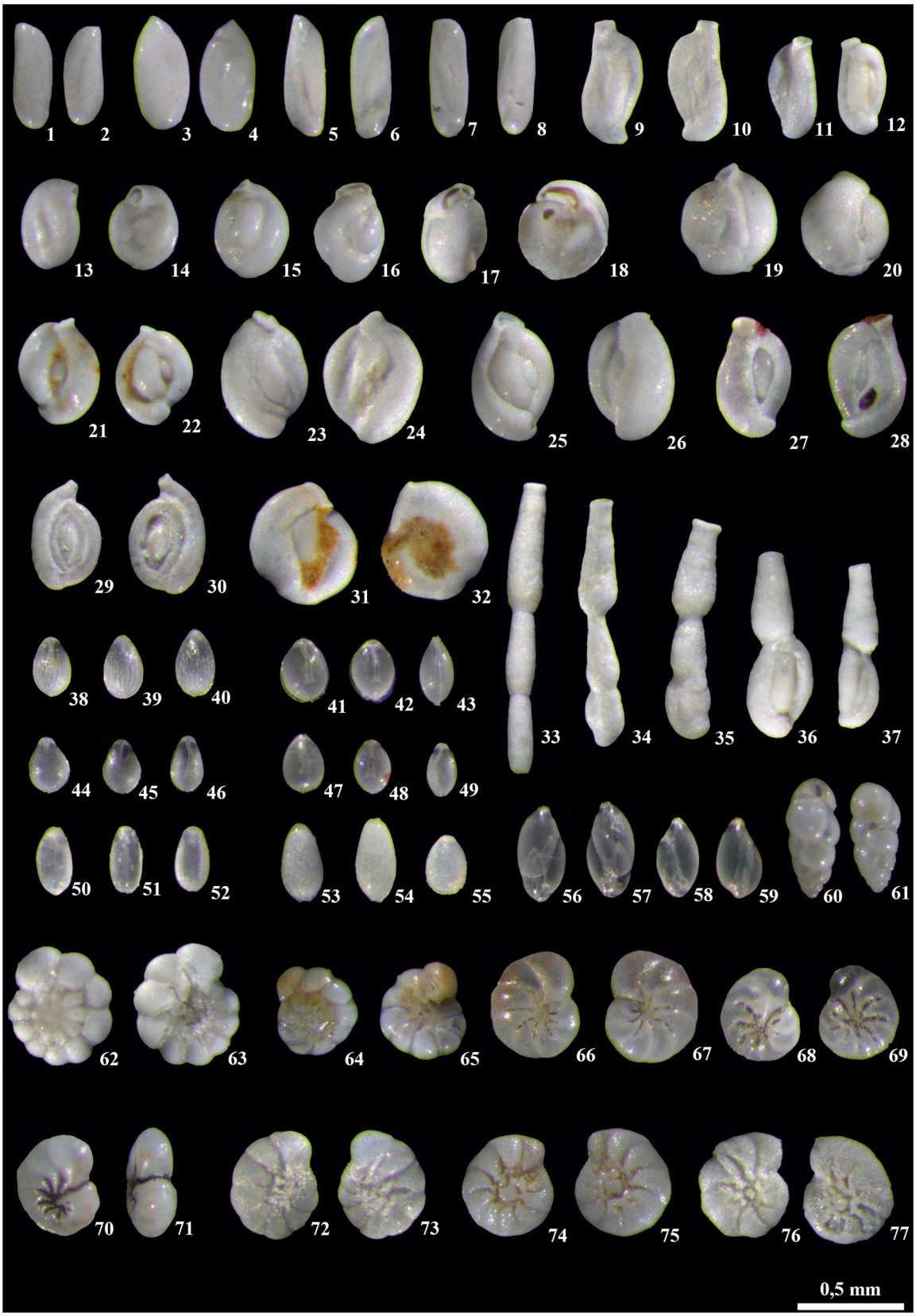

Fig. 9a. Volhynian-Bessarabian foraminifera from the Karagiye Section. 1-6. *Pseudotriloculina* ex. gr. *consobrina*; 7, 8 *Sinuloculina angustioris*; 9–12. *Quinqueloculina collaris;* 13–20. *Varidentella reussi;* 21–26. *Varidentella latelacunata;* 27–28. *Varidentella sarmatica;* 29, 30. *Spiroloculina tenuiseptata;* 31, 32. *Varidentella rosea;* 33–37. *Articulina problema;* 38–40. *Fissurina cubanica;* 41–43. *Fissurina bicaudata;* 44–46. *Fissurina bessarabica;* 47–49. *Fissurina carpathica;* 50–52. *Fissurina elongata;* 53–54. *Fissurina* sp.; 55. *Fissurina daraensis*; 56–59. *Guttulina austriaca;* 60, 61. *Bulimina elongata;* 62–65. *Ammonia* ex. gr. *beccarii;* 66–71. *Nonion bogdanowiczi;* 72–76. *Porosononion* ex. gr. *granosum.*

Fig. 9b. Volhynian-Bessarabian foraminifera from the Karagiye Section. 1-7. *Porosononion* ex. gr. *subgranosum*; 8–14. *Porosononion hyalinum;* 15–20. *Elphidium crispum*; 21,22. *Elphidium antoninum*; 23–25. *Elphidium fichtellianum*; 26–29. *Elphidium hauerinum*; 30,31. *Elphidium aculeatum*; 32–34. *Elphidium josephinum*; 35–37. *Elphidium reginum* var. *caucasica*.

(caption on next page)

Fig. 9c. Volhynian - Bessarabian ostracods from the Karagiye Section. 1-5. *Amnicythere tenuis*; 1, 3. LV, external view; 2, 4. RV, external view; 5. C, dorsal view; 6–10. *Euxinocythere* ex. gr. *praebosqueti*; 6, 8. LV, external view; 7, 9. RV, external view; 10. C, dorsal view; 11–14. *Euxinocythere adelosina*aff. *marginata*; 11, 13. LV, external view; 12, 14. RV, external view; 15–20. *Euxinocythere* sp. 1; 15, 17. LV, external view; 16, 18. RV, external view; 19. C, ventral view; 20. C, dorsal view; 21–26. *Euxinocythere* sp. 2.; 27–32. *Callistocythere multicristata*; 27, 29. LV, external view; 28, 30. RV, external view; 31. C, ventral view; 32. C, dorsal view; 33–38. *Euxinocythere* aff. *naviculata*; 33, 35. LV, external view; 34, 36. RV, external view; 37. C, dorsal view; 38. C, ventral view; 39–43. *Loxoconcha subcrassula*; 39. LV, external view, female; 40. RV, external view, female; 41. LV, external view, male; 42. RV, external view, male; 43. C, ventral view; 44–46. *Loxoconcha* aff. *subcrassula*; 44. C, view from LV; 45. C, view from RV; 46. C, dorsal view; 47–50. *Loxoconcha* ex. gr. *kochi*; 47, 49. V, external view; 48, 50. RV, external view; 51, 52. *Loxoconcha odessaensis*; 51. LV, external view; 52. RV, external view; 53–55. *Loxoconcha valiente*; 53. LV, external view; 54. RV, external view; 55. C, dorsal view.

4.1.4.4. Ostracods. In contrast to the previous interval, the lower Bessarabian ostracod assemblage is low in diversity and abundance. Only in the lower part (25.1–44 m), we identified a few to common specimens of *Amnicythere tenuis* and very rare *Euxinocythere marginata*, *E.* sp. 1 and *E.* sp. 2. as well as the loxoconchid species *Loxoconcha subcrassula* and *Loxoconcha schmidi.* The upper part of SI4 (44–65 m), contains almost no ostracods, except for the sample at 54 m where we identified *E.* ex. gr. *praebosqueti* in large abundance.

4.1.4.5. Nannofossils. Samples from the lower part of SI4 (25.2–44.2 m) contain nannofossil assemblages dominated by *Calcidiscus leptoporus*, *C. tropicus*, *C. pataecus*, *Coronosphaera* sp., small reticulofenestrids (*Reticulofenestra minuta*, *R. minutula*, *R. haqii*) and *Sphenolithus moriformis* (highest amounts in samples from 25.4 m to 25.6 m). Allochthonous nannofossils point to reworking from the Upper Cretaceous and Paleogene. Two levels with common diatoms were observed at 46.3–48.5 m and 54–58.4 m. Samples above these levels are barren of calcareous nannofossils.

4.1.5. Stratigraphic interval 5 (upper Bessarabian, 65–93.2 m)

4.1.5.1. Lithology. Description: SI5 is built up by carbonate rocks with medium-to thickly-bedded alternation of white, pale yellow parallel-laminated to wave-ripple cross-laminated ooidic and bioclastic grainstones and massive wackstones and packstones with ooids and mollusc bioclasts (Fig. 2H); Frequent are up to 1m-thick beds of white mudstones, locally pierced by horizontal and vertical branched burrows. The packstones and grainstones are often followed by greenish grey to beige thinly parallel laminated bindstones (Fig. 2I). There are also occasional up-to-0.5-m-thick beds of white to beige bioclastic rudstones and framestones formed by the up-to-1-m-wide and 40-cm-thick bowl-shaped build-ups of *Sinzowella novorossica* (Fig. 2G). All the beds show sharp, straight, locally slightly undulating contacts. SI5 ends with a remarkable succession represented by highly bioturbated mudstones gradually coarsening upwards into a massive pink medium-grained grainstone.

Interpretation: The sudden switch from clay-prone SI4 to the carbonate-dominated depositional settings of SI5 indicates a progradation of the shallow water nearshore carbonate settings, potentially, due to a relative water-level fall. The horizontally laminated to wave ripple-cross laminated oolites were formed as barriers within the carbonate platform margins, where the depositional processes are strongly controlled by the wave-driven oscillatory currents (Burchette, T. P. et al., 1990; Reading, 1996). The rare foraminifera colonies (framestones) and bindstones represent patch reefs and carbonate mounds respectively – both developed in the low-energy carbonate platform interior (Reading, 1996; Tucker, 1985).

4.1.5.2. Mollusc fauna. Based on mollusc distribution, five units are recognised with decreasing taxonomic richness (12-10-9-7-2 taxa from 5a to 5e, Fig. 3).

Unit 5a (KDM 66.1—KDM 68.9 m, Fig. 3) shows repetitive alternation of limestones and marlstones. In the lower part of Unit 5a, the marlstones comprise loose shells and densely packed shell-debris concentrations. In the upper part they become thinner or absent, contributed by pavements of *S. podolica* or lenses with small *Obsoletiformes* sp. partly in butterfly position. Limestone beds can bear large gastropod shells of *Barbotella hoernesi* and articulated bivalve shells of *S. vitaliana*. The unit is marked by regular presence of *S. podolica, Musculus* cf. *naviculoides* and *Obsoletiformes* sp. The latter taxon, together with *S. vitaliana* and *P. tricuspis* commonly dominates the assemblages in the samples. Unit 5a itself marks the lowermost occurrences of *B. hoernesi* and *Plicatiformes fittoni* in the section.

Unit 5b (KDM 69.3—KDM 74.8 m, Fig. 3) is marked by a continuous presence and the topmost occurrence of *Paradonax lucidus*. The latter species is always found together with *Obsoletiformes* sp. and mostly also by *S. vitaliana* and *Solen subfragilis*. The lowermost sample (KDM 69.3, Fig. 3) bears random shells and lenses of small *Obsoletiformes* sp., partly in a butterfly position. The following sample (KDM 71.15 m, Fig. 3) represents a single pavement with *P. vitalianus,* sole shells of the latter species in living position, as well as a shell-concentration comprising additionally *S. vitaliana* and *P. tricuspis*. The third sample (KDM 73.2 m, Fig. 3) displays shell-debris similar in content to the last one except for showing no dominant species. The topmost sample (KDM 74.8 m, Fig. 3) marks the base of a 1-m-thick interval of thinning upward (5–1 cm) shell-debris interlayers, bearing disarticulated large-sized shells of common *P. tricuspis* and *Obsoletiformes* sp. followed by *B. hoernesi* and *S. vitaliana*, among others.

Unit 5c (KDM 76.2—KDM 79.3 m, Fig. 3) is marked by the regular and common presence of *S. podolica*. Additionally abundant are *P. vitalianus* and *P. tricuspis* in the lowermost and *S. fabreana* in the topmost sample (KDM 79.3 m). The unit shows frequent shell concentrations mostly preserved as steinkerns. Two such 20-cm-thick, reddish-coloured shell beds are prominent markers, the lower one directly underlying the *Sinzowella novorossica* bioherm at 78 m, the upper one marking the sample KDM 79.3 m. They show densely packed unsorted shell material with *B. hoernesi* and large horizontally oriented *S. fabreana* valves.

Unit 5d (KDM 83.8—88.7 m, Fig. 3) built of various limestone facies, is marked by a continuous presence of *P. fittoni* and *Obsoletiformes* sp. The latter taxon dominates the assemblage, commonly associated with *S. subfragilis* and S. *podolica*. Additionally, *P. vitalianus*, *S. vitaliana* and *M. naviculoides* occur. The lowermost mollusc bearing interval (KDM 80.5 m) is a 40-cm-thick shell concentration made by loosely distributed horizontally oriented valves and valve lenses in finely bedded marly limestone. The next one (KDM 83.8 m), superposing a stromatolite bearing interval, represents a 30-cm-thick composite coquina made by a succession of thin pavements of small-sized *Obsoletiformes* sp. valves. The next interval represents occasional bivalve shells and pavements associated with microbiolithic bindstones (KDM 85.10—85.95 m). Finally, in a 2-m-thick horizon marked by the presence of serpulid and bryozoan buildups, the shells-concentrations are represented as thin singular pavements on bedding planes as well as densely packed coquinas with horizontally oriented valves (KDM 87.1—88.7 m). Except for the lowermost interval, the shells are regularly preserved as steinkerns.

Finally, the topmost **Unit 5e** (KDM 93–KDM 93.2, Fig. 3), dominated by light-coloured ooidal limestones, is barren of molluscs. The only exception is its very top, where a 20-cm-thick pink shell concentration by randomly distributed shells of *Obsoletiformes* sp., partly in a butterfly position, is present (KDM 93.0 m). Also rare *S. vitaliana* and *P. fittoni* are present. This level marks the topmost occurrence of Bessarabian mollusc species in the section.

4.1.5.3. Foraminifera. The lower part of SI5 (up to 78 m) displays

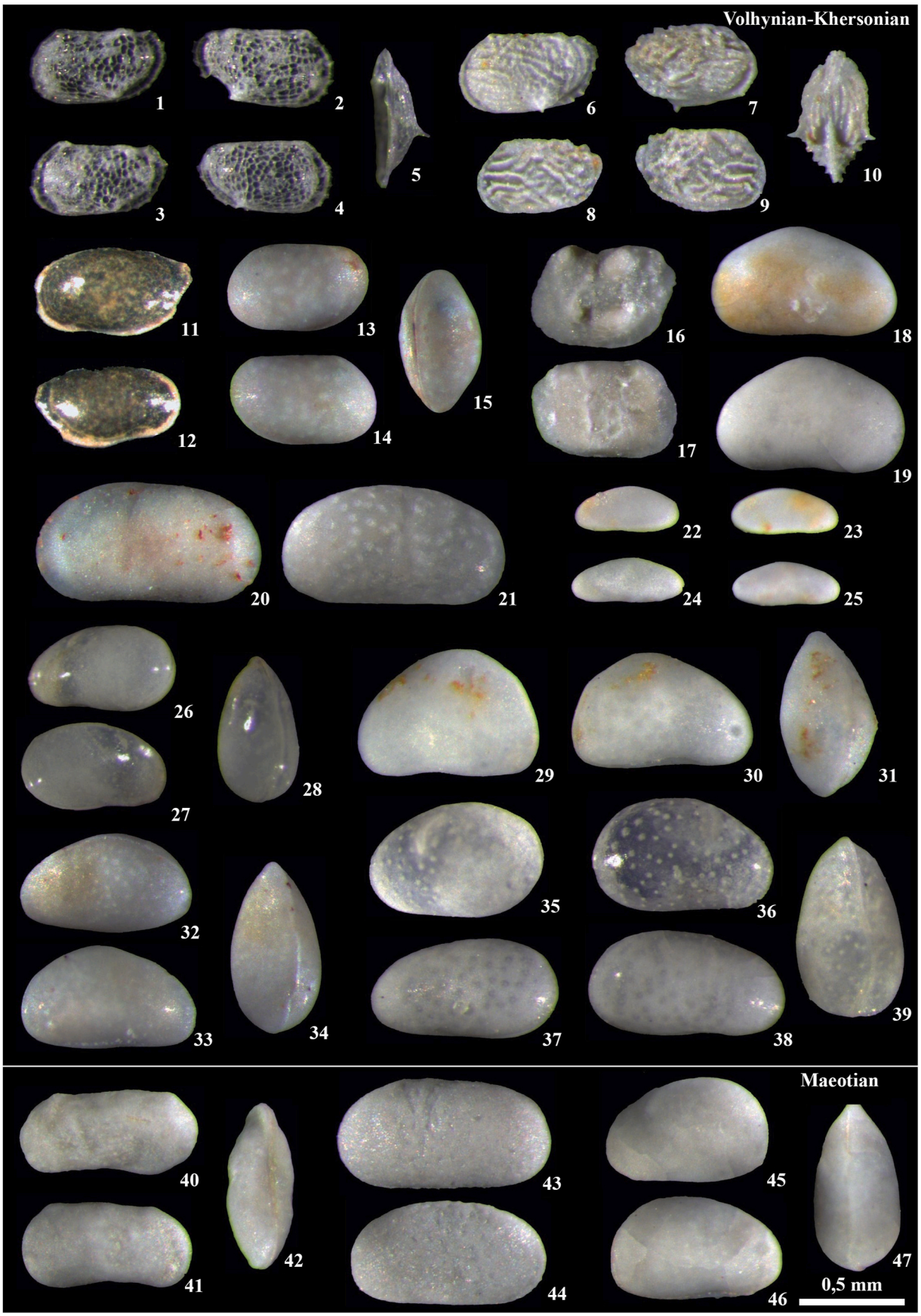

(caption on next page)

Fig. 9d. Volhynian-Khersonian (1–39, 44) and Maeotian (40–47) ostracods from the Karagiye section: 1-5. *Loxocorniculum schmidi*; 1, 3. LV. external view; 2, 4. RV, external view; 5. LV, ventral view; 6–10. *Loxocorniculum ornata*; 6, 8. LV, external view; 7, 9. RV, external view; 10. C, ventral view; 11, 12. *Phlyctocythere fragilis*; 11. LV, external view; 12. RV, external view; 13–15. *Loxoconcha* ex. gr. *muelleri*; 13. LV, external view; 14. RV, external view; 15. C, dorsal view; 16, 17. *Loxoconcha* aff. *quadrituberculata;* 16. LV, external view; 17. RV, external view; 18, 19. *Heterocypris salina*; 18. LV, external view; 19. RV, external view; 20, 21. *Cyprideis* ex. gr. *pannonica*; 20. LV, external view; 21. RV, external view; 22–25. *Cytherois gracilis*; 22. LV, external view, female; 23. RV, external view, female; 24. LV, external view, male; 25. RV, external view, male; 26–28. *Xestoleberis fuscata*; 26. LV, external view; 27. RV, external view; 28. C, dorsal view; 29–31. *Xestoleberis* aff. *castis*; 29. LV, external view; 30. RV, external view; 31. C, dorsal view; 32–34. *Xestoleberis* aff. *dispar*; 32. C, view from LV; 33. C, view from RV; 34. C, dorsal view; 35–39; *Xestoleberis glabrescens*; 35. LV, external view, female; 36. RV, external view, female; 37. LV, external view, ? male; 38. RV, external view, ? male; 39. C, dorsal view; 40–42. *Euxinocythere* aff. *maeotica*; 40. LV, external view; 41. RV, external view; 42. C, ventral view; 43, 44. *Cyprideis* ex. gr. *pannonica*; 43. LV, external view; 44. RV, external view; 45–47. *Xestoleberis maeotica*; 45. C, view from LV; 46. C, view from RV; 47. C, ventral view.

almost the same taxa as below, with even more abundant records (Fig. 5 and 5A-C). The association is dominated by *Porosononion* ex. gr. *granosum, P.* ex. gr. *subgranosum* and *N*onion *bogdanowiczi.* The elphidiids also show an increasing abundance, especially with numerous specimens of *E. crispum* and less frequent *E. josephinum* and *E. reginum* var. *caucasica.* Small-sized *Fissurina* are quite common between 65 and 75 m, the most abundant being *F. carpathica.*

Compared to the lower Bessarabian, the upper Bessarabian specimens have larger and more strongly calcified tests, possibly related to increased calcium carbonate concentration in the water.

The upper part of SI5 (87–93.2 m) is marked by the appearance of the strongly calcified species *Porosononion hyalinum*, associated with numerous specimens of *P.* ex. gr. *subgranosum* (with well-calcified tests) and *E. crispum*. Also, the elphidiids with well-developed marginal spines such as E. josephinum and Elphidium reginum reappear in this interval. The terminal Bessarabian marks the last foraminifera occurrence in the Karagiye section.

4.1.5.4. Ostracods. The interval characteristic for the upper Bessarabian (65–93.2 m) begins with an important diversification and abundance of ostracod species. Most ostracods possess stronger and well-calcified shells, similar to foraminifera.

Leptocytherids include *A. tenuis*, *E.* ex. gr. *praebosqueti, E.* sp. 1, *E.* sp. 2 and *Callistocythere multicristata*. The *Aurila* genus is represented by the well-known *A. merita* and *A. mehesi* species, with stronger valves that differ slightly from the Volhynian specimens. New "aberrant" forms like *Aurila angularis* and *Aurila* sp. appear. From loxoconchids, we identified *L. subcrassula*, with bigger shells than in the Volhynian, associated with new occurrences of *Loxoconcha* ex. gr. *kochi*, *Loxoconcha odessaensis*, *Loxoconcha valiente* and the "aberrant" *Loxoconcha* aff. *quadrituberculata*. Besides them, we frequently identified *Loxocorniculum ornata*, possibly the more robust and ornate variant, the descendent of *L. schmidi* from the Volhynian. The xestoleberids are still represented by *X. fuscata* and *X. glabrescens,* together with more arched species attributed to *Xestoleberis* aff. *castis*. At the top of SI5, we noticed the first occurrence of *Cyprideis* ex. gr. *pannonica*.

During the upper Bessarabian, the ostracod fauna was dominated by forms, with stronger calcified shells and more diversified ornamentation than in Volhynian. The shell peculiarities were possibly a result of the increase in carbonate concentration in the basin. This phenomenon was also described for molluscs in the Central Paratethys by Piller and Harzhauser (2005).

4.1.6. Stratigraphic interval 6 (lower Khersonian, 93.2–112.5 m)

4.1.6.1. Lithology. Description: SI6 begins with pale grey sharp-based rudstone followed by thinly-bedded very-well sorted pale yellowish brown *Chersonimactra* rudstones in beds of 5–10 cm occasionally alternating with beds of pink ooidic sandstones and continuous thin (5–10 cm) lenses of intraformational conglomerates (Fig. 2J). Interestingly, all the beds in this rudstone-oolite-conglomerate alternation gently deepen landwards. At 103.8 m, the rudstones are suddenly covered by light greenish grey massive silty claystones that gradually pass upwards into pale grey sandy marlstones with wave-ripple marks and abundant *Chersonimactra* shells. Above is a series of brown to reddish brown convoluted and pedogenically modified mudstones with rare vertical rootlets and gradual bases (Fig. 2K).

Interpretation: The very well sorted *Chersonimactra* rudstones probably accumulated on the stoss side of the barrier islands formed at the margin of the carbonate platform. Here, the gentle landwards deepening and good sorting suggest high-energy unidirectional wave currents. The poorly sorted ooidic sandstones point to periods of oscillatory wave-driven currents, while conglomerates represent events of exceptionally high waves and/or storm events that caused reworking and redeposition of the barrier sediments. The overlying massive claystone represents a lagoon followed by the progradation of coastal settings and establishment of the backshore environments with palaeosols.

4.1.6.2. Mollusc fauna. The lower Khersonian interval comprises four units marked by monotypic occurrences of *Chersonimactra* species (*C.* cf. *caspia* in 6a, *C. bulgarica* in 6b and 6c and *C. balcica* in 6d). From here, up to the top of the section, the shells are exclusively preserved as steinkerns.

Unit 6a (KDM 93.3—KDM 94.9 m, Fig. 3) starts over a sharp lower boundary with grey bioclastic limestones that contain very common but poorly preserved shells, thus provisory identified as *C.* cf. *caspia*. Already, the very base of the succession is marked by a 30-cm-thick coquina with chaotically oriented shells (KDM 93.3 m). Above, they can additionally occur as horizontally oriented partly articulated shells (KDM 94.9 m) or concentrated in lenses.

Unit 6b (KDM 98.5—101.25 m, Fig. 3) is represented by about 6-m-thick horizontally-bedded bioclastic rudstone, composed exclusively of densely packed randomly oriented single *C. bulgarica* valves.

Unit 6c (KDM 103.2—KDM 103.65 m, Fig. 3) is located directly atop the previous rudstone. It begins with a 10-cm-thick coquina bed with horizontally oriented convex up and remarkably large valves and articulated shells of *C. balci*a (KDM 102.3 m, Fig. 3). Above, a light grey marlstone interval is intercalated by two 15-cm-thick *C. balcica* coquinas with densely packed shells showing no orientation.

Unit 6d (KDM 104.2–KDM 111.7 m) comprises three *C. bulgarica* bearing intervals separated by two barren intervals with loading and water-escape structures and root traces. The lower shell-bearing interval (KDM 104.2—106.0 m) shows in its lower part shells floating in the muddy matrix. They are followed by tiny pavements overlain by a 30-cm-thick coquina comprising convex-up valves and articulated shells *in situ*. Following a short barren interval, another 20-cm-thick coquina with convex-up valves is present. The 70-cm-thick middle mollusc interval (KDM 109.50—110.05 m) consists of stacked pavements by convex-up valves, disturbed by lenses of reworked, partly articulated shells. Finally, the topmost mollusc interval (KDM 111.50—111.7 m) is a 30-cm-thick interval containing accumulations of small-sized disarticulated valves.

4.1.6.3. Foraminifera. No foraminifera have been identified in this stratigraphic interval, possibly due to a salinity drop below their tolerance value (possibly under 9 g/L).

4.1.6.4. Ostracods. The luxuriant ostracod fauna from the upper Bessarabian almost disappears in the Khersonian (Figs. 5 and 9D). Only a few disparate samples, e.g., at 93.8 m, 106 m and 107 m, contain

ostracods. We identified the euryhaline species *C.* ex. gr. *pannonica,* associated mainly with *Euxinocythere* aff. *naviculata*, *Loxoconcha* ex. gr. *muelleri*, *Xestoleberis* sp., *X.* aff. *castis* and *Heterocypris salina*.

Even if the diversity is not great, the respective species appear in abundance and suggest a more restrictive environment.

4.1.7. Stratigraphic interval 7 (upper Khersonian, 112.5–120 m)

4.1.7.1. Lithology. Description: SI7 is characterised by the repetitive alternation of the following beds: 1. white, thinly parallel-laminated (1–2 mm) to wave ripple cross-laminated bindstones in beds of 5–50 cm thick with sharp but blanketing bases; 2. pale grey parallel-stratified mudstones with abundant intraformational angular clasts of reworked bindstones. The mudstone beds have sharp to gradual bases and a thickness of up to 60 cm; 3. Orange-brown to light brown massive to convoluted and aggregated mudstones. The bases of these beds are gradual, often demonstrating a flame-like irregular appearance. These mudstones are rare in the lower part of the unit and become more pronounced and thicker (up to 40 cm) towards the top (Fig. 2L).

Interpretation: The alternation is characteristic of the shallow water tidal plain. Here, the bindstone represents a shallow water microbial flat growth within the intertidal zone (Browne et al., 2000). The appearance of the wave ripple marks represents episodes when the intertidal zone was periodically submerged and affected by the wave-driven oscillatory currents (Reading, 1996). The "reworked horizons" with intraclasts point at a more subaerially exposed part of the tidal plain, where there is more time for the erosion of previously accumulated intertidal deposits. The top orange and red mudstone indicate pedogenic modification within the supratidal zone. Here, the convoluted bedding reflects the rare exceptional episodes of high tides responsible for the soft sediment deformation in palaeosols.

4.1.7.2. Mollusc fauna. The upper Khersonian starts with the topmost *C. bulgarica* occurrence in the section, represented by a shell concentration showing shells in live position at the base of a 50-cm-thick, grey-coloured bindstone (Unit 7a, KDM 113.25 m, Fig. 3). The interval above (Unit 7b, KDM 114.90–KDM 117.15 m, Fig. 3) is marked by the monospecific occurrence of *C. caspia* starting with a 15-cm-thick shell-concentration in light-greyish limestone with densely packed pavements of horizontally, convex-up oriented shells of different growth stages (KDM 114.9 m). Above, a 1-m-thick whitish marl unit bears several tiny pavements (KDM 115.77 m). Finally, a 30-cm-thick microbial bindstone shows horizontally oriented valves in its lower and articulated shells in life-position in its upper part (KDM 117.50 m).

4.1.7.3. Microfauna. In all micropalaeontological samples, taken from this interval, no foraminifera and ostracods could be found.

4.1.8. Stratigraphic interval 8 (lower Maeotian, 120–135.5 m)

4.1.8.1. Lithology. Description: In its lower part (120–124.8 m), SI8 is composed of brown wave-ripple cross-laminated mudstone alternating with greenish-grey wave-ripple cross-laminated to convoluted microbiolithic bindstones. Reworked horizons and palaeosols are rare. From 124.8 m, several 40 cm thick beds of white, very coarse-grained ooidic calcarenites are present, normally graded, fining upwards into medium-grained and with irregular erosive bases. The calcarenites are massive, with faint planar cross-lamination at the base and rare dunes with planar cross-lamination in the middle. Upwards, the calcarenites pass into a pale yellow, 4-m thick small-scale trough cross-laminated oolite followed by a 0.5 m thick framestone formed by dome-shaped branched algae build-ups (Fig. 2M). Above, there is a 3-m thick package of thinly parallel (1–5 mm) laminated bindstone followed by another pinkish-red trough cross-laminated oolite. Among oolites, concentrations of gastropod casts and bivalves are present.

Interpretation: SI8 begins with a small transgression that switched the depositional environments from the inter-/supratidal to subtidal/intertidal. The wave-ripple cross laminated mudstone was formed under the active wave oscillatory action, while the thick microbiolites represent shallower periodically exposed intertidal settings. Starting from 124.8 m, the calcarenites and oolites characterise the switch towards the barrier settings within the shallow water margin of the carbonate platform. The algae build-ups and stromatolithic bindstones indicate the low-energy carbonate platform interior (Reading, 1996; Tucker, 1985).

4.1.8.2. Mollusc fauna. In the lower Maeotian interval (Unit 8a, KDM 129.5–KDM 135.8 m, Fig. 3), only two mollusc-bearing horizons have been detected. The lower one is a 40-cm-thick white oolith bed with common randomly oriented shells of *Potamides taitboutii*, accompanied by *Lampanella maeotica* and single valves of *Mytilaster minor* (KDM 129.5 m). The upper one, representing the topmost layer in the section, is a coarse, porous calcarenite with numerous minute shells of *P. taitboutii*, *M. minor*, *Loripes pseudoniveus* and *Ervilia minuta* (KDM 135.8 m).

4.1.8.3. Foraminifera. No foraminifera have been identified in the lower part of the unit, while the upper part was not sampled for microfauna.

4.1.8.4. Ostracods. Maeotian ostracods have been identified only in a few samples between 122.1 m and 125.7 m below the oolite bed. The most characteristic ostracod species are *Euxinocythere* aff. *maeotica*, *C.* ex. gr. *pannonica. L.* ex. gr. *muelleri* and *Xestoleberis maeotica*.

4.1.8.5. Nannofossils. One investigated sample from SI8 contains a bloom of *Perforocalcinella fusiformis* (ascidians; common name sea squirts). These benthic tunicates commonly occur in shallow marine environments. No other nannofossils were detected. *Perforocalcinella fusiformis* was originally described from the lower Pannonian at Mecsek Mt., Hungary (Bona, 1964), but is also known from the Sarmatian and Badenian (Mandic et al., 2019a; Galović, 2014).

4.2. Vertebrate fauna

The vertebrate finds are grouped and presented by their stratigraphic occurrences and the position of the finding: in layers (*in situ*) or in debris (*ex situ*) (Table 1). The fossil material has different distribution and abundance in different beds (e.g. marlstones, shell-beds, conglomerates) characterising different depositional processes (e.g. accumulations in lagoons, storm deposition). The shell-beds and conglomerates provide the highest number of reworked fossils, whereas the marlstones contain sporadically appearing mostly isolated single bones. Most of the finds are from the outcrop surface (*ex situ*), so only their approximate stratigraphic positions are available. In these cases, the findings could come from the overlying (younger) beds and stratigraphic interpretations are limited.

4.2.1. Fishes

The overall fish diversity has been estimated based on the dentary bones. This bone is the most commonly found and abundant element in the Karagiye fossil record. In situ findings are limited and can be summarised as follows (Table 1): two sciaenids in Konkian; a sciaenid, a perciform and a sparid in Volhynian; a sparid, a gobiid and a probable scombrid in Bessarabian (Fig. 10); only fragmentary material from the micropalaeontological samples in Khersonian. In addition, the Konkian-Bessarabian micropalaeontological samples include rich otolith material. The *ex situ* finds (Table 1), include Pre-Konkian (debris) sharks (Selachia indet.) and a sciaenid, Konkian (debris) sharks, two sciaenids, sparids, three perciform species, Bessarabian (debris) a sparid and a perciform. In the Khersonian, one micropalaeontological sample (at 115 m) contained unidentifiable bone fish fragments, the other samples from

Table 1
Summary of the marine vertebrate fauna (fishes and marine mammals) from the Karagiye Section.

Strat. stage	fish		seals	baleen whales	toothed whales/dolphins
	otolith-based	skeleton-/tooth-based			
Maeotian	–	–	–	–	–
Khersonian	–	Teleostei indet.	–	–	–
Bessarabian	–	Sparidae indet.; Gobiidae indet.; Scombridae indet.; Perciformes indet. 4	*Praepusa* sp.; Phocidae indet.	Cetotheriidae indet.	*Kentriodon fuchsii*; Odontoceti indet.
Bessarabian debris	–	Sparidae indet.; Perciformes indet. 4	*Pachyphoca* sp.	Cetotheriidae indet.	Kentriodontidae indet. Odontoceti indet.
Volhynian	–	Sciaenidae indet.	-	Cetotheriidae indet.; Mysticeti indet.	Kentriodontidae indet.
Volhynian debris	Sciaenidae indet. 1 (? *Trewasciaena*); Sciaenidae indet. 2	Sparidae indet.	*Praepusa* sp.; Phocidae indet.	*Kurdalagonus* cf. *mchedlidzei*; *Otradnocetus virodovi*; Herpetocetinae indet.; Cetotheriidae indet.; Mysticeti indet.	*Pachyacanthus suessi*; ?"*Heterodelphis*" *leiodontus*; *Imerodelphis thabagarii*; *Kentriodon fuchsii*; *Sophianaecetus commenticius*; Kentriodontidae indet.
Konkian	Sciaenidae indet. 1 (? *Trewasciaena*); Sciaenidae indet. 2	Perciformes indet. 3	Phocidae indet.	*Imerocetus* cf. *karaganicus*; *Zygiocetus* cf. *nartorum*; Cetotheriidae indet.	Kentriodontidae indet.
Konkian debris	Sciaenidae indet. 1 (? *Trewasciaena*); Sciaenidae indet. 2	Selachia indet.; Sparidae indet.; Perciformes indet. 1; Perciformes indet. 2; Perciformes indet. 3	*Praepusa* sp.; Phocinae indet.	*Otradnocetus virodovi*; Cetotheriidae indet.	*Pachyacanthus suessi*; *Kentriodon fuchsii*; *Kentriodon* sp.; ?Eurhinodelphidae indet. Kentriodontidae indet.
Pre-Konkian debris	Sciaenidae indet. 1 (? *Trewasciaena*)	Selachia indet.; Perciformes indet. 1	*Praepusa* sp. Phocidae indet.	*Imerocetus* cf. *karaganicus*; *Otradnocetus virodovi*; Cetotheriidae indet.	*Pachyacanthus suessi*; Kentriodontidae indet.

Khersonian-Maeotian beds provided no fish remains.

4.2.2. Marine mammal fauna (whales, dolphins, seals)

4.2.2.1. Konkian. The *in situ* Konkian forms include: three baleen whales *Imerocetus* cf. *karaganicus, Zygiocetus* cf. *nartorum* and a Cetotheriidae indet. (Fig. 10); an unidentified dolphin Kentriodontidae indet.; a new form of a seal Phocinae indet. represented by isolated bones and a partial skeleton, respectively.

The *ex situ* finds (Pre-Konkian and Konkian debris) include: numerous isolated bones of a baleen whale *Otradnocetus virodovi*; several forms of toothed whales as *Kentriodon fuchsii,* other unidentified members of Kentriodontidae and ?Eurhinodelphidae indet. families and a partial skeleton of *Pachyacanthus suessi*; two seals *Praepusa* sp. and Phocinae indet. It should be stressed that their Konkian *ex situ* could be equally originated from the overlying (Volhynian) beds and (considering the large bone size and weight) be transported downslope during weathering processes. Thus, eventual Konkian occurrences of *O. virodovi, P. suessi* and *K. fuchsii* need to be further tested by *in situ* finds.

4.2.2.2. Volhynian. The Volhynian *in situ* finds comprise two whale taxa Cetotheriidae indet. and Mysticeti indet. and one kentriodontid dolphin (Table 1). The *ex situ* finds are very diverse and include more than ten forms. Among baleen whales, *Otradnocetus virodovi* is the most abundant. Other whales include several morphotypes of undetermined members of Cetotheriidae, the most similar to *Kurdalagonus mchedlidzei*, an unnamed whale similar to *Herpetocetus* or *Metopocetus* genera tentatively identified herein as Herpetocetinae indet.; Mysticeti indet. represented by vertebrae of a small unknown whale similar to "*Archaeocetus fockii*". The toothed whales, i.e. dolphins, are present with abundant remains of *Pachyacanthus suessi*, a diverse kentriodontid with at least five taxa (Fig. 10): *Kentriodon fuchsii, Sophianaecetus commenticius, Imerodelphis thabagarii*, a large dolphin similar to "*Heterodelphis" leiodontus* and a dwarf dolphin Kentriodontidae indet. (comparable with "*Phocaena*" *euxina* or *Microphocaena podolica*. The seals are present by *Praepusa* sp. and a Phocidae indet.

4.2.2.3. Bessarabian. In the Bessarabian beds, two seals (*Praepusa* sp., Phocidae indet.), a cetotheriid baleen whale and two toothed whales (*Kentridon fuchsii*, Odontoceti indet.) were found. The Bessarabian surface finds include *Pachyphoca* sp., Cetotheriidae indet. and Kentriodontidae indet.

The Khersonian and the Maeotian layers do not contain any marine mammalian remains.

4.3. Magnetostratigraphy

4.3.1. Rock magnetism

The natural remanent magnetisation (NRM) measurements showed that the Karagiye sediments have a relatively low intensity varying between 200 and 400 μA/m (Supplementary 2). Consequently, the determination of the magnetic mineral carriers performed with the Curie balance resulted in a series of hyperbola-shaped curves (Fig. 11A and B) characteristic of paramagnetic behaviour (Mullender et al., 1993; van et al., 2016b). In the interval with red rootled mudstone (110.5–111.5 m, SI7), three samples demonstrated a high NRM of up to 17000 μA/m. The thermomagnetic runs show a slightly concave curve with irreversible cooling curves gently going down to 580 °C but keeping part of the magnetisation up to 700 °C (Fig. 11C). Such behaviour is characteristic of ferromagnetic minerals (Mullender et al., 1993) that considering the major unlocking temperatures of 580 °C and 700 °C represent magnetite and a minor admix of hematite.

Thermal demagnetisation of IRM samples revealed three distinct groups. The first group, represented by various Konkian, Volhynian and Bessarabian carbonate facies (from wackstones to ooidic grainstones), shows all three coercivity fractions. They display a remarkable reduction at 330 °C indicative for pyrrhotite followed by gradual decline and demagnetisation at 580 °C indicating magnetite as the main magnetic mineral (Fig. 11C) (Dekkers, 1989; O'Reilly, 1984). In the second group, samples from relatively deep-water Bessarabian claystones (SI3), all three orthogonal components gradually decay towards 580 °C, suggesting only magnetite (Fig. 11D). The third group, sampled from Khersonian red mudstones (SI6), show gradual demagnetisation of all three coercivity components towards 660 °C, followed by a sharp drop at 680 °C pointing to hematite as the major magnetic carrier (Fig. 11E) (Lowrie, 1990). Overall, in most samples, the magnetite is the main magnetic mineral carrier (Supplementary 1).

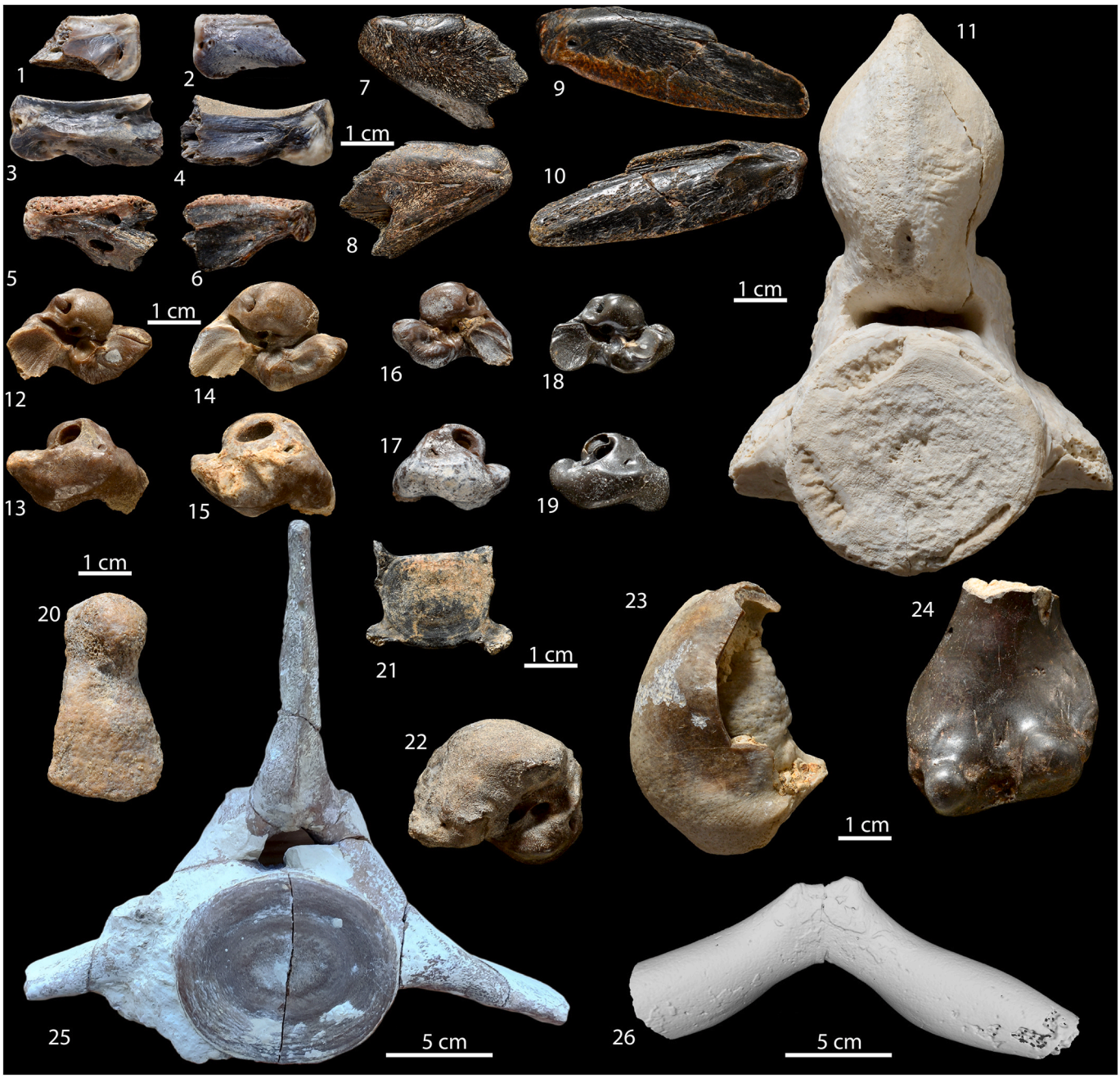

Fig. 10. Marine vertebrate fauna (1-10. fishes and 11-26. marine mammals) from the Karagiye Section. 1, 2. dentary of Perciformes indet. 1 (K23-2), Konkian debris; 3, 4. dentary of Perciformes indet. 2 (KG23-18), Konkian debris; 5, 6. dentary of Perciformes indet. 3 (KG1-213), Konkian debris; 7, 8. dentary of Perciformes indet. 4 (KG22–13.02), Bessarabian (44 m); 9, 10. dentary of Scombridae indet. (KG22-1), Bessarabian (44 m); 11. lumbar vertebra of *Pachyacanthus suessi* (KG22-05), Konkian debris; 12, 13. periotic of *Kentriodon fuchsii* (KG23-1), Volhynian debris; 14, 15. periotic of *Sophianaecetus commenticius* (KG21-1), Volhynian debris; 16, 17. periotic of Kentriodontidae indet. (K23-9a), Konkian debris; 18, 19. periotic of Kentriodontidae indet. (KDFs-23-1c), Bessarabian debris; 20. humerus of *Imerodelphis thabagarii* (KG1-141), Bessarabian debris; 21. vertebra of Odontoceti indet. (KDFs-23-1c), Bessarabian debris; 22. periotic of *Kurdalagonus* cf. *mchedlidzei* (K23-6), Volhynian debris; 23. tympanic bulla of *Zygiocetus* cf. *nartorum* (K23-15), Konkian debris; 24. humerus *Praepusa* sp. (KDFs-23-1b), Bessarabian debris; 25. lumbar vertebra of *Imerocetus* cf. *karaganicus* (K23-10), Konkian, 12 m; 26. hyoid of *Otradnocetus virodovi* (unnumbered), Konkian debris.

Thermal demagnetisation of 344 samples showed the presence of two magnetic components. The low-temperature component (LT) demagnetised at temperatures between 230 and 280 °C (on average around 230 °C) and has positive inclination values (Fig. 11F–H). The LT component mean direction has parameters of declination (D) = 4.62°, inclination (I) = 57.13°, distribution parameter of Fisher (1953) (k) = 21.98, 95% cone of confidence (α95) = 1.9 for a number of accepted samples (N) = 260 in geographic coordinates (Fig. 11I). The low-temperature component is usually linked to the current-day magnetic overprint. The modern magnetic field in the Karagiye section has parameters of D = 7.58° and I = 63° (https://www.ngdc.noaa.gov/ for April 2023). Therefore, we interpret the LT component as a modern-day magnetic overprint complicated by viscous remanent magnetisation.

The second magnetic component commonly demagnetises between 250 and 400 °C (for rare samples with magnetite/hematite, at 690 °C) and has both normal (HT_N) and reversed (HT_R) inclination directions. The mean direction for the HT_R component has parameters of D =

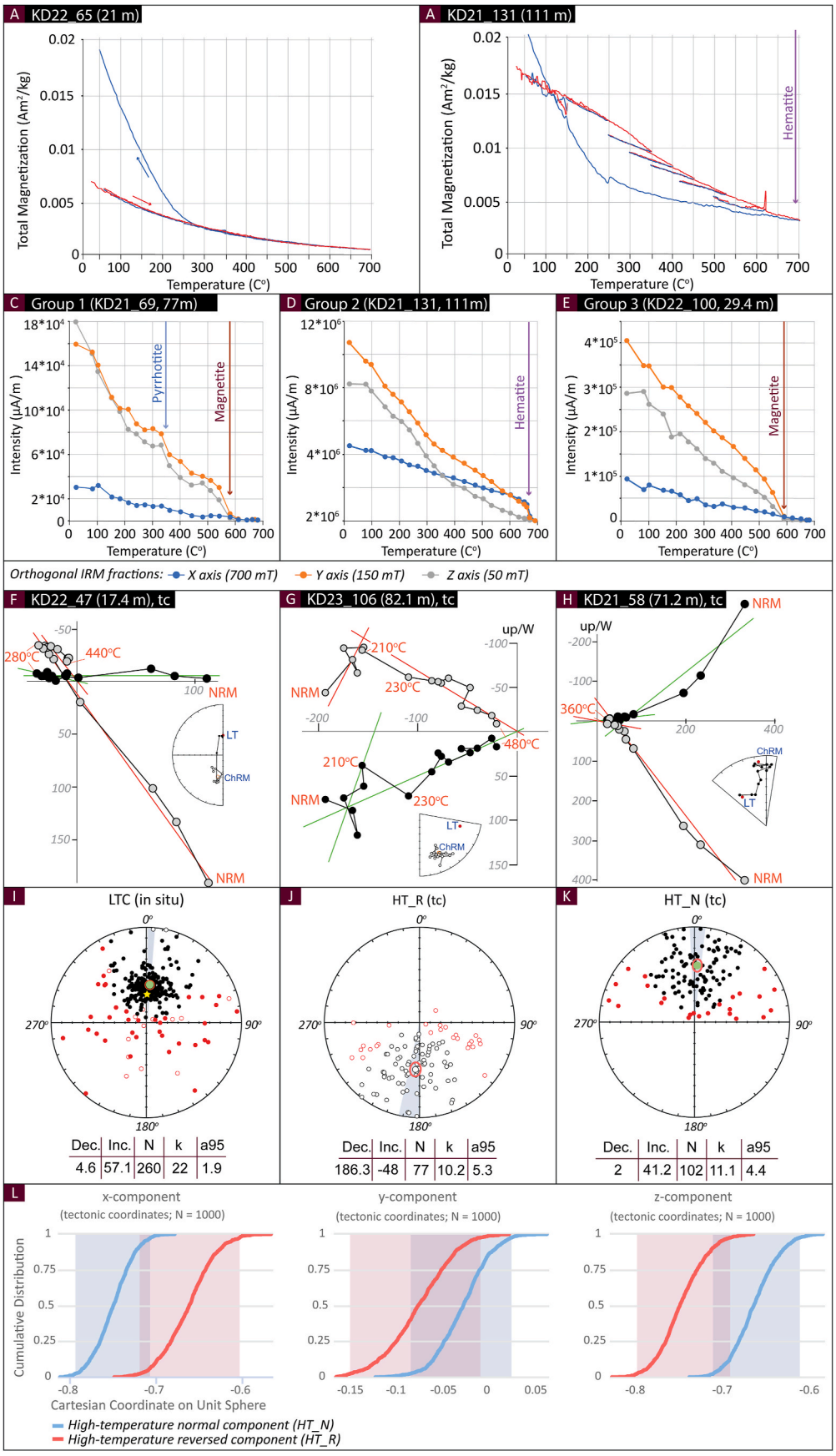

(caption on next page)

Fig. 11. Summary of rock magnetic properties and magnetic components of sediments from the Karagiye outcrop. Curie Balance curve showing: A. paramagnetic behaviour, B. Demagnetisation of hematite-bearing red mudstones; Demagnetisation curves of orthogonal IRM fractions: C. For pyrrhotite and magnetite-bearing carbonates (Group 1), D. For hematite-bearing red mudstones (Group 2), E. For magnetite-bearing claystones (Group 3). Representative Zijderveld diagrams after thermal demagnetisation in tectonic coordinates (tc) for: F. G. Reversed polarity samples, H. Normal polarity samples. Areal plots for: I. Low temperature (LT) directions in geographic coordinates; J. High temperature reversed (HT_R) and K. High temperature normal (HT_N) directions, both in tectonic coordinates. L. Cumulative distributions of Cartesian coordinates of means HT_N and HT_R (Bootstrap reversal test of (Tauxe, 2010)). The reverse polarity has been flipped to antipode. The confidence bounds of three components overlap (e.g. cannot be distinguished at 95% of confidence) and thus pass the reversal test.

186.26°, I = −48°, k = 10.18, α95 = 5.32 for N = 77, while for HT_N component D = 2.04°, I = 41.22°, k = 11.05, α95 = 4.41 for N = 102, both in tectonic coordinates (Fig. 11J and K). These parameters demonstrate that the LT component is clearly distinguishable from the HT_N. The reversal test of McFadden and McElhinny (1990) applied to both HT_N and HT_R is positive (Fig. 11L), and, thus, we interpret the high-temperature component as characteristic of the sedimentation age.

4.3.2. Polarity patterns

Out of 344 measured samples, 22 samples (~7%) had no magnetic signal (diamagnetic), 91 samples (~26%) have undetermined (grey in Fig. 12) directions, 159 samples (~46%) have directions with mean angular deviation (MAD) less than 15°, 34 samples (~10%) have MAD between 15 and 20° and 38 samples (~11%) have MAD exceeding 20° (Fig. 8, Supplementary 1). Conventionally, only directions with MAD <15° are considered reliable (Butler, 1992). The higher MADs likely result from the low NRM of the sediments, and make polarity interpretations less straightforward. Considering that the high-temperature component passes the reversal test, we tend to accept all directions up to MAD ≤20° and we use directions with MAD >20, only to support polarity interpretation of questionable intervals.

The polarity patterns of the studied outcrop comprise 18 polarity zones with nine normal (N1–N9) and nine reversed (R1–R9) (Fig. 11). The measurements of three samples from SI1 (Maykopian) did not deliver reliable results; likely due to the chemical alteration of the sediments (e.g. jarosite powder standing for oxidation of sulfides). The Konkian begins with a series of undetermined directions (8.8–10.5 m) followed by a short normal zone N1 (10.5–13 m) and a reversed zone R1 (13–13.9 m). The Volhynian shows a sharp polarity change towards normal (zone N2, 13.9–16.2 m), followed by reversed zone R2 (16.2–18.1 m), after which the sample directions are indeterminate between 18.1 and 19 m. The normal directions in the remaining upper part of SI3, between 19 and 25 m, form normal polarity zone N3.

The lower Bessarabian (SI4) comprises a long reversed zone R3 (25–50.1 m), among which there are three single normal samples (26.4, 34.65 and 45.5 m). Between 50.1 and 52.9 m, sample polarity fluctuates and thus is uncertain. At 52.9 m, a long normal polarity zone N4 begins, extending into upper Bessarabian (SI5) until 88 m. Within the N4, there are two single reversed polarity samples (75.3 and 82.1 m). Above the N4, between 88 and 90.85 m, there is a series of four reversed samples: three with high and one with low MAD. We interpret this interval as reversed zone R4. Above is a normal zone N5 that passes into the lower Khersonian (SI6) and lasts up to 96.25 m. Between 96.25 and 96.6 m, two reversed samples are situated within a thick package of normally magnetised rudstone. Considering active sedimentary processes within this body, we interpret these two samples as remnants of a small reversed zone R5 (with a question mark). Above lies the normal polarity zone N6 (96.6–101.4 m), which is followed by long reversed polarity zone R6 (101.4–112.5 m) with two single normal polarity samples (107.9, 110.5 m).

The upper Khersonian (SI7) begins with a normal polarity zone N7 (112.5–119.25 m) followed by a short reversed polarity zone R7 (119.25–119.75 m). The Maeotian (SI8) begins in the lowermost part of a normal polarity zone N8 (119.75–121.8 m) followed above by reversed zone R8 (121.8–123.9 m) and normal zone N9 (123.9–125.2 m). Higher up, the polarity becomes less clear; apparently, fragile bindstones and framestones were unsuitable for palaeomagnetic sampling. Between 125.2 and 129, there are three reversed samples, with two having MAD between 15 and 20. We call this interval the polarity zone R9. The last measured sample at 129 m has normal polarity.

5. Discussion

The combination of sedimentological observations, high-resolution palaeomagnetic dating and fossil records of molluscs, microfauna, calcareous nannoplankton and vertebrates allows us to reconstruct the palaeoenvironmental evolution of Karagiye and the Caspian Basin and compare it with other parts of the Eastern Paratethys. The discussion below is built stage-wise, focusing on the correlation of the Karagiye polarity patterns to the GPTS, a comparison of the Karagiye biotic record with other parts of the Eastern Paratethys and a summary of the effects of the Miocene hydrological and biotic events on the Caspian Basin.

5.1. Konkian Stage – pre-isolation phase of the Eastern Paratethys

5.1.1. Correlation to the global polarity time scale (GPTS)

The acquired magnetostratigraphic patterns of the Karagiye section require a cautious correlation to GPTS due to the presence of several hiatuses in the stratigraphic succession. Except for the Konkian part, the combination of magnetostratigraphy and biostratigraphy generally provided solid age constraints (Fig. 13).

The Konkian Stage was previously dated magnetostratigraphically between 13.4 and 12.65 Ma, by correlation to the C5ABn – C5Ar.1r chrons in the GPTS (Fig. 13) (Palcu et al., 2017). In Karagiye, the 6-m-thick Konkian deposits display only one polarity switch from a long normal polarity zone N1 to a short reversed – R1, suggesting an incomplete Konkian record (Fig. 13). Within this interval, a faunal change at 12.6 m from assemblages with *Barnea ustjurtensis* to a faunal complex with *Limacina konkensis* (Fig. 3) marks a lower-middle Konkian (also known as Kartvelian-Sartaganian) biostratigraphic boundary (Popov et al., 2022). This boundary was magnetostratigraphically dated in the Zelenskiy-Panagea (Euxinian Basin) at 12.9 Ma, correlating to the top of the C5Ar.3r reversed chron (Palcu et al., 2017), while in Karagiye it appears in the upper part of the normal zone N1.

We consider two correlation options. Option 1 correlates the N1/R1 polarity switch to the C5AAn-C5Ar.3r reversal (Fig. 13A). Extrapolation of the average sedimentation rates of 0.04 m/kyr from the lithologically similar Volhynian, estimates the base of the Konkian at 13.14 Ma and the Sartaganian faunal change at ~13.03 Ma. This suggests that the Sartaganian marine fauna reached the Caspian Basin about 100 ky earlier than in the Euxinian Basin (e.g. 12.9 Ma, Popov et al., 2022), an unlikely scenario considering this fauna arrived from the Central Paratethyas via the Euxinian Basin.

Option 2 correlates the N1/R1 polarity change to the C5Ar2n-C5Ar.2r reversal (Fig. 13A). This scenario suggests a delayed arrival of the marine Sartaganian faunas to the Caspian Sea at ~12.83 Ma, with the base of the Konkian being ~12.88 Ma. None of the two correlation options are conclusive.

5.1.2. Comparison of the Konkian biotic record within the Caspian Basin and with Euxinian Basins

During the Kartvelian, the Karagiye region was characterised by a sparse faunal assemblage, including the calcareous nannoplankton *Coccolithus pelagicus*, the ostracod *Cytherois gracilis* and the mollusc *Barnea ustjurtensis* (Fig. 14). In the neighbouring Terek-Caspian Depression and Kura Basin, the Kartvelian faunal assemblages are also

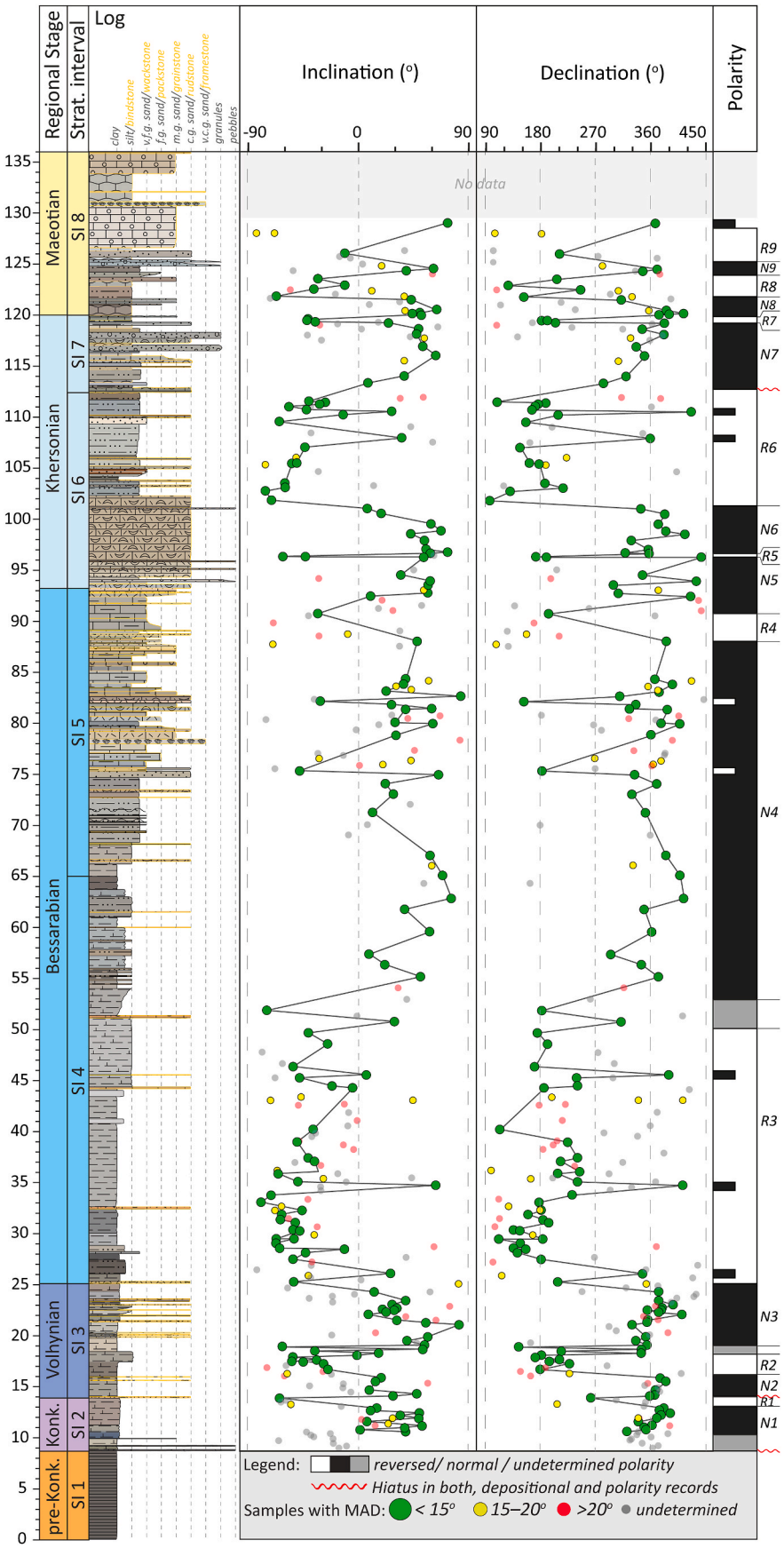

Fig. 12. Magnetic polarity patterns of the Karagiye section.

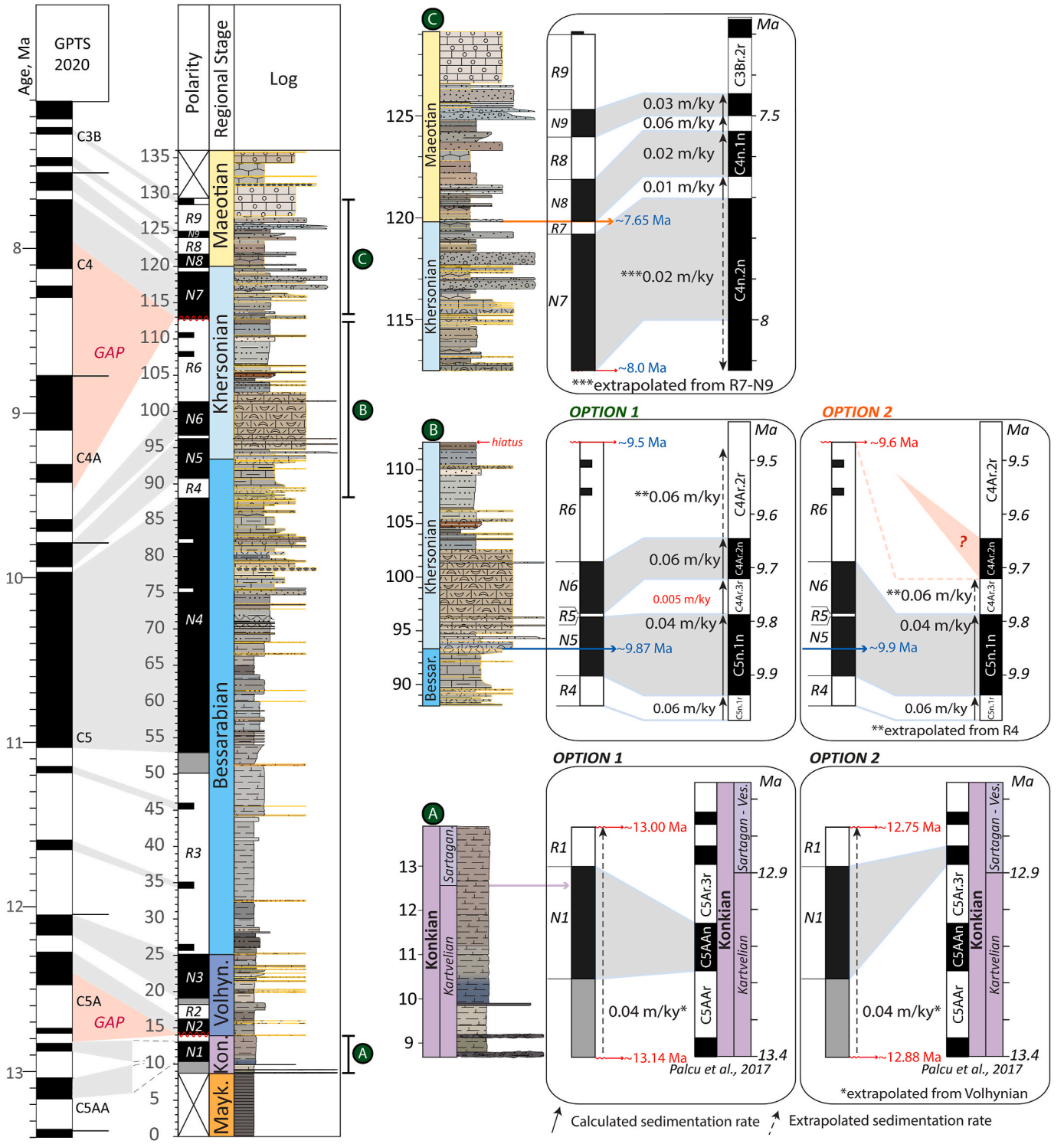

Fig. 13. Correlation of magnetic polarity patterns from Karagiye to the GPTS with a focus on three boundary intervals: A. Kartvelian-Sartaganian (middle-upper Konkian) with two correlation options, both being non-conclusive; B. Bessarabian-Kehrsonian boundary. Here, both options place the boundary at ~9; 9 Ma, but Option 1 is favourable; C. Khersonian-Maeotian transition with the boundary placed at 120 m (7.65 Ma).

impoverished and contain *B. ujratamica*, *B. ustjurtensis*, fish otoliths and almost no microfauna (Muratov and Nevesskaya, 1986). On the Euxinian side of the Caucasian Foreland (Rioni Basin), the Kartvelian fauna is more diverse and contains abundant mollusc taxa of *Barnea* – *B. ustjurtensis*, *B. ujratamica*, *B. scrinia*, *B. kubanica*, *B. sinzovi*, *B. bulgarica*, *Ervillia pussila* and single species of the foraminifera genera *Cassidulina*, *Discorbis*, *Elphidium* and *Ammonia* (Jgenti and Maisuradze, 2016). The Euxinian outcrops of Crimea and the eastern part of the northern Black Sea contain no mollusc fauna but have a foraminifera assemblage dominated by the genera *Cassidulina* and *Discorbis*: *D. kartvelicus, C. bulbiferous, C. bogdanowiczi* and rare *Varidentella* ex gr. *reussi, Ammonia beccarii, Nonion* sp., *Pseudotriloculina* ex gr. *consobrina*, *Articulina vermicularis*, *Reussella spinulosa* and calcareous nannoplankton association with *Braarudosphaera bigelowii*, *Calcidiscus leptoporus*,

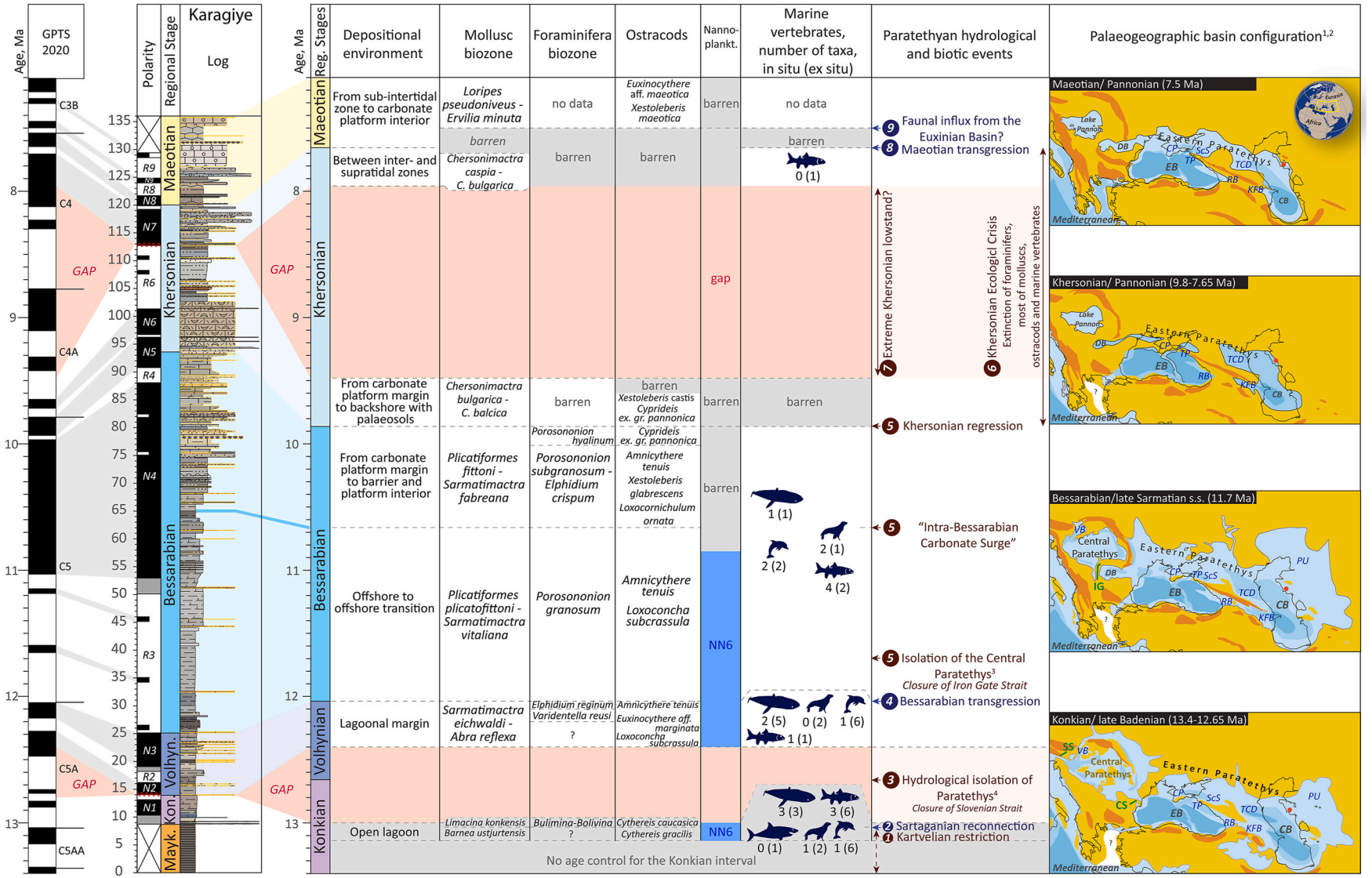

Fig. 14. Correlation of the Karagiye polarity pattern to the GPTS. Mollusc, foraminifera and calcareous nannoplankton biozonations, the most characteristic ostracod fauna and marine vertebrate fauna diversity trends are correlated to major Paratethyan hydrological and biotic events. References: 1 - (Popov, 2004), 2 - (Paramonova, 1994), 3 - (ter Borgh et al., 2014), 4 - (Palcu et al., 2015).

Coccolithus pelagicus, Cyclicar golithus floridanus, Pontosphaera multipora and *Reticulofenestra pseudoumbilicus* (Palcu et al., 2017; Vernyhorova, 2015, 2018; Krasheninnikov et al., 2003; Popov et al., 2016).

A massive Sartaganian faunal influx brought to Karagiye several mollusc taxa such as *Varicorbula gibba, Aporrhais alata* and *Limacina konkensis*, rich foraminifera assemblage with the dominance of *Bolivina dilatata, Bulimina elongata, B. subulata, Porosononion marktobi, Quinqueloculina tortonica, Q. irregularis, Q. akneriana, Q. gracilis, Afinetrina collaris* and *Pseudotriloculina consobrina* etc. (Fig. 6A). The Sartaganian ostracod assemblage is represented by *Cytherois gracilis, Cythereis caucasica, Olimphalunia plicatula* and *Sclerochilus* sp. (Fig. 6B). *Cythereis caucasica* has been described by Schneider (1939) from the Tarkhanian and Chokrakian of the Western Caucasus (Taman Peninsula). It has also been observed in the Konkian of the Western Black Sea, (Tuzlata section, Bulgaria) (M. Stoica unpublished results). However, it never appeared in the Central Paratethys. *Cytherois gracilis* was described by Schneider (1949) from the Karaganian deposits of Azerbaijan. In the Central Paratethys, this species is well known and frequently occurs during the Sarmatian s. str. under the name *Cytherois sarmatica* (Jiříček, 1974). The latter name, in our opinion, should be considered a junior synonym of *C. gracilis*. *Olimfalunia plicatula* is a common species recorded in the late Badenian of the Central Paratethys, described by Reuss in the Viena Basin (see also Gross, 2006). In addition, it is mentioned in the Dacian Basin (Olteanu, 2006), as well in the northern Black Sea (North Caucasus and Crimea) by Schneider (Schneider, 1939, 1949), under the name *Cythereis tschokrakensis*. The Sartaganian deposits of Karagiye also contain rich calcareous nannoplankton with *Braarudosphaera bigelowii, Coccolithus pelagicus, Holodiscolithus macroporus, Rhabdosphaera sicca, Reticulofenestra pseudoumbilicus* and *Syracosphaera mediterranea* (Fig. 8), which based on the absence of *Sphenolithus heteromorphus* can be attributed to the NN6 biozone (Ćorić et al., 2023). Moreover, Sartaganian samples from Karagiye contain endemic *Nivisolithus kovacici* and *N. vrabacii*, originally described from the time-equivalent late Badenian of the Central Paratethys (Bukova Glava, Krndija Mountain, Croatia) (Ćorić et al., 2023), suggesting an active water exchange and similar hydrological conditions across the entire Paratethys domain.

Compared to the other parts of the Caspian Basin, the Sartaganian faunas of Karagiye appear to be taxonomically poorer. In the Terek-Caspian Depression, in addition to the mollusc forms present in Karagiye, there are also *Davidaschvilia sokolovi*, *Abra alba*, *Timoclea konkensis* and *Nassarius Dujardin* (Muratov and Nevesskaya, 1986). In the Kura Basin, the biodiversity is higher and, in addition to listed Karagiye taxa, includes molluscs *Mactra basteroti, Aequipecten malvinae, A. diaphanus, Anomia ephippium, Europicardium multicostatum, Acanthocardia paucicostata, A. andrussovii, Cochlis* cf. *millepunctata* and foraminifers *Angulogerina angulosa, Uvigerina gracilissima, Borelis* (Muratov and Nevesskaya, 1986; Jgenti and Maisuradze, 2016; Rostovtseva et al., 2020).

The Sartaganian fauna of the Euxinian Basin comprises most of the mentioned Caspian fauna but with addition of many other forms: *Anadara turonica, Polititapes vitalianus, Plicatiformes praeplicatus, Ervilia pusilla trigonula, Obsoletiformes ruthenicus, Retusa* sp., *Cochlis* cf. *millepunctata* molluscs (Muratov and Nevesskaya, 1986), dominant stenohaline foraminifers of genera *Lagena, Nodobacullariella, Spirolina, Globulina, Virgulina, Reussella, Pyrgo* (Vernyhorova, 2018; Krasheninnikov et al., 2003) and nearly identical calcareous nannoplankton assemblage (Radionova et al., 2012).

5.1.3. Konkian palaeoenvironment in Karagiye and its response to the Eastern Paratethys – global ocean connectivity dynamics

During the Konkian, the Eastern Paratethys was mostly connected to the global ocean via the Barlad and Carasu Straits – Central Paratethys – Slovenian Strait, although experiencing episodes of pronounced hydrological restriction (Fig. 14) (Popov, 2004; Popov et al., 2022; Studencka et al., 1998). However, the connection with the Central Paratethys was not strong enough to allow a uniform distribution of planktonic foraminifera and radiolarians. At that time, the Caspian Basin was connected with the Euxinian (Black Sea) Basin in the south via the Transcaucasian Strait (Kura and Rioni basins) along the Caucasian Foreland and in the north along the Forecaucasus (Caspian-Terek Depression and Scythian Shelf).

During the Kartvelian, the Karagiye area was occupied by a large open lagoon/shallow littoral zone subject to oscillatory wave action and probably small tidal activity. With the dominance of *Barnea* molluscs, rare calcareous nannoplankton and impoverished foraminifera fauna, both in Karagiye and the neighbouring parts of the Caspian Basin, the Kartvelian palaeosalinity can be estimated as polyhaline. The Eastern Paratethys connection with the global ocean was limited as revealed by the basin-wide development of a poor faunal assemblage dominated by the endemic *Barnea* species and impoverished foraminifera fauna (Jgenti and Maisuradze, 2016; Popov et al., 2022).

Comparing the Kartvelian biotic records between the Caspian and Euxinian basins demonstrates a remarkable westward biodiversity increase, which is likely linked to the presence of a salinity gradient throughout the Eastern Paratethys, with the Euxinian Basin being saltier than the Caspian Basin. The Euxinian Basin, as the closest to the Carasu Strait, received more marine inflow, while in the remote Caspian Basin, the riverine influx played a more prominent role in the basin salinity.

A massive faunal influx marks the onset of the Sartaganian substage. In Karagiye, this event was not accompanied by any changes in the depositional environments, with the open lagoon settings persisting further.

During the Sartaganian, the Eastern Paratethys connection with the global ocean was restored, which facilitated the invasion of numerous euhaline faunal groups (Vernyhorova, 2018; Popov et al., 2022). The occurrence of rich euhaline fauna far east, in the Caspian Basin shows that even the most distal parts of the Eastern Paratethys turned to full marine conditions.

5.2. The Volhynian (sub)stage – the onset of isolation of the Eastern Paratethys

5.2.1. Correlation to the GPTS

The base of the Volhynian is synchronous with the base of the Sarmatian s.s. in the Central Paratethys and has an age of 12.65 Ma, which correlates to the middle of C5Ar.1r (Palcu et al. 2015, 2017; Mandic et al., 2019b). One of the first attempts to date the Volhynian-Bessarabian boundary was made by Chumakov et al. (1992) using the fission track method, who placed the boundary at 12.2 Ma. Later, using the integrated stratigraphic approach (cyclo- and biostratigraphy) for the correlation between the Central and Eastern Paratethys, Harzhauser and Piller (2004) estimated the Volhynian-Bessarabian boundary age at around 11.9 Ma. At the same time, neither palaeomagnetic nor radiometric age constraints were performed in the Eastern Paratethys on the Volhynian-Bessarabian geological records. Considering the mentioned age constraints and anticipating the Volhynian age to be around 12.6–12 Ma, we correlate the Volhynian polarity patterns in Karagiye in the following order: the N2 to C5An.2n, R2 to C5An.1r and N3 to C5An.1n (Fig. 12). Such correlation suggests that a large portion of the Volhynian deposits (reversed polarity chron C5Ar.1r and the lower part of the normal polarity chron C5An.2n) is missing at Karagiye. Calculating the average sedimentation rates from the chrons R2 and N3 (C5An.1r–C5An.1n) results in 0.04 m/kyr. Extrapolation of this rate downwards to the base of the N2 zone results in an age of 12.33 Ma for the basal Volhynian deposits in Karagiye. Therefore, we interpret the presence of a ~670 kyr gap (between 13.0 and 12.33 Ma) straddling the Konkian/Volhynian boundary in the Karagiye section.

5.2.2. Volhynian biotic record of the Caspian Basin and its comparison with the rest of the Eastern Paratethys

The Volhynian fossil record of Karagiye is characterised by a gradual

diversification towards the top of the record (Figs. 3 and 5). The onset begins with a few new rotaliid taxa of rare *Nonion bogdanowiczi, Elphidium crispum* and *Elphidum hauerinum* foraminifers, *Amnicythere tenuis, Euxinocythere marginata* and *Loxoconcha subcrassula* ostracods and *Obsoletoformes* spp., *Musculus* spp. and *Abra* spp. molluscs. In addition to the newly-occurring taxa, several foraminifera taxa such as *Quinqueloculina haueriana, Q. gracilis, Q. pseudoangustissima* and *Pseudotriloculina* ex. gr. *consobrina* and one ostracod species *Cythereis gracilis* passed from the Konkian and persisted during the Volhynian.

Further upwards, the mollusc fauna diversifies gradually, with the new taxa *Ervilia dissita, Sarmatimactra eichwaldi* and *Polititapes vitalianus*, while the microfauna expands stepwise: at 15.6 m occur *Ammonia beccarii, Elphidium crispum, E. hauerinum, Varidentella reussi* and *Quinqueloculina collaris*; and at 18.20 m – *Fissurina carpathica, F. elongata, Porosononion* ex. gr. *subgranosum* and P. ex.gr. *granosum*. The most remarkable Volhynian faunal change in Karagiye happened at 21.3 m, where *Dorsanum duplicatum, Timisia picta* and *Plicatiformes plicatofittoni* molluscs, *Fissurina cubanica, F. bicaudata* and *Elphidium aculeatum, E. josephinum, E. reginum, Guttulina austriaca* foraminifers and *Aurila merita, A. mehesi, Euxinocythere praebosqueti, Loxococncha subcrassula, Loxocornichulum ornata, Xestoleberis* spp. ostracods occur.

In the neighbouring regions of the Caspian Basin, the data on the Volhynian fossil fauna is scarce but generally, resembles those in Karagiye. In the Terek-Caspian Depression, the Volhynian deposits comprise a similar faunal assemblage with *Abra reflexa, Sarmatimactra eichwaldi* and deep water *Cryptomactra pseudotellina* molluscs and *Varidentella reussi* and *Quinqueloculina consorbina* foraminifers (Muratov and Nevesskaya, 1986). In the Kura Basin, similar to Karagiye, the Volhynian fauna is dominated by the indicative molluscs *Polititapes vitalianus, Ervilia dissita, Abra reflexa, Dorsanum duplicatum, Sarmatimactra eichwaldi* with addition of *Donax dentiger* and other taxa of the genera *Trochus, Calliostoma, Gibbula, Solen* and *Acteocina* (Buleyshvili, 1960; Ali-Zade, 1974). In the outcrops of East Georgia (Kura Basin), the Volhynian foraminifera fauna is typically subdivided into three biozones (following upwards): *Elphidium horridum* zone, *Varidentella reussi* zone and *Elphidium aculeatum* zone (also often referred as *Elphidium reginum* zone) with the latter two being identical to Karagiye (Koiava et al., 2008).

In the Euxinian Basin, the Volhynian faunas were studied in more detail, and the faunal assemblages are similar to the ones documented in Karagiye. On the Taman Peninsula (Euxinian Basin), the Volhynian is marked by the mass occurrence of euryhaline molluscs *Abra alba scythica* and rarer *Ervilia dissita, Obsoletiformes* sp., *Sarmatimactra eichwaldi* and *Musculus* sp. The microfaunal assemblages are dominated by *Leptocythere, Loxoconcha, Xestoleberis, Aurila, Denticulocythere, Cytherois, Cythereis* and *Cyprideis* ostracods and *Articulina sarmatica, Elphidium josephinum* and *Varidentella reussi* foraminifers with the latter two constituting the *Varidentella reussi* and *Elphidium reginum* zones (Popov et al., 2016; Karmishina and Shneider, 1986). During the Volhynian, both foraminifera and ostracods have many elements in common with the lower Sarmatian fauna of the Central Paratethys. The Volhynian calcareous nannofossils in Taman are represented by a very poor monospecific assemblage with *Syracosphaera* (Radionova et al., 2012), which is incomparable with a rich complex documented in Karagiye by *Helicosphaera* spp., *Braarudosphaera bigelowii, Cocolithus pelagicus, Reticulofenestra pseudoumbilicus* (Figs. 7 and 8).

5.2.3. Volhynian palaeoenvironments in Karagiye – the onset of hydrological isolation of the EP and its expression in the Caspian Basin

The Volhynian marks the onset of the hydrological isolation of the Paratethys from the global ocean. This conclusion is based on a sharp extinction of stenohaline taxa at the Badenian-Sarmatian (in the Central Paratethys) and Konkian-Volhynian (in the Eastern Paratethys) boundaries known as the BSEE (see Chapter 2). A major role in this process was attributed to the Slovenian Strait, whose termination stopped the marine inflow and led to a basin-wide salinity drop. However, no faunal-independent geochemical constraints exist to confirm this hypothesis.

Between 12.33 and 12.0 Ma, Karagiye was at the margin of a large open lagoon with oscillatory wave- and small tidal currents, active bioturbation and episodes of subaerial exposure. As the upper Konkian – lowermost Volhynian are missing in the section, it is impossible to estimate the impact of the Paratethyan hydrological isolation on the area. The Volhynian in Karagiye largely misses most of the Konkian foraminifers, marine ostracods and, most remarkably, sharks, which likely points to a salinity decrease (lack of fully marine conditions). At the same time, four foraminifera taxa, one marine ostracod and, most importantly, all Konkian nannoplankton taxa passed into the Volhynian.

Comparison of the Volhynian biotic record and biozonation from Karagiye with the other parts of the Caspian and Euxinian basins shows the uniformity of Volhynian ecosystems across the Eastern Paratethys, which is essential for inter-basinal correlations and application of biozones.

5.3. Bessarabian Stage – from a maximum transgression to the first hydrological disruption of the Eastern Paratethys

5.3.1. Correlation to the GPTS

The Bessarabian in Karagiye starts at 25.2 m, marked by a large transgression event and a first occurrence of indicative Bessarabian *Plicatiformes plicatofittoni* molluscs. The Bessarabian palaeomagnetic record in Karagiye comprises magnetic zones ranging from R3 to the middle of N5 (Fig. 13). Considering the conformable position of Bessarabian on top of Volhynian, we correlate these zones in the following order: long reversed zone R3 with three single normal samples is correlated to the chron C5r (that comprises several short normal polarity intervals according to Krijgsman and Kent, 2004); long normal zone N4 – to the C5n.2n; reversed one R4 corresponds to the C5n.1r and the following normal zone N5 correlates to the C5n.1n (Fig. 13).

The Volhynian-Bessarabian boundary is located only a few centimetres above the C5An.1n–C5r.3r reversal that has an age of 12.045 Ma. Such age is generally in line with the age model of Harzhauser and Piller (2004) who correlated the boundary slightly above the C5An.1n–C5r.3r reversal. Therefore, we date the Volhynian-Bessarabian boundary at ~12.05 Ma.

5.3.2. Bessarabian fossil record in Karagiye and its comparison with other parts of the Eastern Paratethys

From the faunal point of view, the Bessarabian deposits in Karagiye are subdivided into lower and upper intervals (Fig. 14). For the lower Bessarabian, the most characteristic fauna includes *Sarmatimactra vitaliana, Obsoletiformes* spp., *Plicatiformes plicatofittoni, Ervillia dissita, Polititapes vitalianus* molluscs, *Nonion bogdanowiczi, Porosononion granossum, Elphidium crispum* foraminifers, minor presence of *Amnicythere tenuis* and *Loxoconcha subcrassula* ostracods and rich but upwards-decreasing calcareous nannoplankton assemblage with *Calcidiscus* spp., *Coronasphaera* sp., *Reticulofenestra pseudoumbilicus* and *Sphenolithus moriformis*.

The base of the Bessarabian is marked by an abundant occurrence of *Calcidiscus* spp. nannoplankton, resembling similar forms of the Našice section, Croatia (Ćorić, 2006; Galovic and Young, 2012) suggesting uniform basin-wide ecological conditions.

In the upper Bessarabian, the molluscs fauna is represented by *Sarmatimactra podolica, S. fabreana, Plicatiformes fittoni, Solen subfragilis, Polititapes tricuspis, Barbotella hoernesi, Paradonax lucidus* and minor presence of *Gibbula feneoniana*. The upper Bessarabian foraminifera assemblage is similar to the lower Bessarabian except for the new *Porosononion hyalinum* appearing in the very top and other taxa such as *Porosononion* ex. gr. *granosum, P.* ex. gr. *subgranosum* and *Elphidium reginum* becoming abundant. The ostracod fauna shows numerous new taxa, with *Callistocythere* sp., *Loxoconcha* ex. gr. *kochi, Cyprideis* ex. gr. *pannonica* and *Loxoconcha* aff. *quadrituberculata*. No nannoplankton was detected in the upper Bessarabian. Ostracod fauna from the Karagiye

section is similar to the fauna described from the northern Black Sea, Caucasus and Caspian areas, although some differences in taxonomic approach exist (Schneider, 1939, 1949, 1953; Suzin, 1956; Pobedina et al., 1956; Stancheva, 1990).

Similar to Karagiye, the two-member subdivision of the Bessarabian into lower (known as the "Novomoscovian layers") and upper (also known as the "Dnipropetrovsk-Vasilevka layers") has been traced across the Euxinian and Caspian basins of the Eastern Paratethys (Paramonova, 1994). In the stratotypes of Southern Ukraine, the lower Bessarabian fauna comprises *Obsoletiformes obsoletum*, *Cerastoderma plicatum plicatum*, *Sarmatimactra vitaliana*, *Calliostoma podolica*, while the upper Bessarabian deposits include *Plicatiformes fittoni*, *Sarmatimactra fabreana*, *Barbotella intermedia* and others (Muratov and Nevesskaya, 1986). In the Taman Peninsula (Euxinian Basin), Kura Basin and Terek-Caspian Depression (both in the Caspian Basin), the lower Bessarabian is represented by deep-water claystone facies, which contains characteristic deep-water assemblage dominated by *Cryptomactra pesanseris*, *C. pseudotellina* and *Sarmatimactra urupica* molluscs, rare foraminifers of the genera *Nonion* and *Elphidium* and *Reticulofenestra* sp. and *Coccolithus pelagicus* calcareous nannoplankton (Muratov and Nevesskaya, 1986; Nevesskaya and Trubikhin, 1984; Popov et al., 2016).

The upper Bessarabian deposits in the Kura Basin and the Terek-Caspian Depression are represented by shallow water marlstone facies that contain assemblages similar to Karagiye with *Plicatiformes fittoni*, *Sarmatimactra fabreana, Ervilia dissita* (Muratov and Nevesskaya, 1986).

5.3.3. Bessarabian palaeoenvironments in Karagiye

During the Bessarabian Stage, the Eastern Paratethys reached its maximum Middle-Late Miocene water level (Fig. 14). The large transgression started at 12.05 Ma and extended far inland, in the direction of Central Asia and north of the Black Sea (Popov et al., 2022).

In Karagiye, the Bessarabian transgression changed the shallow-water marginal lagoon environments to relatively deep-water offshore settings. Remarkably for the Bessarabian, the faunal assemblages demonstrate a quantitative explosion in the first meter above the transgressive contact at 25.2 m. This fauna almost disappeared above 27 m as the water level continued to rise.

The observations on the lower Bessarabian facies in Karagiye show that the depositional settings fluctuated between offshore and offshore transition. One of the most remarkable transgressive surfaces occurred at 32.5 m dated at ~11.8 Ma, with the offshore setting lasting up until 41 m or ~11.6 Ma, afterwards switching back to offshore transition environments. During this time, the water level rise in the Euxinian Basin reached its maximum as the basin ingressed far north into the Palaeo-Don Valley, where the Bessarabian transgression was dated at 11.5 Ma (Danišík et al., 2021).

At 11.7 Ma (below C5r.2n), the closure of the Iron Gate Strait separated the Central Paratethys from the Eastern Paratethys and turned it into a gradually freshening brackish lake (ter Borgh et al., 2014). As observed in Karagiye, neither the water balance nor the faunal record was affected by this event.

At 10.67 Ma (65 m), the depositional setting abruptly switched to the carbonate platform interior, followed by the appearance of new late Bessarabian faunas. A similar transition from clastic to shallow carbonate depositional settings has been previously observed in all other parts of the Eastern Paratethys, such as the Bulgarian coast of the Black Sea (Koleva-Rekalova, 1994), Crimea and north of the Black Sea (Muratov and Nevesskaya, 1986).

We assume that this event, called here the "Intra-Bessarabian Carbonate Surge," was linked to the water-level-drop-related increase in carbonate saturation. Carbonates were constantly delivered into the isolated Eastern Paratethys from the surrounding land masses and mountain ranges (Carpathians, Caucasus). Observations on the microfauna in Karagiye showed a remarkable thickening of ostracod and foraminifer shells, which indicates a rise in the water alkalinity.

During the late Bessarabian, between 10.7 and 9.9 Ma, Karagiye was a shallow water carbonate platform interior inhabited by serpulid colonies, microbial mats and rich invertebrate faunas.

5.4. Khersonian Stage – onset of hydrological and biotic instability

5.4.1. Correlation to the GPTS

The Khersonian deposits in Karagiye begin at 93.2 m with the first occurrence of *Chersonimactra* cf. *caspia* and span the N5-N8 polarity interval (Fig. 13). The transition from the upper Bessarabian (SI5) carbonate platform interior grainstones to Khersonian barrier island rudstones has an erosional appearance and thus requires cautious correlation to the GPTS.

The Bessarabian-Khersonian boundary is located in the middle of the normal zone N5. The following R5 and N6 are located in rudstones accumulated in high-energy environments, making the chrons thicker (as for N6) or extremely short/incomplete (as for R5). The R6 spans the fine-grained lagoon to backshore deposits and is incomplete as it is followed by a hiatus at 112.5 m.

For the correlation of N5-R6 to GPTS, we discuss two options (Fig. 13): **Option 1** correlates N5 to C5n.1n, R5 to C4Ar.3r, N6 to C4Ar.2r and R6 to C4Ar.2r. With such correlation, the transition to rudstones demonstrates a slight increase in the average sedimentation rates from 0.04 to 0.06 m/kyr. Extremely low sedimentation rates in R5 are in disagreement with observed coarse-grained lithology, which suggests the incompleteness of the chron. Extrapolation of the 0.04 m/kyr rates within the N5 zone results in a Bessarabian-Khersonian boundary age of 9.87 Ma. If extrapolating the sedimentation rates from R4 up to the boundary (R4 and the lower part of N5 have similar lithology), the boundary arrives at 9.9 Ma.

The reversed zone R6 has a similar lithology as R4. Extrapolation of the sedimentation rates of 0.04 m/kyr from R4 to the R6 results in the uppermost age limit for R6 of ~9.46 Ma, which is still within C4Ar.2r (Fig. 13).

Option 2 assumes that R5 is not a chron but an anomaly; both N5 and N6 correlate to the C5n.1n, and R6 correlates to C4Ar.3r. Such correlation implies a decrease of sedimentation rates from 0.06 to 0.04 m/kyr, contradicting the observed sedimentological transition towards higher energy depositional settings. Option 2 also results at the Bessarabian-Khersonian boundary age of 9.9 Ma. For calculation of the R6 upper age limit, extrapolation of sedimentation rates from R4 (lithologically similar to R6) results in an age of ~9.6 Ma, meaning, that there must be a missing C4Ar.2n normal chron, somewhere between 101.4 and 112.5 m. Overall, both correlation options indicate an age of the Bessarabian-Khersonian boundary at ~9.9 Ma, but option 1 better agrees with the lithological changes and provides more logical ages for the R6 zone.

The Bessarabian-Khersonian boundary was also magnetostratigraphically dated in the Panagiya outcrop (Russia, Black Sea Basin) at 9.6 Ma, corresponding to the lower part of C4Ar.2r chron (Palcu et al., 2021). However, the lack of diagnostic fauna in the large parts of layers 14 and 15 in Panagiya (Popov et al., 2016) creates an additional uncertainty of at least 200 ky (9.75–9.55 Ma). Moreover, the biostratigraphic, palaeomagnetic and sedimentological data in Panagiya were collected sequentially, which could potentially contribute to the boundary position discrepancy.

The polarity patterns of the upper Khersonian (112.5–120 m) between N7 and N8 do not fit into subsequent GPTS patterns (Fig. 13). A simultaneous sharp change in both the magnetic polarity and the depositional environments at the SI6/SI7 transition (lower-upper Khersonian) points to the presence of a hiatus.

Considering the biostratigraphic data from the upper Khersonian–lower Maeotian of the Karagiye section, the polarity zones N7 – R9 can be correlated to the GPTS in the following order: N7 to C4n.2n, R7 to C4n.1r, N8 to C4n.1n, R8 to C3Br.3r, N9 to C3Br.2n, R9 to C3Br.2r (Fig. 13). Calculating sedimentation rates from complete chrons C4n.1r – C3Br.2n (R7-N9) results in an average rate of 2.55 cm/ky. Using these

rates, the age of the last Khersonian molluscs in Karagiye section at 117.5 m can be estimated at ~7.8 Ma, while the appearance of the first Maeotian ostracods at 122.1 m is around 7.5 Ma. Therefore, with a time window of 300 kyr between the last Khersonian and first Maeotian faunas, a firm placement of the boundary between these two stages in Karagiye section is complicated.

In other parts of the Eastern Paratethys, such as the Dacian (Lazarev et al., 2020; Palcu et al., 2019) and the Euxinian basins (Palcu et al., 2021) the Khersonian-Maeotian boundary was dated at 7.65 Ma, correlating to the C4n.1n – C4n.1r boundary. Geochronologically, the 7.65 Ma level correlates to 120 m, where the depositional record displays a small transgression event marked by the disappearance of coarse-grained sandstones with reworked bindstone fragments and becomes dominated by wave-ripple cross-laminated mudstones. We tentatively place the Khersonian – Maeotian boundary at that level.

5.4.2. Khersonian ecological crisis

The Khersonian faunal assemblage of Karagiye is remarkably poor and contains only *Chersonimatra balcica*, *Ch. caspia* and *Ch. bulgarica* molluscs and rare ostracods of the genera *Xestoleberis*, *Callistocythere*, *Euxinocythere*, *Heterocypris* and *Loxoconcha*. Overall, compared to the Bessarabian, the biodiversity of Khersonian molluscs shrunk from 17 taxa to 3 (with complete turnover) and ostracods from 19 to 7 taxa. Neither foraminifers nor nannoplankton and marine vertebrates (except for one sample with a few fish remains) were found. This extensive interval of ecological turnover, called here the Khersonian Ecological Crisis, was also observed in other parts of the Eastern Paratethys.

In the Terek-Caspian Depression, the Khersonian fauna is mainly represented by *Chersonimactra* molluscs and rare freshwater genera such as *Unio*, *Melanopsis* and *Viviparus*. In the Kura Basin, besides those molluscs, Khersonian deposits occasionally comprise *Solen subfragilis* molluscs, *Cyprideis littoralis* ostracods and rare *Ammonia beccarii* foraminifers. Two latter taxa may indicate a slightly higher salinity than in Karagiye and Terek-Caspian Depression. The Khersonian fauna of the Euxinian Basin is more diverse than in the Caspian. On the Taman Peninsula, it includes the molluscs *Chersonimactra* and foraminifers *Ammonia* (Muratov and Nevesskaya, 1986). In the Dacian Basin, the Khersonian interval is characterised by molluscs *Chersonimactra*, *Coelogonia* and *Potamides*, rare foraminifers *Ammonia* and frequent ostracods *Cyprideis torosa* (Palcu et al., 2019; Lazarev et al., 2020).

The comparison of faunal records across the Eastern Paratethys shows a heavy impact of the Khersonian Ecological Crisis on the biotic record. Besides the catastrophic decline of invertebrate communities, the fossil record lost nearly all large marine faunas such as whales, dolphins and seals. The exact driver(s) of this process remain nebulous. The lack of foraminifers in the Caspian Basin (except for some rare *Ammonia*) suggests that the salinity of the basin dropped below 9‰. Overall, the faunal-based salinity of the Eastern Paratethys during the Khersonian was estimated between 5 and 12‰ (Paramonova, 1994), but requires further fauna-independent confirmation.

5.4.3. Khersonian-Maeotian palaeoenvironmental evolution

During the Khersonian, the Eastern Paratethys started experiencing extreme water level fluctuations with suggested amplitudes of up to 300 m (Popov et al., 2010), which were linked to the climatically driven disruption of the water budget. During the lowstand episodes, some parts (basins/subbasins) disconnected, exposing large areas of the former shelf. In the Euxinian Basin, three extreme lowstand events were recognised from seismic profiles: one large event spanning the Bessarabian-Khersonian transition, one minor event in the middle of the Khersonian and the strongest one in the terminal Khersonian (Popov et al. 2010, 2022).

The expression and timing of these events in the Caspian Sea remain blank. During the Khersonian, the Caspian Sea retreated from the vast areas of the Ustyurt Plateau of Central Asia (Paramonova, 1994). Moreover, the first Khersonian water drop at the Bessarabian-Khersonian transition along with the tectonic pulse in the Caucasus caused a closure of the Transcaucasian Strait (Popov et al. 2010, 2022). As a result, the sea retreated from the upper Kura Basin (Kartli Depression) (Buleyshvili, 1960) making the Caspian Basin connected to the rest of the Eastern Paratethys only via the northern Pre-Caucasus Strait (Scythian Shelf – Caspian-Terek Depression) (Popov, 2004).

The observations on the lithofacies in Karagiye suggest that during the Khersonian, also the Caspian Basin experienced some water-level fluctuation. In the late Bessarabian, the carbonate platform was gradually shallowing upwards and later, with erosional contacts, became covered with Khersonian barrier rudstones. Such reorganisation may be linked with the end-Bessarabian water level fall, which quickly rebounded with the Khersonian transgression. As this event appears within the 47-kyr-long C5n.1n chron, this process was rather rapid and should not have caused much loss of the depositional record. Hence, the Bessarabian-Khersonian transition in the Caspian Basin was not as dramatic as in the Euxinian Basin, potentially because the major water level drop in the Caspian Basin happened earlier, at the early-late Bessarabian boundary (65 m, 10.67 Ma) where the facies change seems to be more severe.

Between 9.87 and 9.48 Ma (SI6, 93.2–112.5 m), the Karagiye record demonstrates a gradual progradation from a carbonate platform barrier to a lagoon and further to a backshore with palaeosols. Higher up, the depositional record comprises a 1.5-Myr-long hiatus (between 9.5 and 8.0 Ma) that, in our opinion, characterises a strong water level drop. Future focus on geochronological, sedimentological and seismic constraints from the deep-water parts of the basin is needed to verify this.

With the return of aquatic environments at ~8.0 Ma (112.5 m), Karagiye turned into a tidal plain with frequent *Chersonimactra* molluscs and microbial mats. At ~7.8 Ma, prior to the Khersonian–Maeotian boundary, the last Khersonian fauna disappeared, characterising the culmination of the Khersonian Ecological Crisis. A similar faunal trend identified as the "Barren Zone" (Paramonova, 1994; Kojumdgieva et al., 1989), was previously documented in the Euxinian and Dacian basins and was linked to the effect of the final and strongest Khersonian water level drop (Lazarev et al., 2020; Palcu et al., 2019).

The Khersonian lowstand was terminated by a large Maeotian transgression at 7.65 Ma dated in the Euxinian and the Dacian basins (Palcu et al. 2019, 2021; Lazarev et al., 2020). The appearance of new invertebrates of Mediterranean affinity (Popov et al., 2022) and the rise of the $^{87}Sr/^{86}Sr$ isotopic ratio towards the oceanic values (Vasiliev et al., 2021) may suggest a short reconnection of the Eastern Paratethys with the global ocean.

In Karagiye, the Maeotian transgression was accompanied by neither faunistic nor remarkable depositional changes. At 7.65 Ma (120 m), the late Khersonian inter-to-supratidal environments became slightly deeper – sub-to intertidal and contained no fauna. Only at 7.5 Ma, the first characteristic Maeotian ostracod and mollusc assemblage appeared in the record. The delayed occurrence of Maeotian molluscs in the Caspian Basin could be linked with a slightly delayed reconnection between the Caspian and the Euxinian Basins.

At around 7.3 Ma, the depositional settings in Karagiye changed towards the shallow water carbonate platform interior with widespread oolithic barriers and microbial mats.

The comparison of the extreme Khersonian water level oscillation of the Euxinian Basin with the facies and faunal trends in Karagiye suggests that the Caspian Basin had its own hydrological evolution, which does not correlate with the Euxinian Basin. The Bessarabian-Khersonian and terminal Khersonian water level drops did not greatly impact the depositional system of Karagiye. Instead, the early-late Bessarabian (10.67 Ma) and the middle Khersonian (between ~9.5 and ~8 Ma) regressions had the strongest effect on the basin.

5.5. "Marine" vertebrate fauna

Though most of the vertebrate remains come from *ex-situ* finds, the tentative reconstruction of the fauna allowed the following conclusions. The Konkian stage was richer in fish diversity in comparison to younger sediments and included fully marine organisms such as sharks, perciforms and otolith-based large-sized sciaenids (Fig. 14). Among the latter, the small-sized form represents a new, undescribed sciaenid species, whereas the large-sized form can be assigned to the genus *Trewaschiaena* (Bannikov et al., 2018). The latter represents the oldest representative of the genus and, at the same time, counts as the second Konkian species of the genus in the Eastern Paratethys.

The marine mammal fauna of Karagiye is rather diverse, with at least five *in-situ* taxa and a few additional *ex-situ* taxa (*Otradnocetus virodovi, Praepusa, Kentridon fuchsii*, etc.). Among them, the baleen whales *Imerocetus* and *Otradnocetus* were previously documented from the Karaganian-Konkian (without precise dating) of other parts of the Eastern Paratethys (south-western (Mchedlidze, 1964) and north-western Caucasus (Gol'din, 2018; Mchedlidze, 1984). The Karagiye record extends the palaeogeographic distribution of the genera, further for the *Otradnocetus* with much longer probable Volhynian stratigraphic occurrence.

A partial skeleton of *Pachyacanthus* was found in the Konkian sediment debris, making its stratigraphic position uncertain. A second partial skeleton, with a similar body size and similar fossilisation state (bone colour and appearance), has been found on the Volhynian beds (ex-situ), suggesting that the Konkian (ex-situ) find should also be considered Volhynian. The Karagiye record, which indicates a Volhynian age, has the same age as the Central Paratethyan record, suggesting that this toothed whale had a basin-wide (Paratethyan) distribution.

Interestingly, some of Karagiye's marine mammalian taxa have ages similar to the Atlantic Ocean record. Herpetocetinae indet. found from Volhynian debris (dated younger than 12.4 Ma) shares characters similar to *Herpetocetus* and *Metopocetus*. The oldest *Metopocetus* is known from the Nomini Cliffs, USA, which was dated 14–13.5 Ma (Kodama and Pazzaglia, 2023). In general, Herpetocetinae becomed widespread worldwide since the Late Miocene (Boessenecker, 2011). The most probable scenario that explains the Paratethyan and out-of-Paratethyan occurrences of Herpetocetinae would be that the faunal exchanges occurred between the Paratethys and the global ocean before the isolation and afterwards the fauna radiated in the isolated Eastern Paratethyan Basin. Previously, the Paratethys has already been suggested as a diversification hotspot of whales, as it has been demonstrated by Gol'din (2018) on the example of Cetotheriidae and some clades of Phocinae (Koretsky, 2001). Further findings in and outside Paratethys, as well as a comparison with another faunistic record, will be necessary to reconstruct the basin's role in the biotic record's palaeobiogeographic history.

The Bessarabian fauna replaced the Konkian and Volhynian with an assemblage including sparids, a small-sized gobiid, a perciform taxon and a large-sized scombrid. A similar association could be found also in the Sarmatian of the Vienna Basin, Central Paratethys (DV personal observations). A marine mammal fauna includes Paratethyan endemic taxa, widely distributed across the Eastern Paratethys. The lack of any vertebrates in the Khersonian and Maeotian beds suggests that this part of the region was not favourable for their life.

6. Conclusion

Using the integrated stratigraphic approach, we have created well-dated and almost complete palaeoenvironmental and biotic records of the Karagiye section, which provide insight into the evolution of the Caspian Basin before (Konkian), during (Volhynian—Khersonian) and after (Maeotian) the major endorheic phase of the Eastern Paratethys.

Before the major endorheic phase, during the present portion of lower Konkian (Kartvelian), the Karagiye area was an open lagoon with very low faunal diversity. During this period, the Eastern Paratethys had a restricted or closed connection to the global ocean; and the Caspian Basin was fresher than the Euxinian Basin, with salinity ranging within the polyhaline values. Later, the appearance of the numerous middle Konkian marine faunal assemblages marked the restoration of connectivity with the global ocean via the Central Paratethys and the establishment of normal marine environments in the Caspian Basin.

The geological record of the Konkian–Volhynian boundary is missing in Karagiye, hampering the expression of the Paratethyan isolation at 12.65 Ma. After the marine connectivity cut off at 12.65 Ma, the Caspian faunal record underwent a remarkable biotic turnover. Through the preserved portion of the Volhynian (12.33–12.0 Ma), the Karagiye was a shallow-water marginal lagoon inhabited by new endemics, including a few taxa inherited from the Konkian.

At 12.0 Ma, the large Bessarabian transgression established a relatively deep-water offshore environment and introduced new faunas. At ~10.7 Ma, the sudden progradation of shallow water carbonate platform followed by new molluscs and foraminifers indicate the late Bessarabian time. Across the Eastern Paratethys, this event, named here the intra-Bessarabian Carbonate Surge, is characterised by a remarkable increase of carbonate precipitation that was potentially caused by a tectonically driven increase of erosion on land with further supply into a landlocked Eastern Paratethys. Widespread oolite formation and hypercalcification of microfauna suggest high anomalohaline salinity at that time.

In the terminal Bessarabian, the sea retreated from Karagiye but briefly returned with a small-scale Khersonian transgression at 9.9 Ma that established here the marginal carbonate platform barrier with new highly impoverished fauna. Compared to the Bessarabian, the Khersonian fossil record shows no foraminifers, most of the ostracods and all marine vertebrate mammals and the biodiversity of molluscs shrunk to a single genus. This event, called here the Khersonian Ecological Crisis (KEC), was probably linked to strong salinity changes.

The gradual early Khersonian shallowing in Karagiye culminated in palaeosol formation at ~9.5 Ma, which was followed by a 1.5-My-long hiatus (until ~8.0 Ma) that was linked to one of the extreme Khersonian lowstands of the Caspian Basin. In the late Khersonian over the hiatus, the Karagiye represented a shallow-water tidal plain. At around 7.8 Ma, the Khersonian fauna disappeared in Karagiye, marking the peak of the KEC. This event was potentially linked to the freshening and disconnection of the Caspian Basin from the Euxinian Basin, which at that time experienced the terminal Khersonian water level drop.

At 7.65 Ma, a small-scale transgression in Karagiye tentatively marks the Khersonian–Maeotian boundary. However, the first Maeotian faunas appeared here only at 7.5 Ma, which was likely caused by a delayed reconnection with the Euxinian Basin.

Our study shows that while being a part of the Eastern Paratethys, the Caspian Basin still had its unique palaeohydrological evolution. During the isolation phase of the Eastern Paratethys, the Caspian Basin faunal record followed a similar trend with high diversification during the Volhynian-Bessarabian to a near-total faunal extinction during the Khersonian. However, the facies trend of Karagiye shows a significant difference in the number and amplitude of extreme Khersonian water level fluctuations compared to the neighbouring Euxinian Basin and, thus, requires an in-depth sedimentological analysis.

Integrating high-resolution dating with documentation of biotic records creates an important framework for more precise intra-basinal biostratigraphic correlations. It is especially crucial for the dating of the marginal Paratethyan outcrops that, along with marine faunas, often contain land mammals whose dating can be challenging. However, further work on the dating and distribution of biozones across the Eastern Paratethys is highly encouraged.

CRediT authorship contribution statement

Sergei Lazarev: Writing – review & editing, Writing – original draft,

Methodology, Investigation, Formal analysis, Data curation, Conceptualization. **Oleg Mandic:** Methodology, Investigation, Formal analysis. **Marius Stoica:** Methodology, Investigation, Formal analysis, Data curation. **Pavel Gol'din:** Methodology, Formal analysis, Data curation. **Stjepan Ćorić:** Methodology, Formal analysis, Data curation. **Mathias Harzhauser:** Writing – review & editing, Formal analysis, Data curation. **Wout Krijgsman:** Writing – review & editing, Data curation. **Dias Kadirbek:** Writing – review & editing, Formal analysis. **Davit Vasilyan:** Writing – review & editing, Writing – original draft, Supervision, Project administration, Methodology, Funding acquisition, Formal analysis, Data curation.

Declaration of competing interest

The authors declare that they have no known competing financial interests or personal relationships that could have appeared to influence the work reported in this paper.

Acknowledgements

Our study is dedicated to the memory of our friend and colleague Professor Laurent Richard, Nazarbayev University, who enthusiastically supported us and the project from the beginning of the joint research. We want to thank: Sergey Popov for valuable discussions on different aspects of the Paratethys research; Milovan Fustic for the support in the organisation of the fieldwork and fruitful discussions on the depositional history of the Paratethys; Renaud Roch for valuable assistance in the fossil excavation in the field and fossil preparation in the lab; Bettina Reichenbacher and Werner Schwarzhans for the guidance in the identification of the otolith material; Pavlo Otriazhyi for the help with the organisation and identification of the fossil record of the Karagiye; Mark Dekkers for guidance in IRM measurements; our driver Vadik Gassiev for our safe and smooth steppe rides, patience and all logistic support which made our ambitious field campaigns possible. We are grateful to all geology students of the Nazarbaev University who contributed from 2019 to 2024 to the study of the geology and fossil record of the Karagiye section. Special thanks to two anonymous reviewers whose comments helped to improve the manuscript. The study has been funded by the Swiss National Science Foundation project # 200021_197323 and a seed funding grant from the University of Geneva SFG 772 (to DV).

Appendix A. Supplementary data

Supplementary data to this article can be found online at https://doi.org/10.1016/j.marpetgeo.2025.107288.

Data availability

All data associated with this manuscript is available as Supplementary materials.

References

Ali-Zade, A.A., 1974. The Sarmatian of Azerbaijan. Moscow: Nedra.
Allen, Jessica L., Johnson, Cari L., 2011. Architecture and formation of transgressive-regressive cycles in marginal marine strata of the John Henry Member, Straight Cliffs Formation, Upper Cretaceous of Southern Utah, USA. Sedimentology 58 (6), 1486–1513. https://doi.org/10.1111/j.1365-3091.2010.01223.x.
Andreetto, F., Aloisi, G., Raad, F., Heida, H., Flecker, R., Agiadi, K., et al., 2021. Freshening of the Mediterranean salt giant: controversies and certainties around the terminal (Upper Gypsum and Lago-Mare) phases of the Messinian salinity crisis. Earth Sci. Rev. 216, 103577. https://doi.org/10.1016/j.earscirev.2021.103577.
Bannikov, Alexandre F., Schwarzhans, Werner, Carnevale, Giorgio, 2018. Neogene Paratethyan Croakers (Teleostei, Sciaenidae). Riv. Ital. Paleontol. Stratigr. 124 (3). https://doi.org/10.13130/2039-4942/10696, 2018.
Boessenecker, R.W., 2011. Herpetocetine (Cetacea: Mysticeti) dentaries from the upper Miocene Santa Margarita Sandstone of Central California. PaleoBios 30 (1). https://doi.org/10.5070/P9301021792.
Bogdanovich, A.K., 1952. ИскопаеМЫые фораМиниферы СССР. Милиолиды и пенероплиды. [Fossil foraminifers of the USSR. Miliolids and Peneroplids]. In: Trudy VNIGRI, pp. 1–338, 64.
Bona, J., 1964. Coccolithophoriden – Untersuchungen in der neogenen Schichtenfolge des Mecsek Gebirges. Földtani közlöny 94, 121–131.
Brandt, J.F., 1873. Untersuchungen über die fossilen und subfossilen Cetaceen Europa's. Mémoires de l'Académie Impériale des Sciences de St.-Pétersbourg, 7e série 22 (1), 1–361.
Brânzilă, M., 1999. Geologia părţii sudice a Câmpiei Moldove. [The Geology of the Southern Part of the Moldavian Plain]. Corson Press, Iasi.
Brestenská, E., 1974. Die Foraminiferen des Sarmatien s. str. In: Papp, A., Marinescu, F., Seneš, J. (Eds.), Chronostratigraphie und Neostratotypen. Miozän der Zentralen Paratethys, M5 Sarmatien, pp. 243–293 (sensu E.Suess, 1866). Die Sarmatische Schichtengruppe und ihr Stratotypus, IV. Bratislava (4).
Browne, Kathleen M., Golubic, Stjepko, Seong-Joo, Lee, 2000. Shallow marine microbial carbonate deposits. In: Riding, Robert E., Awramik, Stanley M. (Eds.), Microbial Sediments. Springer Berlin Heidelberg, Berlin, Heidelberg, pp. 233–249.
Buleyshvili, D.A., 1960. Geology and Oil and Gas Potential of the Intermontane Depression of Eastern Georgia. Gostoptekhizdat, Leningrad [in Russian].
Burchette, T.P., Wright, V.P., Faulkner, T.J., 1990. Oolitic sandbody depositional models and geometries, Mississippian of southwest Britain: implications for petroleum exploration in carbonate ramp settings. Sediment. Geol. 68 (1), 87–115. https://doi.org/10.1016/0037-0738(90)90121-9.
Butler, Robert F., 1992. Paleomagnetism. Magnetic Domains to Geologic Terranes. Blackwell Scientific Publ, Boston.
Cavazza, William, Gusmeo, Thomas, Zattin, Massimiliano, Alania, Victor, Enukidze, Onise, Corrado, Sveva, Schito, Andrea, 2024. Two-step exhumation of Caucasian intraplate rifts: a proxy of sequential plate-margin collisional orogenies. Geosci. Front. 15 (2), 101737. https://doi.org/10.1016/j.gsf.2023.101737.
Cernajsek, T., 1974. Die Ostracodenfaunen der Sarmatischen Schichten in Österreich. In: Papp, A., Marinescu, F., Seneš, J. (Eds.), Chronostratigraphie und Neostratotypen. Miozän der Zentralen Paratethys, M5 Sarmatien, vol. 4. Die Sarmatische Schichtengruppe und ihr Stratotypus, Bratislava, pp. 458–491 (sensu E.Suess, 1866).
Chumakov, I.S., Byzova, S.L., Ganzei, S.S., 1992. Late Cenozoic Geochronology and Correlation of the Paratethys. Nauka, Moscow [in Russian].
Ćorić, S., 2006. Middle/Upper Miocene (Sarmatian/Pannonian) endemical calcareous nannoplankton from the central Paratethys. In: 11th Interantional Nannoplankton Association Conference. Nebraska, Lincoln, pp. 24–29. September. Lincoln.
Ćorić, S., Galovic, I., Matošević, M., 2023. New calcareous nannofossils from the Middle to Late Miocene of the North Croatian Basin, Central Paratethys. J. Nannoplankt. Res. 41 (1), 1–12. https://doi.org/10.58998/jnr2059.
Damholt, Tove, Surlyk, Finn, 2004. Laminated–bioturbated cycles in Maastrichtian chalk of the North Sea: oxygenation fluctuations within the Milankovitch frequency band. Sedimentology 51 (6), 1323–1342. https://doi.org/10.1111/j.1365-3091.2004.00672.x.
Danišík, Martin, Ponomareva, Vera, Portnyagin, Maxim, Popov, Sergey, Zastrozhnov, Andrei, Kirkland, Christopher L., et al., 2021. Gigantic eruption of a Carpathian volcano marks the largest Miocene transgression of Eastern Paratethys. Earth Planet Sci. Lett. 563, 116890. https://doi.org/10.1016/j.epsl.2021.116890.
De Leeuw, A., Bukowski, K., Krijgsman, W., Kuiper, K.F., 2010. Age of the Badenian salinity crisis; impact of Miocene climate variability on the circum-Mediterranean region. Geol. 38 (8), 715–718. https://doi.org/10.1130/G30982.1.
Dekkers, M.J., 1989. Magnetic properties of natural pyrrhotite. II. High- and low-temperature behaviour of Jrs and TRM as function of grain size. Phys. Earth Planet. In. 57 (3–4), 266–283. https://doi.org/10.1016/0031-9201(89)90116-7.
Didkowski, V.I., 1961. Neogene miliolids from the south-western part of the Russian Platform (Quinqueloculina and Triloculina genera) [Miliolidi neogenovikh pivdeno-zakhidnoi chastini rosiiskoi platformi (Rodi: Quinqueloculina to Triloculina)]. In: Gn. AN USRS, Ser. Stratigrafii Ta Paleontologii, vol. 39.
Didkowski, V.I., Satanovskaja, Z.N., 1970. Foraminifery miocena Ukrainy [Foraminifera of the Miocene of Ukraine]. In: Paleontologiceskij Spravochnik, pp. 1–166, 4.
Dott, R.H., Bourgeois, Joanne, 1982. Hummocky stratification: significance of its variable bedding sequences. Geol. Soc. Am. Bull. 93 (8), 663. https://doi.org/10.1130/0016-7606(1982)93<663:HSSOIV>2.0.CO;2.
Dumitriu, Simina Dumitriţa, Loghin, Sergiu, Dubicka, Zofia, Dobrinescu, Melinte, Carmen, Mihaela, Paruch-Kulczycka, Jolanta, Ionesi, Viorel, 2017. Foraminiferal, ostracod, and calcareous nannofossil biostratigraphy of the latest Badenian – Sarmatian interval (Middle Miocene, Paratethys) from Poland, Romania and the Republic of Moldova. Geol. Carpathica 68 (5), 419–444. https://doi.org/10.1515/geoca-2017-0028.
Filipescu, S., 1996. Stratigraphy of the neogene from the western border of the Transylvanian Basin. Stud. Univ. Babes-Bolyai Geol. 2 (41), 3–75.
Filipescu, S., Silye, L., Krézsek, C., 2005. Sarmatian micropaleontological assemblages and sedimentary paleoenvironments in the Southern Transylvanian Basin. Acta Palaeontol. Romaniae 5, 173–179.
Filipescu, Sorin, Miclea, Angela, Gross, Martin, Harzhauser, Mathias, Zágoršek, Kamil, Jipa, Cătălin, 2014. Early Sarmatian paleoenvironments in the easternmost Pannonian Basin (Borod Depression, Romania) revealed by the micropaleontological data. Geol. Carpathica 65 (1), 67–81. https://doi.org/10.2478/geoca-2014-0005.
Fisher, R., 1953. Dispersion on a sphere. Proc. R. Soc. A 217 (1130), 295–305. https://doi.org/10.1098/rspa.1953.0064.
Flecker, Rachel, Krijgsman, Wout, Capella, Walter, Martíns, Castro, de, Cesar, Dmitrieva, Evelina, Mayser, Jan Peter, et al., 2015. Evolution of the Late Miocene Mediterranean–Atlantic gateways and their impact on regional and global environmental change. Earth Sci. Rev. 150, 365–392. https://doi.org/10.1016/j.earscirev.2015.08.007.

Fordinál, K., Zágorsek, K., Zlinská, A., 2006. Early Sarmatian biota in the northern part of the Danube Basin (Slovakia). Geol. Carpathica 57 (2), 123–130.
Frisch, Konstantin, Voigt, Silke, Voigt, Thomas, Hellwig, Alexandra, Verestek, Verena, Weber, Yuki, 2019. Extreme aridity prior to lake expansion deciphered from facies evolution in the Miocene Ili Basin, south-east Kazakhstan. Sedimentology 66 (5), 1716–1745. https://doi.org/10.1111/sed.12556.
Galovic, Ines, Young, Jeremy, 2012. Revised taxonomy and stratigraphy of Middle Miocene calcareous nannofossils of the Paratethys. Micropaleontology 58 (4), 305–334. https://doi.org/10.47894/mpal.58.4.01.
Galović, I., 2014. Palaeoecological changes through the Sarmatian based on calcareous nannofossils of North Croatia, Central Paratethys. Mater. Geonviron. 61 (2–3), 75–208.
Gani, M.R., Ranson, A., Cross, D.B., Hampson, G.J., Gani, N.D., Sahoo, H., 2015. Along-strike sequence stratigraphy across the Cretaceous shallow marine to coastal-plain transition, Wasatch Plateau, Utah, U.S.A. Sediment. Geol. 325, 59–70. https://doi.org/10.1016/j.sedgeo.2015.05.003.
Gebhardt, H., Zorn, I., Roetzel, R., 2009. The initial phase of the early Sarmatian (Middle Miocene) transgression. Foraminiferal and ostracod assemblages from an incised valley fill in the Molasse Basin of Lower Austria. Austr. J. Earth Sci. 102 (2), 100–119.
Gol'din, Pavel, 2018. New Paratethyan dwarf baleen whales mark the origin of cetotheres. PeerJ 6, e5800. https://doi.org/10.7717/peerj.5800.
Gol'din, Pavel, Startsev, Dmitry, 2017. A systematic review of cetothere baleen whales (Cetacea, Cetotheriidae) from the Late Miocene of Crimea and Caucasus, with a new genus. Papers Palaeontol. 3 (1), 49–68. https://doi.org/10.1002/spp2.1066.
Görög, Á., 1992. Sarmatian foraminifera of the Zsámbék basin, Hungary. In: Annales Universitatis Scientiarium Budapestinensis de Rolando Eötvös nominatae, Geologica, vol. 29, pp. 31–153.
Gross, Martin, 2006. Mittelmiozäne Ostracoden aus dem Wiener Becken (Badenium/Sarmatium, Österreich). Verlag der Österreichischen Akademie der Wissenschaften.
Harzhauser, Mathias, 2021. The Cainozoic to present-day record of Circum-Mediterranean, NE Atlantic and North Sea Cantharidinae and Trochinae (Trochoidea, Gastropoda)-a synopsis. Zootaxa 4902 (1). https://doi.org/10.11646/zootaxa.4902.1.1 zootaxa.4902.1.1.
Harzhauser, Mathias, Guzhov, Aleksandr, Landau, Bernard, 2023. A revision and nomenclator of the Cainozoic mudwhelks (Mollusca: Caenogastropoda: Batillariidae, Potamididae) of the Paratethys Sea (Europe, Asia). Zootaxa 5272 (1), 1–241. https://doi.org/10.11646/zootaxa.5272.1.1.
Harzhauser, Mathias, Kranner, Matthias, Mandic, Oleg, Daneshian, Jahanbakhsh, Asgharian, Fezeh, Mohtat, Tayebeh, et al., 2024a. Middle Miocene (Chokrakian, Karaganian) depositional environments of the Eastern Paratethys Sea in the southern Caspian Basin (Mazandaran Province, northern Iran). Int. J. Earth Sci. 113 (2), 389–415. https://doi.org/10.1007/s00531-023-02379-2.
Harzhauser, Mathias, Landau, Bernard, Mandic, Oleg, Neubauer, Thomas A., 2024b. The Central Paratethys Sea-rise and demise of a Miocene European marine biodiversity hotspot. Sci. Rep. 14 (1), 16288. https://doi.org/10.1038/s41598-024-67370-6.
Harzhauser, Mathias, Mandic, Oleg, Kranner, Matthias, Lukeneder, Petra, Kern, Andrea K., Gross, Martin, et al., 2018. The Sarmatian/Pannonian boundary at the western margin of the Vienna Basin (City of Vienna, Austria). AJES 111 (1). https://doi.org/10.17738/ajes.2018.0003, 26-A4.
Harzhauser, Mathias, Piller, Werner E., 2004. Integrated stratigraphy of the Sarmatian (Upper Middle Miocene) in the western Central Paratethys. Strat 1 (1), 65–86. https://doi.org/10.29041/strat.01.1.04.
Harzhauser, Mathias, Piller, Werner E., 2007. Benchmark data of a changing sea — Palaeogeography, Palaeobiogeography and events in the Central Paratethys during the Miocene. Palaeogeogr. Palaeoclimatol. Palaeoecol. 253 (1–2), 8–31. https://doi.org/10.1016/j.palaeo.2007.03.031.
Healy, Terry, Kenichi, Harada, 1991. Editorial: Enclosed and Semi-Enclosed Coastal Seas. J. Coast Res. 7 (1), i–v. Available online at: http://www.jstor.org/stable/4297799.
Hoyle, Thomas M., Leroy, Suzanne A.G., Lopez-Merino, Lourdes, Miggins, Daniel P., Koppers, Anthony A.P., 2020. Vegetation succession and climate change across the Plio-Pleistocene transition in eastern Azerbaijan, central Eurasia (2.77–2.45 Ma). Palaeogeogr. Palaeoclimatol. Palaeoecol. 538, 109386. https://doi.org/10.1016/j.palaeo.2019.109386.
Iljina, L.A., Nevesskaja, L.A., Paramonova, N.P., 1976. Regularities of Mollusc Development in the Neogene Semimarine and Brackishwater Basins of Eurasia (Late Miocene - Early Pliocene). Publishing house "Nauka", Moscow.
Iljina, L.B., 1993. Handbook for identification of the marine Middle Miocene gastropods of Southwestern Eurasia. Trudi Paleontologičeskogo instituta 255, 1–151.
Ionesi, Viorel, 2006. Sarmaţianul dintre Valea Siretului şi Valea Şomuzului Mare [the Sarmatian between the Siret Valley and the Big Şomuz Valley]. Alexandru Ioan Cuza Univeristy of Iaşi Press, Iasi.
Jgenti, E.M., Maisuradze, L.S., 2016. Karaganian, Kartvelian and Konkian regional stages of Georgia. History of the Development of Molluscs and Foraminifera and Their Stratigraphic Significance [in Russian], Tbilisi.
Jiříček, R., 1974. Biostratigraphische Bedeutung der Ostracoden des Sarmats s. str. In: Papp, A., Marinescu, F., Seneš, J. (Eds.), Chronostratigraphie und Neostratotypen. Miozän der Zentralen Paratethys, M5 Sarmatien, vol. 4. Die Sarmatische Schichtengruppe und ihr Stratotypus, Bratislava, pp. 434–458 (sensu E.Suess, 1866).
Jiříček, R., 1983. Redefinition of the Oligocene and Neogene ostracod zonation of the Paratethys. In: Misc. Micropalaentol. Mem, 18th. Eur. Colloq. Micropaleontol., pp. 195–236
Jorissen, Elisabeth L., Leeuw, Arjan de, van Baak, Christiaan G.C., Mandic, Oleg, Stoica, Marius, Abels, Hemmo A., Krijgsman, Wout, 2018. Sedimentary architecture and depositional controls of a Pliocene river-dominated delta in the semi-isolated Dacian Basin, Black Sea. Sediment. Geol. 368, 1–23. https://doi.org/10.1016/j.sedgeo.2018.03.001.
Karmishina, G.I., Shneider, G.F., 1986. Arthropods: Crustacea: Ostracods. In: Muratov, M.V., Nevesskaya, L.A. (Eds.), Stratigraphy of the USSR. The Neogene Sytem, vol. 2, pp. 289–295. With assistance of A. K. Bogdanovich, O. S. Vyalov, L. K. Gabuniya, Yu. B. Gladenkov, B. P. Zhizhchenko, Ilyina L. B. et al. 2 volumes. Moscow: Nedra (1).
Kazár, E., 2006. Odontocete periotics (Mammalia: Cetacea) from the Carpathian Basin, Middle Miocene (Badenian and Sarmatian Stages), including the Vienna Basin, Austria. Beiträge Paläontol. 30, 269–292.
Kieft, R.L., Hampson, G.J., Jackson, C.A.-L., Larsen, E., 2011. Stratigraphic Architecture of a Net-Transgressive Marginal- to Shallow-Marine Succession: Upper Almond Formation, Rock Springs Uplift, Wyoming, U.S.A. J. Sediment. Res. 81 (7), 513–533. https://doi.org/10.2110/jsr.2011.44.
Kodama, K.P., Pazzaglia, F.J., 2023. New paleomagnetic and rock-magnetic cyclostratigraphy-determined age, deposition rates, and processes for a part of the Calvert Cliffs (Miocene) passive margin deposits. Earth Sci. Rev. 245, 104570. https://doi.org/10.1016/j.earscirev.2023.104570.
Koiava, K., Maissuradze, L., Shatilova, I., Spezzaferri, S., Strasser, A., the Scopes Project: IB 7320-110693 partners, 2008. The Subdivision of Sarmatian deposits of Eastern Georgia based on foraminifera. In: The Fifth Conference on Environmental Micropalaeontology, Microbiology and Meiobenthology. The Fifth Conference on Environmental Micropalaeontology, Microbiology and Meiobenthology. University of Madras, India, pp. 150–153. February 17 - 25.
Kojumdgieva, E.I., 1969. Fosilite Na Bulgaria VIII Sarmat. Sofija.
Kojumdgieva, E.I., Paramonova, N.P., Belokrys, K.S., Muskhelishvili, L.V., 1989. Ecostratigraphic subdivision of the Sarmatian after molluscs. Gologica Carpathica 40 (1), 81–84.
Koleva-Rekalova, E., 1994. Sarmatian aragonite sediments in north-eastern Bulgaria - origin and diagenesis. Geol. Balc. 24 (5), 47–64.
Korecz-Laky, I., 1968. A keleti Mecsek miocén Foraminiferái. [Miocene Foraminifera of the eastern Mecsek Mountains]. Magy. All. Foldt. Intez. Evk. 52 (1), 1–229.
Koretsky, I., 2001. Morphology and systematics of Miocene Phocinae (Mammalia: Carnivora) from Paratethys and the North Atlantic region. Geologica Hungarica Series Palaeontologica 54, 1–109.
Koymans, M.R., Langereis, C.G., Pastor-Galan, D., Hinsbergen, D.J.J., 2016. Paleomagnetism.org: An online multi-platform open source environment for paleomagnetic data analysis. Comput. Geosci. 93, 127–137.
Krasheninnikov, V.A., 1959. Характеристика фауны воraМинифер среднего Миоцена [Characteristics of the foraminifera fauna of the Middle Miocene]. In: Zhizhtschenko, B.P. (Ed.), Атлас СреднеМиоценовой Фауны Северного Кавказа И КрыМа [Atlas of the Middle Miocene Fauna of the North Caucasus and Crimea]. Trudy VNIGAZ, Moscow, pp. 15–103.
Krasheninnikov, V.A., Basov, I.A., Golovina, L.A., 2003. Eastern Paratethys: Tarkhanian and Konkian Regional Stages. Scientific World, Moscow (stratigraphy, micropaleontology, bionomics, paleogeography).
Krijgsman, Wout, Kent, Dennis V., 2004. Non-Uniform Occurrence of Short-Term Polarity Fluctuations in the Geomagnetic Field? New Results from Middle to Late Miocene Sediments of the North Atlantic (DSDP Site 608). In: Channell, J.E.T., Kent, D.V., Lowrie, W., Meert, J.G. (Eds.), Timescales of the Paleomagnetic Field. American Geophysical Union (Geophysical Monograph Series), Washington, D. C., pp. 161–174
Laskarev, V., 1924. Sur les equivalentes du Sarmatien supérieur en Serbie. In: Recueil de traveaux ofert a M. Jovan Cvijic par ses amis et collaborateurs, pp. 73–85.
Lazarev, S., Leeuw, A. de, Stoica, M., Mandic, O., van Baak, C.G.C., Vasiliev, I., Krijgsman, W., 2020. From Khersonian drying to Pontian "flooding": late Miocene stratigraphy and palaeoenvironmental evolution of the Dacian Basin (Eastern Paratethys). Global Planet. Change 192, 103224. https://doi.org/10.1016/j.gloplacha.2020.103224.
Lowrie, W., 1990. Identification of ferromagnetic minerals in a rock by coercivity and unblocking temperature properties. Geophys. Res. Lett. 17 (2), 159–162. https://doi.org/10.1029/GL017i002p00159.
Łuczkowska, E., 1974. Miliolidae (Foraminiferida) from Miocene of Poland. Part II. Biostratigraphy, Paleoecology and Systematics. Acta Paleontol. Polonica 19 (1), 1–176.
Maissuradze, L., Koiava, K., 2011. Biodiversity of Sarmatian Foraminifera of the Eastern Paratethys. Bull. Georgian Natl. Acad. Sci. 5 (1).
Maisuradze, L.S., 1971. Sarmatian Foraminifera of the West Georgia [in Russian]. Tbilisi: Metznereba.
Maisuradze, L.S., 1980. К палеобиологической истории фораМинифер позднего Миоцена ЧерноМорско-Каспийского бассейна [On the paleobiological history of foraminifera of the late Miocene of the Black Sea-Caspian basin]. Metznereba, Tbilisi.
Mandic, O., Rundić, L., Ćorić, S., Pezelj, D., Theobalt, D., Sant, K., Krijgsman, W., 2019a. Age and mode of the middle Miocene marine flooding of the Pannonian Basin—constraints from central Serbia. Palaios 34 (2), 71–95. https://doi.org/10.2110/palo.2018.052.
Mandic, Oleg, Sant, Karin, Kallanxhi, Mădălina-Elena, Ćorić, Stjepan, Theobalt, Dörte, Grunert, Patrick, et al., 2019b. Integrated bio-magnetostratigraphy of the Badenian reference section Ugljevik in southern Pannonian Basin - implications for the Paratethys history (middle Miocene, Central Europe). Global Planet. Change 172, 374–395. https://doi.org/10.1016/j.gloplacha.2018.10.010.
Martini, E., 1970. Standard Tertiary and Quaternary Calcareous Nannoplankton Zonation. In: Proceedings of the 2nd Planktonic Conference, pp. 739–785.
McFadden, P.L., McElhinny, M.W., 1990. Classification of the reversal test in palaeomagnetism. Geophys. J. Int. 103 (3), 725–729. https://doi.org/10.1111/j.1365-246X.1990.tb05683.x.

Mchedlidze, G.A., 1964. Fossil Cetaceans of the Caucasus. Metzniereba, Tbilisi.
Mchedlidze, G.A., 1984. ИскопаеМый Кит Из Миоценовых ОтлоЖений Окрестностей Станицы Отрадная (Северный Кавказ). [Fossil Whale from Miocene Deposits in the Vicinity of the Village of Otradnaya (North Caucasus)]. Tbilisi, Mecniereba.
Méhes, Gy, 1908. Adatok Magyarország pliocén Ostracodáinak ismeretéhez II. Az alsópannóniai emelet Darwinulidae-i és Cytheridae-i. Bull. Hungarian Geol. Soc. 38, 61–65.
Meijer, P.Th, 2012. Hydraulic theory of sea straits applied to the onset of the Messinian Salinity Crisis. In: Marine Geology, pp. 131–139. https://doi.org/10.1016/j.margeo.2012.09.001, 326-328.
Mosar, Jon, Kangarli, Talat, Bochud, Martin, Glasmacher, Ulrich A., Rast, Annick, Brunet, Marie-Francoise, Sosson, Marc, 2010. Cenozoic-Recent tectonics and uplift in the Greater Caucasus: a perspective from Azerbaijan. Geol. Soc., Lond., Special Publ. Publ. 340 (1), 261–280. https://doi.org/10.1144/SP340.12.
Mullender, T.A.T., Velzen, A.J., Dekkers, M.J., 1993. Continuous drift correction and separate identification of ferrimagnetic and paramagnetic contributions in thermomagnetic runs. Geophys. J. Int. 114 (3), 663–672. https://doi.org/10.1111/j.1365-246X.1993.tb06995.x.
Muratov, M.V., Nevesskaya, L.A. (Eds.), 1986. Stratigraphy of the USSR. The Neogene Sytem, vol. 2. Nedra, Moscow. With assistance of A. K. Bogdanovich, O. S. Vyalov, L. K. Gabuniya, Yu. B. Gladenkov, B. P. Zhizhchenko, Ilyina L. B. et al. Paleontological Institute AS USSR.
Murray, John W., 2009. Ecology and Applications of Benthic Foraminifera. Cambridge University Press.
Nemčok, M., Glonti, B., Yukler, A., Marton, B., 2013. Development history of the foreland plate trapped between two converging orogens; Kura Valley, Georgia, case study. In: Geological Society, vol. 377. Special Publications, London, pp. 159–188. https://doi.org/10.1144/SP377.9, 1.
Nevesskaja, L.A., Goncharova, I.A., Paramonova, N.P., Popov, S.B., Babak, E.B., Bagdasarjan, K.G., Voronina, A.A., 1993. Opredelitelj Miocenovjih Dvustvorchatjih Molljuskov Jugo-Zapadnoi Evrazii. Nauka, Moscow.
Nevesskaya, L.A., Goncharova, I.A., Ilyina, L.B., Paramonova, N.P., Khondkarian, S.O., 2003. The Neogene Stratigraphic Scale of the Eastern Paratethys. Stratigr. Geol. Correl. 11 (2), 105–127.
Nevesskaya, L.A., Trubikhin, V.M., 1984. History of the Caspian Basin and its mollusc fauna in the Late Pliocene - Early Pleistocene. In: Kamaletdinov, M.A., Yakhimovich, V.L. (Eds.), Antropogen of Eurasia. Nauka, Moscow, pp. 19–27.
Nichols, Gary, 2009. Sedimentology and Stratigraphy, second ed. Wiley-Blackwell, Chichester.
O'Reilly, W., 1984. Magnetic properties of other mineral systems. In: O'Reilly, W. (Ed.), Rock and Mineral Magnetism. Springer US, Boston, MA, pp. 172–193.
Olteanu, R., 1989. La faune d'ostracodes pontiens du Bassin Dacique. In: Chronostratigraphie und Neostratotypen, Pliozän Pl1, pp. 722–752. Pontien.
Olteanu, R., 1998. Orthogenesis and Orthoselection. Leptocythere lineages in brackish-water Neogene (Ostracoda). Rev. Roum. Geol. 42, 141–153.
Olteanu, R., 1999. The Loxoconcha genus (Ostracda, Crustacea) within Paratethys area. Mem. Inst. Geol. Rom. 37, 17–90.
Olteanu, R., 2006. Monografia ostracodelor terţiare din arealul carpatic/Monograph of Tertiary ostracods from the Carpathian area. Edit. Acad. Române, Bucharest.
Orbigny, Alcide Dessalines d, Delarue, Jean, 1846. Foraminifères fossiles du bassin tertiaire de Vienne (Autriche) : découverts par … Joseph de Hauer. Gide et Compe, Paris.
Palcu, D.V., Golovina, L.A., Vernyhorova, Y.V., Popov, S.V., Krijgsman, W., 2017. Middle Miocene paleoenvironmental crises in Central Eurasia caused by changes in marine gateway configuration. Global Planet. Change 158, 57–71. https://doi.org/10.1016/j.gloplacha.2017.09.013.
Palcu, Dan V., Tulbure, Maria, Bartol, Milos, Kouwenhoven, Tanja J., Krijgsman, Wout, 2015. The Badenian–Sarmatian Extinction Event in the Carpathian foredeep basin of Romania: Paleogeographic changes in the Paratethys domain. Global Planet. Change 133, 346–358. https://doi.org/10.1016/j.gloplacha.2015.08.014.
Palcu, Dan Valentin, Patina, Irina Stanislavovna, Şandric, Ionuţ, Lazarev, Sergei, Vasiliev, Iuliana, Stoica, Marius, Krijgsman, Wout, 2021. Late Miocene megalake regressions in Eurasia. Sci. Rep. 11 (1), 11471. https://doi.org/10.1038/s41598-021-91001-z.
Palcu, Dan Valentin, Vasiliev, Iuliana, Stoica, Marius, Krijgsman, Wout, 2019. The end of the Great Khersonian Drying of Eurasia: Magnetostratigraphic dating of the Maeotian transgression in the Eastern Paratethys. Basin Res. 31 (1), 33–58. https://doi.org/10.1111/bre.12307.
Chronostratigraphie und Neostratotypen: Miozän der Zentralen Paratethys, Band VI. In: Papp, A., Cicha, I., Senes, J., Steininger, F. (Eds.), 1978. M4 Badenien (Moravien, Wielicien, Kosovien). Schweizerbart Science Publishers, Stuttgart, Germany. Available online at: http://www.schweizerbart.de//publications/detail/isbn/9783510600069/Nww. _Chronostratigraphie_und_Neostrat.
Papp, A., Marinescu, F., Senes, J., 1974a. M5 Sarmatien (sensu E. SUESS, 1866). Die Sarmatische Schichtengruppe und ihr Stratotypus. Chronostratigr. Neostratotypen 4, 1–707.
Papp, A., Marinescu, F., Seneš, J. (Eds.), 1974b. Chronostratigraphie und Neostratotypen. Miozän der Zentralen Paratethys, vol. 4. M5 Sarmatien (sensu E. Suess, 1866). Die Sarmatische Schichtengruppe und ihr Stratotypus,. Bratislava.
Papp, Adolf, Schmid, Manfred E., 1985. Die fossilen Foraminiferen des tertiären Beckens von Wien. In: Revision der Monographie von Alcide d'Orbigny (1846). Geologischen Bundesanstalt, Wien.
Paramonova, N.P., 1994. History of Sarmatian and Akchagylian Bivalves. Nauka, Moscow.
Perch-Nielsen, K., 1985. Cenozoic Calcareous Nannofossils. In: Bolli, H.M., Sanders, J.B., Perch-Nielsen, K. (Eds.), Plankton Stratigraphy. Cambridge University Press, Cambridge, pp. 427–554.
Peryt, Tadeusz Marek, 2006. The beginning, development and termination of the Middle Miocene Badenian salinity crisis in Central Paratethys. In: Sedimentary Geology, pp. 379–396. https://doi.org/10.1016/j.sedgeo.2006.03.014, 188-189.
Piller, Werner E., Harzhauser, Mathias, 2005. The myth of the brackish Sarmatian Sea. Terra. Nova 17 (5), 450–455. https://doi.org/10.1111/j.1365-3121.2005.00632.x.
Pishanova, L.S., 1969. Stratigraphical and facial distribution of foraminifera in Miocene deposits of the western part Ukrainian SSR. Rocz. Pol. Tow. Geol. 39 (1–3), 335–351.
Pobedina, V.M., Voroshilova, A.G., Rybina, O.I., Kuznetsova, Z.V., 1956. Справочник по Микрофауне средне- и верхнеМиоценовых отлоЖений АзербайдЖана: Справочник по Микрофауне АзербайдЖана. [Handbook of microfauna of the Middle and Upper Miocene deposits of Azerbaijan: Handbook of microfauna of Azerbaijan]. Aznefteizdat, Baku. Available online at: https://books.google.ch/books?id=8GWMDwAAQBAJ.
Popescu, G., 1995. Contribution to the knowledge of the Sarmatian Foraminifera of Romania. Roman. J. Paleontol. 76, 85–98.
Popescu, G., Grihan, I.M., 2002. Contributions to the knowledge of the marine Middle Miocene Miliolida from Romania. Acta Palaeontol. Romaniae 3, 371–397.
Popescu, G., Grihan, I.M., 2004. Contributions to the knowledge of the calcareous unicameral foraminifeara from the Middle Miocene of Romania. Acta Palaeontol. Romaniae 4, 403–421.
Popescu, G., Grihan, I.M., 2005. Middle Miocene Foraminifera from Romania: Order Buliminida. Part 1. Acta Palaeontol. Romaniae 5, 379–396.
Popescu, G., Grihan, I.M., 2008. Contributions to the knowledge of the rotaliiform foraminifera from the marine middle Miocene deposits from Romania. Acta Palaeontol. Romaniae 6, 287–324.
Popov, S.V., 2004. Lithological-paleogeographic maps of Paratethys. 10 Maps Late Eocene to Pliocene. E Schweizerbart'sche Verlagsbuchhandlung, Stuttgart (Courier Forschungsinstitut Senckenberg).
Popov, S.V., Antipov, M.P., Zastrozhnov, A.S., Kurina, E.E., Pinchuk, T.N., 2010. Sea-level fluctuations on the northern shelf of the Eastern Paratethys in the Oligocene-Neogene. Stratigr. Geol. Correl. 18 (2), 200–224. https://doi.org/10.1134/S0869593810020073.
Popov, S.V., Golovina, L.A., Palcu, D.V., Goncharova, I.A., Pinchuk, T.N., Rostovtseva, Yu V., et al., 2022. Neogene Regional Scale of the Eastern Paratethys, Stratigraphy and Paleontological Basis. Paleontol. J. 56 (12), 1557–1720. https://doi.org/10.1134/S0031030122120024.
Popov, S.V., Rostovtseva, Yu V., Fillippova, N. Yu, Golovina, L.A., Radionova, E.P., Goncharova, I.A., et al., 2016. Paleontology and stratigraphy of the Middle–Upper Miocene of the Taman Peninsula: Part 1. Description of key sections and benthic fossil groups. Paleontol. J. 50 (10), 1039–1206. https://doi.org/10.1134/S0031030116100014.
Raaf, J.F.M., Boersma, J.R., Gelder, A., 1977. Wave-generated structures and sequences from a shallow marine succession, Lower Carboniferous, County Cork, Ireland. Sedimentology 24 (4), 451–483. https://doi.org/10.1111/j.1365-3091.1977.tb00134.x.
Radionova, Eleonora, Golovina, Larisa, Filippova, Natalia, Trubikhin, Valery, Popov, Sergey, Goncharova, Irina, et al., 2012. Middle-Upper Miocene stratigraphy of the Taman Peninsula, Eastern Paratethys. Open Geosci. 4 (1), 925. https://doi.org/10.2478/s13533-011-0065-8.
Raffi, I., Wade, B.S., Pälike, H., Beu, A.G., Cooper, R., Crundwell, M.P., et al., 2020. The Neogene Period. In: Geologic Time Scale 2020, pp. 1141–1215.
Reading, Harold G., 1996. Sedimentary environments. In: Reading, H.G. (Ed.), Processes, Facies, and Stratigraphy, third ed. Blackwell Science, Cambridge, Mass., Oxford.
Reineck, Hans-Erich, Wunderlich, Friedrich, 1968. Classification and origin of flaser and lenticular bedding. Sedimentology 11 (1–2), 99–104. https://doi.org/10.1111/j.1365-3091.1968.tb00843.x.
Rögl, F., 1999. Mediterranean and Paratethys. Facts and hypotheses of an Oligocene to Miocene paleogeography (Short overview). Geol. Carpathica 50 (4), 339–349.
Rostovtseva, Yu V., Koiava, K.P., Rybkina, A.I., 2020. The Cyclostratigraphy of the Konkian Deposits of Eastern Georgia (Eastern Paratethys, Kura Basin). Moscow Univ. Geol. Bull. 75 (6), 579–588. https://doi.org/10.3103/S0145875220060101.
Schneider, G.F., 1939. Остракоды Миоцена КрыМско-Кавказского бассейна. [Ostracodes of the Miocene of the Crimean-Caucasian Basin]. Problemy Paleontol. 5, 177–208.
Schneider, G.F., 1949. Миоценовая фауна остракод Кавказа и КрыМа. Микрофауна нефтяных МестороЖдений СССР, Сборник II. [Miocene fauna of ostracods of the Caucasus and Crimea. Microfauna of oil fields of the USSR, Collection II]. Trudy VNIGRI 34 (M-L), 89–189.
Schneider, G.F., 1953. Фауна остракод из Миоценовых отлоЖений западной части Украины. [Ostracod fauna from the Miocene deposits of the western part of Ukraine]. Geologicheskiy sbornik: Doklady i statyi 2, 101–132.
Schobben, Martin, Stebbins, Alan, Ghaderi, Abbas, Strauss, Harald, Korn, Dieter, Korte, Christoph, 2016. Eutrophication, microbial-sulfate reduction and mass extinctions. Commun. Integr. Biol. 9 (1), e1115162. https://doi.org/10.1080/19420889.2015.1115162.
Schulz, H., Bechtel, A., Sachsenhofer, R., 2005. The birth of the Paratethys during the Early Oligocene. From Tethys to an ancient Black Sea analogue? Global Planet. Change 49 (3–4), 163–176. https://doi.org/10.1016/j.gloplacha.2005.07.001.
Serova, M. Ya, 1955. Стратиграфия и фауна фораМинифер Миоценовых отлоЖений Предкарпатья. [Stratigraphy and foraminifera fauna of the Ciscarpathian Miocene depoits]. Materials for the biostratigraphy of the western regions of the Ukrainian SSR, pp. 261–451.

Silye, Lóránd, 2015. Sarmatian Foraminiferal Assemblages from Southern Transylvanian Basin and Their Significance for the Reconstruction of Depositional Environments. Presa Universitară Clujeană, Cluj-Napoca.
Simon, Dirk, Palcu, Dan, Meijer, Paul, Krijgsman, Wout, 2019. The sensitivity of middle Miocene paleoenvironments to changing marine gateways in Central Europe. Geol. 47 (1), 35–38. https://doi.org/10.1130/G45698.1.
Sladkovskaya, M.G., 2017. Trochidae (Gastropoda) from the Sarmatian Basin of the Eastern Paratethys. Paleontol. J. 51 (14), 1453–1583. https://doi.org/10.1134/S0031030117140039.
Sokhadze, G., Floyd, M., Godoladze, T., King, R., Cowgill, E.S., Javakhishvili, Z., et al., 2018. Active convergence between the Lesser and Greater Caucasus in Georgia: Constraints on the tectonic evolution of the Lesser–Greater Caucasus continental collision. Earth Planet Sci. Lett. 481, 154–161. https://doi.org/10.1016/j.epsl.2017.10.007.
Stancheva, M., 1963. Ostracodna fauna ot neogena v severozapadna Bulgariia. II: sarmatskii ostracodi. Tr. geol. ma Bulgaria, Ser. pal 5, 1–75.
Stancheva, M., 1972. Sarmatian ostracods from north-eastern Bulgaria. In: *Bulletin of Geological Institute, Series Paleontological* 21, pp. 103–128.
Stancheva, M., 1990. Upper Miocene Ostracods from Northern Bulgaria. Bulgarian Academy of Science, Sofia.
Studencka, B., Gontsharova, I.A., Popov, S.V., 1998. The bivalve faunas as a basis for reconstruction of the Middle Miocene history of the Paratethys. Acta Geol. Pol. 48 (3), 285–342.
Subbotina, N.N., Pishanova, L.S., Ivanova, l.V., 1960. Стратиграфия олигоценовых и Миоценовых отлоЖений Предкарпатья по фораМинифераМ [Stratigraphy of Oligocene and Miocene deposits of the Ciscarpathian region based on foraminifera]. Sbornik: Microfauna SSSR. Trudy VNIGRI 11, 5–156.
Suess, E., 1866. Untersuchungen über den Charakter der österreichischen Tertiärbildungen II. Über die Bedeutung der sogenannten „brackischen Stufe" oder der „Cerithienschichten". Sitzungsberichte der Akademie der Wissenschaften, mathematisch-naturwissenschaftliche Klasse 54, 218–259.
Suzin, A.V., 1956. Остракоды Третичных ОтлоЖений Северного Предкавказья [Ostracods of the Tertiary Deposits of the Northern Ciscaucasus]. Moscow: Gostoptekhizdat.
Szczechura, J., 1982. Middle Miocene foraminiferal biochronology and ecology of SE Poland. Acta Palaeontol. Pol. 27 (1–4).
Szuromi-Korecz, Andrea, Magyar, Imre, Sztanó, Orsolya, Csoma, Vivien, Botka, Dániel, Sebe, Krisztina, Tóth, E.M.Ő.K.E., 2021. Various marginal marine environments in the Central Paratethys: Late Badenian and Sarmatian (middle Miocene) marine and non-marine microfossils from Pécs-Danitzpuszta, southern Hungary. Foldtani Kozlony 151 (3), 275–305. https://doi.org/10.23928/foldt.kozl.2021.151.3.275.
Tauxe, Lisa, 2010. Essentials of Paleomagnetism. University of California Press, Berkeley. Available online at: http://gbv.eblib.com/patron/FullRecord.aspx?p=1219560.
ter Borgh, Marten, Stoica, Marius, Donselaar, Marinus E., Matenco, Liviu, Krijgsman, Wout, 2014. Miocene connectivity between the Central and Eastern Paratethys: Constraints from the western Dacian Basin. Palaeogeogr. Palaeoclimatol. Palaeoecol. 412, 45–67. https://doi.org/10.1016/j.palaeo.2014.07.016.
ter Borgh, Marten, Vasiliev, Iuliana, Stoica, Marius, Knežević, Slobodan, Matenco, Liviu, Krijgsman, Wout, et al., 2013. The isolation of the Pannonian basin (Central Paratethys): New constraints from magnetostratigraphy and biostratigraphy. Global Planet. Change 103, 99–118. https://doi.org/10.1016/j.gloplacha.2012.10.001.
Tóth, E.M.Ő.K.E., 2008. Sarmatian (Middle Miocene) ostracod fauna from the Zsámbék Basin, Hungary. Geologica Pannonica 36, 101–151.
Tóth, E., Görög, Á., Lécuyer, C., Moissette, P., Balter, V., Monostori, M., 2010. Palaeoenvironmental reconstruction of the Sarmatian (Middle Miocene) Central Paratethys based on palaeontological and geochemical analyses of foraminifera, ostracods, gastropods and rodents. Geol. Mag. 147 (2), 299–314. https://doi.org/10.1017/S0016756809990203.
Tucker, M.E., 1985. Shallow-marine carbonate facies and facies models. Geol. Soc., Lond., Special Publ. 18 (1), 147–169. https://doi.org/10.1144/GSL.SP.1985.018.01.08.
van, Baak, Christiaan, G.C., Vasiliev, Iuliana, Palcu, Dan V., Dekkers, Mark J., Krijgsman, Wout, 2016a. A Greigite-Based Magnetostratigraphic Time Frame for the Late Miocene to Recent DSDP Leg 42B Cores from the Black Sea. Front. Earth Sci. 4. https://doi.org/10.3389/feart.2016.00060.
van, Baak, Christiaan, G.C., Stoica, Marius, Grothe, Arjen, Aliyeva, Elmira, Krijgsman, Wout, 2016b. Mediterranean-Paratethys connectivity during the Messinian salinity crisis: The Pontian of Azerbaijan. Global Planet. Change 141, 63–81. https://doi.org/10.1016/j.gloplacha.2016.04.005.
van der Merwe, Willem C., Flint, Stephen S., Hodgson, David M., 2010. Sequence stratigraphy of an argillaceous, deepwater basin-plain succession: Vischkuil Formation (Permian), Karoo Basin, South Africa. Mar. Petrol. Geol. 27 (2), 321–333. https://doi.org/10.1016/j.marpetgeo.2009.10.007.
Vasiliev, Iuliana, Stoica, Marius, Grothe, Arjen, Lazarev, Sergei, Palcu, Dan Valentin, van Baak, Christiaan, et al., 2021. Hydrological Changes in Restricted Basins: Insights From Strontium Isotopes on Late Miocene-Pliocene Connectivity of the Eastern Paratethys (Dacian Basin, Romania). Geochem. Geophys. Geosyst. 22 (7), e2020GC009369. https://doi.org/10.1029/2020GC009369.
Venglinsky, I.V., 1953. Микропалеонтологическая характеристика сарМатских отлоЖений Закарпатской области [Micropaleontological characteristics of Sarmatian deposits of the Transcarpathian region]. Nauk Zapiski, Geologicheskaya seria 23 (6).
Venglinsky, I.V., 1958. Miocene foraminifera from the Transcarpathian area. Vidavictvo Akademia Nauk Ukrainskoi RSR, Kyiv [Foraminiferi miocenu Zakarpatja].
Venglinsky, I.V., 1962. The biostratigraphy of the Miocene from the Pericarpathian area based on foraminifera [Biostratigrafia miocenu Zakarpatja za faunaju foraminifer]. Vidavictvo Akademia Nauk Ukrainskoi RSR, Kyiv.
Venglinsky, I.V., 1975. ФораМиниферы и биостратиграфия Миоценовых отлоЖений Закарпатского прогиба [Foraminifera and biostratigraphy of Miocene deposits from the Transcarpathian Depression. Naukova Dumka, Kyiv.
Vernyhorova, YuV., 2015. The criteria of the Konkian deposits stratigraphy of the eastern Paratethys based on molluscs and foraminifers. Geol. J. 0 (4), 77–86. https://doi.org/10.30836/igs.1025-6814.2015.4.139037.
Vernyhorova, Yulia, 2018. Biostratigraphy of the Konkian (Middle Miocene of the Eastern Paratethys) deposits of Southern Ukraine based on foraminifera. Geol Cro 71 (3), 135–146. https://doi.org/10.4154/gc.2018.18.
Vernyhorova, Yuliia V., Holcová, Katarína, Doláková, Nela, Reichenbacher, Bettina, Scheiner, Filip, Ackerman, Lukáš, et al., 2023. The Miocene Climatic Optimum at the interface of epicontinental sea and large continent: A case study from the Middle Miocene of the Eastern Paratethys. Mar. Micropaleontol. 181, 102231. https://doi.org/10.1016/j.marmicro.2023.102231.
Voigt, Silke, Weber, Yuki, Frisch, Konstantin, Bartenstein, Alexander, Hellwig, Alexandra, Petschick, Rainer, et al., 2017. Climatically forced moisture supply, sediment flux and pedogenesis in Miocene mudflat deposits of south-east Kazakhstan, Central Asia. The Depositional Record 3 (2), 209–232. https://doi.org/10.1002/dep2.34.
Voloshinova, N.A., 1952. Fossil foraminifera of the USSR. Nonionids. In *Trudy VNIGRI*, 63, 11–75.
Voloshinova, N.A., 1958. О новой систеМатике нонионид. Микрофауна СССР, Сборник 9 [On the new systematics of nonioninds. Microfauna of the USSR, Volume 9]. Trudy VNIGRI 115, 117–191.
Yoshida, S., 2000. Sequence and facies architecture of the upper Blackhawk Formation and the Lower Castlegate Sandstone (Upper Cretaceous), Book Cliffs, Utah, USA. Sediment. Geol. 136 (3–4), 239–276. https://doi.org/10.1016/S0037-0738(00)00104-4.
Zalányi, B., 1913. Magyarországi miocén ostracodák. In: Kir, A.M. (Ed.), Földt. Int. Évkönyve 4 (21), 75–133.
Zelenka, J., 1990. A review of the Sarmatian Ostracoda of the Vienna Basin. In: Whatley, R., Maybury, C. (Eds.), Ostracoda and Global Events, 1. Chapman and Hall, London u.a., pp. 263–270 (British Micropalaeontological Society publication series).
Zhao, Zhe, Hou, Zhong-E, Li, Shu-Qiang, 2022. Cenozoic Tethyan changes dominated Eurasian animal evolution and diversity patterns. Zool. Res. 43 (1), 3–13. https://doi.org/10.24272/j.issn.2095-8137.2021.322.
Zhizhtschenko, B.P. (Ed.), 1959. Атлас СредниеМиоценовой Фауны Северного Кавказа И КрыМа [Atlas of the Middle Miocene Fauna of the North Caucasus and Crimea]. Trudy VNIGAZ, Moscow.